ISSN 0038-531X

Russian Original Vol. 57, No. 3, September, 1984

March, 1985

SATEAZ 57(3) 577-672 (1984)

SOVIET ATOMIC ENERGY

АТОМНАЯ ЭНЕРГИЯ
(ATOMNAYA ÉNERGIYA)

TRANSLATED FROM RUSSIAN

c/b CONSULTANTS BUREAU, NEW YORK

SOVIET ATOMIC ENERGY

Soviet Atomic Energy is abstracted or indexed in *Chemical Abstracts, Chemical Titles, Pollution Abstracts, Science Research Abstracts, Parts A and B, Safety Science Abstracts Journal, Current Contents, Energy Research Abstracts,* and *Engineering Index.*

Mailed in the USA by Publications Expediting, Inc., 200 Meacham Avenue, Elmont, NY 11003.

POSTMASTER: Send address changes to *Soviet Atomic Energy,* Plenum Publishing Corporation, 233 Spring Street, New York, NY 10013.

Soviet Atomic Energy is a translation of *Atomnaya Énergiya,* a publication of the Academy of Sciences of the USSR.

An agreement with the Copyright Agency of the USSR (VAAP) makes available both advance copies of the Russian journal and original glossy photographs and artwork. This serves to decrease the necessary time lag between publication of the original and publication of the translation and helps to improve the quality of the latter. The translation began with the first issue of the Russian journal.

Consultants Bureau journals appear about six months after the publication of the original Russian issue. For bibliographic accuracy, the English issue published by Consultants Bureau carries the same number and date as the original Russian from which it was translated. For example, a Russian issue published in December will appear in a Consultants Bureau English translation about the following June, but the translation issue will carry the December date. When ordering any volume or particular issue of a Consultants Bureau journal, please specify the date and, where applicable, the volume and issue numbers of the original Russian. The material you will receive will be a translation of that Russian volume or issue.

Subscription (2 volumes per year)
Vols. 56 & 57: $560 (domestic), $621 (foreign)
Vols. 58 & 59: $645 (domestic), $715 (foreign)
Single Issue: $100
Single Article: $8.50

CONSULTANTS BUREAU, NEW YORK AND LONDON

c/b
233 Spring Street
New York, New York 10013

Published monthly. Second-class postage paid at Jamaica, New York 11431.

SOVIET ATOMIC ENERGY

A translation of *Atomnaya Énergiya*

March, 1985

Volume 57, Number 3 **September, 1984**

CONTENTS

CONTENTS

(continued)

Engl./Russ.

The Russian press date (podpisano k pechati) of this issue was 8/27/1984. Publication therefore did not occur prior to this date, but must be assumed to have taken place reasonably soon thereafter.

ARTICLES

COST OF INFORMATION IN NUCLEAR POWER

Ya. V. Shevelev

UDC 33.621.039.003

Statement of the Problem. Appreciable information on the interaction of neutrons with matter has accumulated in nuclear and reactor physics. There are many programs for the calculation of neutron fields. One can obtain an answer with this or the other accuracy to almost any practically significant question on the number of reactions of this or the other kind between neutrons and the materials of a nuclear reactor. If this accuracy is limited by incompleteness of information about the cross sections or other characteristics of the nuclei, a dilemma arises: whether to tolerate this inaccuracy and the nonoptimality of the engineering solutions associated with it or to run experiments which refine the nuclear data.

In order to solve this problem, it is necessary to know, on the one hand, the cost of the experiment and, on the other hand, its usefulness [1], i.e., the decrease of loss associated with availability of the necessary information. The experiment is profitable if its usefulness is greater than its cost. In this paper methods are discussed for determining the usefulness of an experiment which refines nuclear data and other parameters affecting the operation of a nuclear reactor as well as the usefulness of parallel design-structural developments of competing installations or alternatives of their elements.

Mathematical Model. Let $f(x, y)$ be the expenditures for an economic measure, for example, for construction or operation (and perhaps for something else) of the installation; more exactly, these are the discounted (reduced) costs [2]. The parameter x should be selected from some set of permissible values; this is the parameter to be controlled. It is impossible to change the parameter y; it is associated with objectively acting and uncontrollable factors, i.e., the organization of the world. However, it is not known completely accurately. One can express the set of values of y by means of the subjective probability density distribution for y in the form $p(y|y_0, \sigma_0)$, namely,

$$\int p(y|y_0, \sigma_0)\,dy = 1; \quad \int p(y|y_0, \sigma_0)\,y\,dy = y_0; \quad \int p(y|y_0, \sigma_0)\,(y-y_0)^2\,dy = \sigma_0^2. \tag{1}$$

The subjective probability is specified on a set of differently constructed (having different values of y) worlds, among which the real world was mislaid. It characterizes our idea of the plausibility of the assumption that apparently the world with the parameter y is the real world.

The optimal choice of the parameter x should be aimed at minimization of the anticipated costs*

$$x_{opt}: \min_x \int f(x, y)\,p(y|y_0, \sigma_0)\,dy. \tag{2}$$

It is proposed to run an experiment which will refine our ideas about y. After the experiment we shall obtain a new subjective probability density for y. We shall denote it as $p(y|y_1, \sigma_1)$; similarly to the expression (1),

$$\int p(y|y_1, \sigma_1)\,dy = 1; \quad \int p(y|y_1, \sigma_1)\,y\,dy = y_1; \quad \int p(y|y_1, \sigma_1)\,(y-y_1)^2\,dy = \sigma_1^2. \tag{3}$$

*Reference [4] is devoted to the controversy with the other viewpoints, for example, those expounded in [3].

Translated from Atomnaya Énergiya, Vol. 57, No. 3, pp. 147-153, September, 1984. Original article submitted December 5, 1983.

0038-531X/84/5703-0577$08.50

The quantity

$$\Delta\sigma^2 = \sigma_0^2 - \sigma_1^2 \tag{4}$$

is a measure of the information content of the experiment and can be estimated prior to its execution. The cost of the experiment Δf can be estimated. The value of y_1 is not known in advance. We shall denote the probability density of obtaining the value y_1 as a result of the planned experiment by $p(y_1|y_0, \sigma_0, \sigma_1)$. The experiment is profitable if Δf in the sum of the expected costs after the experiment with an optimally selected (after the experiment) x is less than the anticipated costs without doing the experiment, but again with an optimally selected x. Of course, the optimal x will be different. The economic effect from performance of the experiment is equal to

$$Ef = \{\min_x \langle f\rangle_0\} - \{\Delta f + \langle \min_x \langle f\rangle_1\rangle_{01}\}, \tag{5}$$

where $\langle\rangle_0$, $\langle\rangle_1$, and $\langle\rangle_{01}$ are the averaging signs with the weights $p(y|y_0, \sigma_0)$, $p(y|y_1, \sigma_1)$, and $p(y_1|y_0, \sigma_0, \sigma_1)$, so that

$$Ef = \left\{\min_x \int f(x, y)\, p(y|y_0, \sigma_0)\, dy\right\} - \left\{\Delta f + \int p(y_1|y_0, \sigma_0, \sigma_1)\, dy_1 \left[\min_x \int f(x, y)\, p(y|y_1, \sigma_1)\, dy\right]\right\}. \tag{6}$$

If $Ef \geqslant 0$, the economic advisability of doing the experiments is proven.

The function $p(y_1|y_0, \sigma_0, \sigma_1)$ which enters into the expression (6) should satisfy the equation

$$p(y|y_0, \sigma_0) = \int p(y_1|y_0, \sigma_0, \sigma_1)\, p(y|y_1, \sigma_1)\, dy_1. \tag{7}$$

Actually, one can treat the averaging of y as a two-stage process. In the first stage an inaccurate experiment gives the parameter y_1 with the probability $p(y_1|y_0, \sigma_0, \sigma_1)$, after which an accurate measurement gives the value y with the probability $p(y|y_1, \sigma_1)$. The final distribution of y cannot differ from that existing prior to the experiment $p(y|y_0, \sigma_0)$, as long as the possible results of its execution are being discussed. In particular, we find from Eq. (7), using the expressions (1), (3), and (4),

$$y_0 = \int p(y|y_0, \sigma_0)\, y\, dy = \int p(y_1|y_0, \sigma_0, \sigma_1)\, dy_1 \int p(y|y_1, \sigma_1)\, y\, dy = \int p(y_1|y_0, \sigma_0, \sigma_1)\, y_1\, dy,$$

$$\int p(y_1|y_0, \sigma_0, \sigma_1)\, y_1\, dy_1 = y_0; \tag{8}$$

$$\sigma_0^2 = \int p(y|y_0, \sigma_0)\,(y - y_0)^2\, dy = \int p(y_1|y_0, \sigma_0, \sigma_1)\, dy_1 \int p(y|y_1, \sigma_1)\,(y_1 - y_0 +$$

$$+ y - y_1)^2\, dy = \int p(y_1|y_0, \sigma_0, \sigma_1)\, dy_1\, [(y_1 - y_0)^2 + \sigma_1^2];$$

$$\int p(y_1|y_0, \sigma_0, \sigma_1)\,(y_1 - y_0)^2\, dy_1 = \Delta\sigma^2. \tag{9}$$

If there are grounds for assuming $p(y|y_0, \sigma_0)$ and $p(y|y_1, \sigma_1)$ to be normal distributions, $p(y_1|y_0, \sigma_0, \sigma_1)$ is also a normal distribution with a mathematical expectation y_0 and a dispersion $\Delta\sigma^2$.

Simplest Quadratic Model. Let the choice of x be unconstrained in any way, and let f be approximated with good accuracy by a quadratic function of x and y. One can, without restricting generality, figure x from the optimum point at $y = y_0$ and f from its value at this optimum. Then

$$f = f_y \cdot (y - y_0) + f_{yy} \cdot (y - y_0)^2/2 + f_{xx}x^2/2 + f_{xy}x \cdot (y - y_0), \tag{10}$$

$$f_{xx} > 0. \tag{11}$$

Integrating the expression (10) with the weight $p(y|y_0, \sigma_0)$, we obtain according to the expression (1)

$$\langle f\rangle_0 = f_{yy}\sigma_0^2/2 + f_{xx}x^2/2.$$

The optimal x is equal to zero, so that

$$\min_x \langle f\rangle_0 = f_{yy}\sigma_0^2/2. \tag{12}$$

Integrating the expression (10) with the weight $p(y|y_1, \sigma_1)$, we obtain, according to Eq. (3),

$$\langle f\rangle_1 = f_y\cdot(y_1-y_0) + f_{yy}\cdot[(y_1-y_0)^2+\sigma_1^2]/2 + f_{xx}x^2/2 + f_{xy}x\cdot(y_1-y_0).$$

The optimal x is equal to $-f_{xy}\cdot(y_1-y_0)/f_{xx}$, so that

$$\min_x \langle f\rangle_1 = f_y\cdot(y_1-y_0) + f_{yy}\cdot[(y_1-y_0)^2+\sigma_1^2]/2 - (f_{xy})^2(y_1-y_0)^2/(2f_{xx}). \tag{13}$$

Averaging this quantity with the weight $p(y_1|y_0, \sigma_0, \sigma_1)$, we obtain, according to the expressions (7) and (8),

$$\langle\min_x \langle f\rangle_1\rangle_{01} = f_{yy}\cdot(\Delta\sigma^2+\sigma_1^2)/2 - (f_{xy})^2\Delta\sigma^2/(2f_{xx}). \tag{14}$$

Substituting Eq. (2) and the expression (14) into formula (5) and using the quantity (4), we find

$$Ef = \{f_{yy}\sigma_0^2/2\} - \{\Delta f + f_{yy}\sigma_0^2/2 - \Delta\sigma^2(f_{xy})^2/(2f_{xx})\},$$

$$Ef = C\,\Delta\sigma^2 - \Delta f, \tag{15}$$

where

$$C = (f_{xy})^2/(2f_{xx}). \tag{16}$$

The quantity $C\Delta\sigma^2$ is the economic cost of the information, i.e., the usefulness of the experiment. If its value is greater than the cost of the experiment Δf, the experiment is profitable. The economic value of the information turns out in this case to be proportional to the information content of the experiment $\Delta\sigma^2$. One can call the proportionality coefficient C the information cost. According to the expression (11), this is a positive quantity. If the experiment is accurate, $\Delta\sigma^2 = \sigma_0^2$. The usefulness of an accurate experiment $C\sigma_0^2$ coincides with the disadvantage from a lack of information prior to the experiment:

$$L = C\,\sigma_0^2. \tag{17}$$

Possible Generalizations of the Quadratic Model. A rather simple generalization of the model consists of replacing the scalars x and y with vectors x and y. The expansion (10) takes the form (to shorten the writing we set $y_0 = 0$)

$$f = y^t f_y + \frac{1}{2}y^t f_{yy}y + \frac{1}{2}x^t f_{xx}x + x^t f_{xy}y, \tag{18}$$

where "t" denotes transposition, f_y is a vector whose components are the derivatives of f with respect to the components of y, and f_{yy}, f_{xx}, and f_{xy} are matrices whose elements are the corresponding derivatives. In order that $x = 0$ be a minimum point of f at $y = y_0 = 0$, the matrix f_{xx} should be positive definite. Then

$$\min_x \langle f\rangle_0 = \frac{1}{2}\langle y^t f_{yy}y\rangle_0, \tag{19}$$

where $\langle\rangle_0$ is, as before, the averaging symbol for the distribution of probabilities for y prior to performance of the experiment. This distribution is now characterized (besides the mathematical expectation $y_0 = 0$) not by the number σ_0^2 but by the covariant matrix $\langle yy^t\rangle_0$ with the elements $\langle y_i y_j\rangle_0$. We shall find the loss from inaccurate knowledge of the value of y. Assuming that the planned experiment gives an accurate value of y, we obtain in place of the expression (5)

$$Ef = \min_x \langle f\rangle_0 - \Delta f - \langle\min_x f\rangle_0. \tag{20}$$

The optimal value of x for an accurately measured value of y is equal to $-f_{xx}^{-1}f_{xy}y$. Substituting it into the expansion (18) and averaging, we obtain

$$\langle \min_x f \rangle_0 = \frac{1}{2} \langle y^t f_{yy} y \rangle_0 - \frac{1}{2} \langle y^t f_{xy}^t f_{xx}^{-1} f_{xy} y \rangle_0,$$

so that

$$Ef = \frac{1}{2} \langle y^t f_{xy}^t f_{xx}^{-1} f_{xy} y \rangle_0 - \Delta f. \tag{21}$$

The economic loss from a lack of information is equal to

$$L = \sum_i \sum_j C_{ij} \langle y_i y_j \rangle. \tag{22}$$

where C_{ij} are the elements of the cost matrix

$$C = \frac{1}{2} f_{xy}^t f_{xx}^{-1} f_{xy}. \tag{23}$$

The matrix C, just as f_{xx}, is positive definite. Therefore the loss calculated from formula (22) is always positive.

Constraints can be imposed on x. If at y = 0 the optimal x does not lie on the boundary, formulas (22) and (23) remain in force for covariant matrices $\langle yy^t \rangle_0$ which are sufficiently small in the norm, since the probability of the optimal value of x lying on the boundary is small for a small indeterminacy in the values of y.

Let us consider the case in which at y = 0 the optimal value of x lies on the boundary of the authorized region. If the boundary is smooth in the neighborhood of the optimal value of x, one can reduce the problem to the preceding one by selecting new generalized coordinates on the boundary. The new vector x will have a smaller dimensionality, and its choice will not be constrained in any way. If the optimal (at y = 0) value of x is located at a singular point of the boundary (at a "corner"), so that the optimum point is not shifted upon small changes in y, the cost of the information for a matrix $\langle yy^t \rangle_0$ which is sufficiently small in the norm is equal to zero (ignorance of the value of y does not impose a loss).

Finally, if upon a change in y in the region in which the probability is not small the optimal value of x can switch from the boundary into the volume or from one boundary to another, the analytic calculation of the usefulness of the experiment is complicated. One can do it by using the Monte Carlo method.

A Model of a Different Type. In a number of cases the transition of the parameter x through some boundary whose position is not known completely accurately will result in large economic losses. Moreover, if there were not these losses, the optimum would lie on the boundary. The simplest mathematical model of such a situation is expressed by the following dependence of the expenditures on the parameter being controlled x and the poorly known value of the parameter y:

$$f(x, y) = -cx + \text{Ш} E(x - y), \quad c > 0, \quad \text{Ш} > 0. \tag{24}$$

Here the function E is equal to zero for nonpositive and to unity for positive values of the argument. The statistical properties of y are determined by the expression (1); $y_0 = 0$, and the distribution for y is Gaussian:

$$p(y|y_0, \sigma_0) = \exp[-y^2/(2\sigma_0^2)]/(\sqrt{2\pi}\sigma_0). \tag{25}$$

In addition to a local minimum at x = y, the function f formally has a global minimum as $x \to \infty$. However, we shall assume that larger values for x are forbidden.

Averaging f over the distribution (25), we obtain

$$\langle f \rangle_0 = -cx + \text{Ш} \int_{-\infty}^{x} p(y|y_0, \sigma_0)\, dy. \tag{26}$$

If

$$\text{Ш} > c\sqrt{2\pi}\sigma_0, \tag{27}$$

a minimum of $\langle f\rangle_0$ is observed at

$$\begin{aligned} -c+\text{III}p(x_{\text{opt}}|y_0,\ \sigma_0)=0;\\ dp(x_{\text{opt}}|y_0,\ \sigma_0)/dx_{\text{opt}}>0, \end{aligned} \tag{28}$$

whence according to the distribution (25),

$$x_{\text{opt}}=-\sigma_0\sqrt{\ln\frac{\text{III}^2}{2\pi\sigma_0^2c^2}}. \tag{29}$$

Substituting the expression (29) into formula (26), we find

$$\begin{aligned} \min_x\langle f\rangle_0=\sigma_0c\cdot\left\{\left(\ln\frac{\text{III}^2}{2\pi\sigma_0^2c^2}\right)^{1/2}+\right.\\ \left.+\frac{\text{III}}{\sigma_0c}\operatorname{erfc}\left[\left(\ln\frac{\text{III}^2}{2\pi\sigma_0^2c^2}\right)^{1/2}\right]\right\}, \end{aligned} \tag{30}$$

where

$$\operatorname{erfc}(z)=\frac{2}{\sqrt{\pi}}\int_z^\infty e^{-t^2}dt\approx\frac{1}{\sqrt{\pi}\,z}e^{-z^2}. \tag{31}$$

An approximate formula which is valid for large values of z gives

$$\min_x\langle f\rangle_0\approx\sigma_0c\cdot\left[\left(\ln\frac{\text{III}^2}{2\pi\sigma_0^2c^2}\right)^{1/2}+\left(\ln\frac{\text{III}^2}{2\pi\sigma_0^2c^2}\right)^{-1/2}\right];\ \frac{\text{III}}{\sqrt{2\pi}\,\sigma_0c}\gg1. \tag{32}$$

If y were to become known accurately as a result of the performance of an experiment, we would have

$$x_{\text{opt}}=y,\ \min_x f=-cy,$$

so that

$$\langle\min_x f\rangle_0=0 \tag{33}$$

and the economic loss from a lack of information is

$$L=\min_x\langle f\rangle_0. \tag{34}$$

In agreement with the expression (32), this loss vanishes when $\sigma_0 = 0$. However, in contrast to the preceding models, the loss is not proportional to the dispersion σ_0^2. In the first approximation it is proportional to σ_0, i.e., to the root of the dispersion (the proportionality coefficient depends on σ_0 logarithmically, i.e., very weakly), and with good accuracy

$$\frac{dL}{d\sigma_0}\approx c\cdot\left(\ln\frac{\text{III}^2}{2\pi\sigma_0^2c^2}\right)^{1/2}. \tag{35}$$

The loss increases slowly as III increases and is almost proportional to c.

An Example of the Application of the Simplest Quadratic Model. Let it be known that the annual volumes of plutonium extracted from fast reactors which are subject to refabrication vary linearly with time:

$$q=q_0+\dot{q}t \tag{36}$$

The rate of growth of the refabrication volumes $\dot{q}/q_0$ is equal to the rate of growth of the total installed capacity of breeder reactors. We shall assume that it is limited by the arrival of excess plutonium from these reactors. Actually, thermal reactors also supply plutonium. But ignoring this source of plutonium, we overestimate the cost of the information which we are talking about. Consequently, we shall assume that $\dot{q}/q_0$ is proportional to the excess of the value of the breeding ratio of the breeder reactors above unity.

We shall denote the relative error in this excess, and this also means in $\dot{q}$, as σ_0. Very large expenditures have been consumed throughout the world in the last decade for a

decrease of σ_0, and right now the absolute error of the breeding ratio is 3.5% [5, 6], so that $\sigma_0 \approx 0.10$.* Was there an economic necessity to refine the breeding ratio? Should one refine it further?

Automated assembly lines should be constructed for the refabrication of plutonium. We shall assume that the design capacity of the assembly line Q is not expressed in that part of the instantaneous flow rates which is proportional to the load of the undertaking. One can ignore this part of the flow rates by selecting the design capacity of successively installed assembly lines Q_j, j = 0, 1,... . In other words, we shall represent the expenditures for construction and operation of the assembly line reduced to the time of its startup which are not associated with the load of the undertaking as a linear function of Q [7, 8]:

$$\varphi(Q) = \mathcal{K} + kQ, \; Q > 0. \tag{37}$$

At time $t_0 = 0$ a line should be introduced with a capacity Q_0 subject to determination. The times of introduction of the lines t_1, t_2, ... are uniquely determined by the design capacities Q_0, Q_1, ..., since it is advisable to introduce a new line prior to exhausting the production reserve of the lines already operating:

$$t_{j+1} - t_j = Q_j/\dot{q}, \; j > 1; \; t_1 - t_0 = (Q_0 - q_0)/\dot{q}. \tag{38}$$

The true value of $\dot{q}$ will be determined up to the time of exhaustion of the production capacity Q_0.

The part of the reduced costs subject to minimization is equal to

$$f = \varphi(Q_0) + \sum_{j=1}^{\infty} \varphi(Q_j) \exp(-Pt_j), \tag{39}$$

where P is the discount norm, i.e., the norm of the reduction of nonsimultaneous costs to a single time [2]. When $\dot{q}$ becomes known, the equal intervals between the introduction of the lines and accordingly the equal values of the design capacity

$$t_2 - t_1 = t_3 - t_2 = \ldots = \Delta t, \tag{40}$$

$$Q_1 = Q_2 = \ldots = Q \tag{41}$$

will be optimal by virtue of the time-independent nature of the problem, so that we obtain from the expressions (37)-(41)

$$f = \mathcal{K} + kQ_0 + (\mathcal{K} + k\dot{q}\Delta t) \exp[-(Q_0 - q_0) P/\dot{q}] \; [1 - \exp(-P\Delta t)]^{-1}. \tag{42}$$

Let us introduce the dimensionless parameters

$$z = P\Delta t; \; a = (Q_0 - q_0) k/\mathcal{K}; \; \mu = P\mathcal{K}/(k\dot{q}). \tag{43}$$

We obtain

$$f/\mathcal{K} = 1 + kq_0/\mathcal{K} + a + \frac{1 + z/\mu}{1 - \exp(-z)} \exp(-\mu a) \tag{44}$$

instead of the expression (42). After $\dot{q}$, and this means μ also, are determined, one should for minimization of the costs find a z (and this means Δt also) such that the expression

$$(1 + z/\mu)[1 - \exp(-z)]^{-1} \; .$$

is a minimum. Equating the derivative with respect to z to zero, we obtain an equation for z [8]:

*If b.r. = 1.5(1 + ε), where ε is the relative error of the breeding ratio, the relative error (b.r. − 1) will amount to ε b.r./(b.r. − 1) = 3ε.

$$\exp(z) - 1 - z = \mu. \tag{45}$$

With this equation taken into account the expression (44) is transformed:

$$f/\mathcal{K} = 1 + kq_0/\mathcal{K} + a + \frac{1+\mu+z}{\mu}\exp(-\mu a). \tag{46}$$

Here the parameter being optimized is a, and μ is undetermined. In order to reduce the problem to the simplest quadratic model discussed earlier, we shall assume

$$\mu = \mu_0/(1+y); \tag{47}$$

$$a = a_0 \cdot (1+x), \tag{48}$$

where

$$\mu_0 = P\mathcal{K}/(k\langle\dot{q}\rangle_0); \tag{49}$$

$$a_0 = z_0/\mu_0; \tag{50}$$

$$\exp(z_0) - 1 - z_0 = \mu_0 \tag{51}$$

It follows from the expressions (43) and (47) that

$$\dot{q} = \langle\dot{q}\rangle_0 (1+y), \tag{52}$$

so that the relationships (1) with $y_0 = 0$ are valid for y. It is easy to see that for $y = 0$ the optimal value of a is equal to a_0, and accordingly the optimal value of x is equal to zero. Next

$$f_x/\mathcal{K} = a_0 - a_0 \cdot (1+\mu+z)\exp[-\mu a_0 \cdot (1+x)];$$
$$f_{xx}/\mathcal{K} = \mu_0 a_0^2 \cdot (1+\mu_0+z_0)\exp(-\mu_0 a_0);$$
$$f_{xy}/\mathcal{K} = [a_0^2(1+\mu_0+z_0)\mu_y - a_0 \cdot (\mu_y + z_y)]\exp(-\mu_0 a_0),$$

where

$$\mu_y = -\mu_0; \quad z_y = \mu_y/[\exp(z_0) - 1].$$

We obtain from formula (16) after simple transformations using the expressions (50) and (51)

$$C/\mathcal{K} = \frac{1}{2}\mu_0\left(\frac{1}{z_0+\mu_0} - \frac{z_0}{\mu_0}\right)^2. \tag{53}$$

The dependence of $C/\mathcal{K}$ on the optimal dimensionless intervals between introductions of assembly lines z_0 is given in Table 1 (the corresponding values of μ_0 are also given there).

The intervals between the introductions of lines should scarcely exceed 10 yr, so that with $P \approx 10^{-1}$ yr^{-1} we obtain $z_0 < 1$ and

$$C \approx \mathcal{K}/4 \tag{54}$$

We shall assume that $\mathcal{K}$ is evaluated as 10^8 rubles. Then an experiment run with the aim of decreasing the error from $\sigma_0 = 15\%$ to $\sigma_1 = 10\%$ would be justified by the economy in the construction and operation of assembly lines for refabrication if it would cost no more than 300 thousand rubles, i.e., would not require the creation of engineering facilities.

TABLE 1. Dependence among z_0, μ_0, and $C/\mathcal{K}$

z_0	μ_0	$C/\mathcal{K}$
0	0	0,250
1	0,718	0,235
2	4,39	0,196

An Example of the Application of a Different Type of Model. We shall assume that at each time the capacity of the reactor is selected to be optimal with account taken, on the one hand, of the benefit from its overloading and, on the other hand, of the danger of damage to the heat-generating assembly (HGA). There is a productivity reserve in the thermopower part of the installation which is sufficient for the undertaking of a forced capacity. The exact value of the capacity leading to damage to the assembly is unknown. It varies with time. During a certain time, on the average equal to T, changes accumulate in the reactor which require the adoption of a new solution of the permissible (optimal) reactor capacity. The changes can consist of a creeping of the hot spot to a new HGA or may be associated with overloads of fuel. One can assume that "tests" of the reactor for the stability of its HGA are performed at intervals of T; a positive result of the test (the assemblies passed) gives useful information only during the interval T, i.e., the average correlation interval of those unknown factors which affect the stability of the fuel.

Let x be the relative difference between the reactor capacity selected for the next interval T and the mathematical expectation of the capacity at which damage to the HGA at the hot spot of the active zone occurs. The loss from such damage shall be denoted as Ш, and the advantage from forcing of the capacity (without a change in the reactor construction) and the generation as a result of this additional unit of energy shall be denoted as ΔC. If y is the relative deviation of the damaged capacity from its mathematical expectation, which has a dispersion σ_0^2, the loss in the calculation for a single reactor and a single "test" from inaccurate knowledge of the damaged capacity will, according to the expressions (29) and (32), amount to

$$\min_x \langle f \rangle_0 \approx z\sigma_0 \Delta C\, TQ_0, \tag{55}$$

where

$$z = |x_{opt}|/\sigma_0 = \left[\ln \frac{Ш^2}{2\pi\sigma_0^2 (\Delta C\, TQ_0)^2} \right]^{1/2}. \tag{56}$$

The loss per unit generated energy, i.e., the increase in the price of energy due to lack of knowledge, is calculated according to the expression (55) from the formula

$$\delta C = z\sigma_0 \Delta C. \tag{57}$$

The value of ΔC — the difference between the total cost of the electric power generated by a nuclear power plant and its fuel component — is approximately equal to 1 kopeck/kWh (the fuel component C_f is about 0.3 kopeck/kWh [9]).

In high-powered water-cooled channel reactors (RBMK-1000) in which increases in the time for an unstable harmonic of the neutron field to accelerate to 1 h are achieved by different means, the value of T can be estimated to be 1 h (when it is 1/4 h or less, the operation of the reactor is complicated) [10]. Assuming (which some understating) that the loss upon the HGA getting out of order is equal to the contribution of its cost to C_f, we obtain

$$\frac{Ш}{\Delta C\, Q_0 T} = \frac{C_f}{\Delta C} \cdot \frac{\tau}{NT}, \tag{58}$$

where N is the number of assemblies in the reactor and τ is the duration of their excess in the reactor at nominal capacity. With N = 1600, τ = 25,000 h [10], and σ_0 = 0.05, we obtain the value 2.6 for z according to the expressions (56) and (58), so that with formula (57) taken into account $\delta C \approx 0.13$ kopeck/kWh. If the error is reduced as a result of scientific investigations from σ_0 = 5% to σ_1 = 4%, the electric power becomes cheaper by 0.026 kopeck/kWh. Since there is a large program for the introduction of RBMK-1000 (more than 10 units) [11], this price reduction will provide an appreciable economy exceeding 10^8 rubles. Therefore the costs for the investigations are undoubtedly repaid.

Optimal Time for Cessation of the Investigations. In the initial stage of development of a new facility many versions of the engineering schemes and structures of this facility and its subassemblies are usually considered. Certainly the noncompetitive versions are gradually eliminated, and several schemes and structural designs remain, from which it is not easy to select the best one. The following problem arises: whether to continue parallel developments or to finally select a version by using unreliable information and risking

making a mistake. Parallel developments require costs which may or may not be repaid. The costs are inappreciable at the stage of draft designing, larger at the stage of engineering design, and very large at the stage of preparation and test operation of pilot plants. But even at the stage of penetration of a small series the choice of the best version sometimes requires obtaining reliable statistics which are collected for one year.

We shall formulate a mathematical model of this complex problem as follows. The most probable value of the economic advantage of the version which seems the best over its competition is estimated by the monetary sum f_0.* However, the estimate is not reliable. The uncertainty of f_0 has also been estimated and is expressed as the dispersion of the economic advantage σ_0^2, or $f_0 \pm \sigma_0$, as σ_0 is comparable to f_0 and perhaps exceeds f_0.

The next stage in the developments requires additional (in comparison with the development of a single selected version) discounted costs Δf but promises a decrease in the dispersion by $\Delta\sigma^2$. Has the continuation of parallel developments been justified or not? In this problem we have a poorly known value of the vector y with the components f_b and f_w — the costs for the apparent best and worst versions. The parameter to be controlled x can take two values. If the apparent best version is selected, x = b; in the opposite case x = w. Let f_{b0} and σ_{b0} be the parameters of the probability distribution $p(f_b|f_{b0}, \sigma_{b0})$ for f_b in the initial stage of developments; f_{w0} and σ_{w0} are the same for f_w. The next stage of parallel developments will give the distributions $p(f_b|f_b, \sigma_{b1})$ and $p(f_w|f_{w1}, \sigma_{w1})$; the information content of the developments is known:

$$\Delta\sigma_b^2 = \sigma_{b0}^2 - \sigma_{b1}^2; \quad \Delta\sigma_w^2 = \sigma_{w0}^2 - \sigma_{w1}^2. \tag{59}$$

Evidently,

$$f_0 = \langle f_w - f_b \rangle_0 = f_{w0} - f_{b0}; \quad \sigma_0^2 = \sigma_{b0}^2 + \sigma_{w0}^2. \tag{60}$$

In the next stage the dispersion of $(f_w - f_b)$ will be $\sigma_{b1}^2 + \sigma_{w1}^2$, so that

$$\Delta\sigma^2 = \Delta\sigma_b^2 + \Delta\sigma_w^2. \tag{61}$$

The probability distribution for f_{b1} is found from Eq. (7). We shall assume that $p(f_b|f_{b0}, \sigma_0)$ and $p(f_b|f_{b1}, \sigma_{b1})$ are normal distributions. Then $p(f_{b1}|f_{b0}, \sigma_{b0}, \sigma_{b1})$ is also a normal distribution with the mathematical expectation f_{b0} and the dispersion $\Delta\sigma_b^2$. We obtain

$$p(f_{b1}|f_{b0}, \sigma_{b0}, \sigma_{b1})\; p(f_{w1}|f_{w0}, \sigma_{w0}, \sigma_{w1}) = \exp\left[-\frac{(f_{b1}-f_{b0})^2}{2\Delta\sigma_b^2} - \frac{(f_{w1}-f_{w0})^2}{2\Delta\sigma_w^2}\right] \Big/ (2\pi\Delta\sigma_b\Delta\sigma_w) \tag{62}$$

for the probability density of the vector y_1 with the components f_{b1} and f_{w1}. Now one can use the general formula (5). Evidently,

$$f = \begin{pmatrix} f_b & \text{for} & x=b \\ f_w & \text{for} & x=w \end{pmatrix}; \quad \langle f \rangle_0 = \begin{pmatrix} f_{b0} & \text{for} & x=b \\ f_{w0} & \text{for} & x=w \end{pmatrix}; \tag{63}$$

$$\min_x \langle f_0 \rangle = f_{b0}.$$

*This is the discounted economic effect from the introduction of a series of installations.

TABLE 2. The Dependence of ψ on v According to the Expression (65)

v	ψ	v	ψ
0	0	3,0	0,763
0,5	0,00425	3,5	0,953
1,0	0,0833	4,0	1,145
1,5	0,227	4,5	1,339
2,0	0,396	5,0	1,534
2,5	0,576		

Next

$$\langle f\rangle_1=\begin{pmatrix} f_{b1} & \text{for} & x=b\\ f_{w1} & \text{for} & x=w\end{pmatrix};$$

$$\min_x\langle f\rangle_1=\begin{pmatrix} f_{b1} & \text{for} & f_{b1}\leqslant f_{w1}\\ f_{w1} & \text{for} & f_{b1}>f_{w1}\end{pmatrix};$$

$$\langle\min_x\langle f\rangle_1\rangle_{01}=\int\begin{pmatrix} f_{b1} & \text{for} & f_{b1}<f_{w1}\\ f_{w1} & \text{for} & f_{b1}>f_{w1}\end{pmatrix}\times$$

$$\times\exp\left[-\frac{(f_{b1}-f_{b0})^2}{2\Delta\sigma_b^2}-\frac{(f_{w1}-f_{w0})^2}{2\Delta\sigma_w^2}\right]\frac{df_{b1}\,df_{w1}}{2\pi\Delta\sigma_b\,\Delta\sigma_w}.$$

Simple but cumbersome rearrangements lead to the formula

$$\langle\min_x\langle f\rangle_1\rangle_{01}\approx f_{b0}-f_0\psi(\Delta\sigma/f_0), \tag{64}$$

where

$$\psi(v)=\frac{1}{\sqrt{2\pi}}\int_{1/v}^{\infty}(vt-1)\,e^{-t^2/2}\,dt. \tag{65}$$

Substituting the expressions (63) and (66) into formula (5), we obtain

$$\mathrm{Ef}=f_0\psi(\Delta\sigma/f_0)-\Delta f. \tag{66}$$

The funcion $\psi(v)$ increases monotonically from zero, becoming linear for large values of v (Table 2). Upon a very large reduction of the dispersion as a result of the continuation of parallel developments, when $\Delta\sigma/f_0\gg 1$,

$$\mathrm{Ef}=\Delta\sigma/\sqrt{2\pi}-f_0/2-\Delta f. \tag{67}$$

Since $\Delta\sigma\leqslant\sigma_0$, the relationship (67) can be satisfied only for a very large initial indeterminacy of information,

$$\sigma_0/f_0>\Delta\sigma/f_0\gg 1.$$

In those cases in which a reduction of the dispersion occurs as a result of the multiple recurrence of uniform experiments or observation of the behavior of the installations, the approximation

$$\Delta\sigma^2=\Delta\sigma_\infty^2\frac{\Delta f}{\Delta f_0+\Delta f} \tag{68}$$

is valid. By estimating $\Delta\sigma_\infty$ and Δf_0, one can with the help of the expression (66) establish whether or not $\mathrm{Ef}>0$ for some $\Delta f>0$. If this is not so, the experiment (set of statistics) should be curtailed. It follows to continuously check the advisability of continuation of an experiment as long as it lasts, since f_0 varies in the course of the experiment.

LITERATURE CITED

1. A. S. Kochenov and Ya. V. Shevelev, "The problem of the cost of a neutron in a research reactor," Preprint IAÉ-2590, Moscow (1975).
2. N. P. Fedorenko, N. Ya. Petrakov, and D. S. L'vov, Ekonomika Mat. Metody, 23, No. 2 (1982).
3. S. Ya. Chernavskii, "Taking account of the indeterminacy factor in prediction of the development of nuclear power," At. Energ., 46, No. 1, 13-19 (1979).
4. Ya. V. Shevelev, "Game approaches to problems of planning the national economy of the USSR," Preprint IAÉ-3489/3, Moscow (1981).
5. A. S. Van'kov, A. I. Voropaev, and L. N. Yurova, Analysis of a Reactor Physics Experiment [in Russian], Atomizdat, Moscow (1977).

6. P. N. Alekseev, G. N. Manturov, and M. N. Nikolaev, "An estimate of the error in the calculation of the criticality and productivity coefficients of fast power reactors due to inaccuracy of the neutron data," At. Energ., 49, No. 4, 221-224 (1980).
7. I. I. Arushanyan, V. Z. Belen'kii, A. M. Belostotskii, and S. V. Obraztsov, "A time-independent optimization model of the development of a capital-capacity branch," Ekonomika Mat. Metody, 13, No. 6, 1229-1241 (1977).
8. Ya. V. Shevelev and A. V. Klimenko, "Optimization of the development of a fuel base of nuclear power on the basis of simple models," Vopr. At. Nauki Tekh., Ser. Fiz. Tekh. Yad. Reaktorov, No. 5 (27), 12-14 (1982).
9. F. Ya. Ovchinnikov, L. N. Golubev, V. D. Dobrynin, et al., The Operational Regimes of Water–Water Nuclear Power Reactors [in Russian], Atomizdat, Moscow (1979).
10. N. A. Dollezhal' and I. Ya. Emel'yanov, A Channel Nuclear Power Reactor [in Russian], Atomizdat, Moscow (1980).
11. A. M. Petros'yants, Atomic Science and Technology — for the National Economy [in Russian], Énergoizdat, Moscow (1981).

USING IN-REACTOR MEASUREMENTS TO REDUCE THE INDETERMINACY OF THE PHYSICAL CALCULATION OF FIELDS OF ENERGY RELEASE

V. K. Goryunov and Ya. V. Shevelev

UDC 621.039.51:681.3.06

Monitoring of the fields of energy release is an important measure for ensuring the safe and, at the same time, economic operation of modern energy-intensive reactors. For certain reasons, however, for most reactors it is deemed inappropriate to equip all the fuel assemblies (FA) in succession with detectors. Usually, the number of such detectors constitutes $\sim 10\%$ of the number of FA.

At the same time, when physical calculations of energy-release fields are performed on computers in a computing center, despite the increasing power of the computers and improvements in the computing programs it is not possible to take all the design features of the reactor into account and, most important of all, unknown random deviations of the properties of the FA from their design values cannot be taken into account.

Under these conditions the accuracy of physical calculation can be enhanced substantially only by tying its results with measurements, naturally with allowance for the reliability of the calculation and the measurements [1]. In this paper in order to determine the energy-release field more precisely and to indicate the optimum method of locating detectors we make use of the specific characteristic of the random component of the error of the physical calculation from the random scatter of the properties of the FA, viz., the correlative nature of errors at a considerable distance [2-6]. We shall explain the appearance of this characteristic feature.

Suppose that the reactor core is made up of FA that are identical as far as design is concerned but in fact differ in composition from each other and from the design. In the computational model these deviations are expressed in terms of the mean deviations over a cell of the interaction cross sections, scattered over the reactor in a random and uncorrelated manner.

Thus far, while the fluctuations of the cross sections are still relatively small, we can apply first-order perturbation theory to evaluate the response in the neutron field, to which the energy-release field is proportional. In particular, in the one-group diffusion approximation the difference in the neutron fields before and after perturbation is expressed in terms of the eigenfunctions Φ_k and the simple discrete eigenvalues λ_k of the unperturbed problem $L\Phi = \lambda\Phi$,

$$\tilde{\Phi}_0 = \Phi_0 + \varepsilon \sum_{k \neq 0} \frac{(\Phi_k^*, L'\Phi_0)}{\lambda_0 - \lambda_k} \Phi_k + O(\varepsilon^2), \quad (1)$$

Translated from Atomnaya Énergiya, Vol. 57, No. 3, pp. 153-157, September, 1984. Original article submitted March 8, 1984.

0038-531X/84/5703-0587$08.50

where $\varepsilon L'$ is the perturbation operator in the equation $(L+\varepsilon L')\tilde{\Phi} = \lambda\tilde{\Phi}$, describing the neutron balance in the perturbed reactor.

The neutron-flux fluctuations $\delta\Phi = (\tilde{\Phi}_0 - \Phi_0)/\Phi_0$ relative to the average value Φ_0 are zero when averaged over the set of realizations $\langle\delta\Phi\rangle = 0$, while for the autocorrelation function (ACF) of relative fluctuations in the one-velocity approximation we have the expression [4]

$$R(\mathbf{r}, \mathbf{r}') \equiv \langle\delta\Phi(\mathbf{r})\,\delta\Phi^*(\mathbf{r}')\rangle = \langle\varepsilon^2\rangle \sum_{k,\,k'\neq 0} a_{kk'} \frac{\Phi_k(\mathbf{r})\,\Phi_{k'}^*(\mathbf{r}')}{\Phi_0(\mathbf{r})\Phi_0(\mathbf{r}')}, \tag{2}$$

where

$$a_{kk'} = \frac{(\Phi_k^*\Phi_0,\ \Phi_{k'}\Phi_0)}{(\lambda_0-\lambda_k)(\lambda_0-\lambda_{k'})}. \tag{3}$$

If not only the average compositions of the FA fluctuate but so also do the average compositions of the individual fuel elements and details of the FA, the form of formula (2) does not change; only the factor $\langle\varepsilon^2\rangle$ in front of the summation sign changes. Upon making a detailed analysis of formulas (2) and (3) we found the following [4, 6].

1. Regardless of the geometry considered, reactors with any quality of reflector are characterized by the anisotropy and inhomogeneity of the random field of the neutron-flux fluctuations. The amplitude of the relative fluctuations increases toward the periphery of the reactor core. This is due to the predominant contribution of "low" spatial harmonics, i.e., those modes to which there correspond smaller eigenvalues of the unperturbed problem and a small difference $\lambda_0 - \lambda_k$ in the denominator of formula (3). The anisotropy is conserved in the transition to a normalized field of fluctuations.

2. Even a homogeneous reactor with "point" spatially uncorrelated white-noise type of perturbations of the cross sections is characterized by neutron-flux fluctuations that are correlated at a distance on the order of the linear size of the reactor core. This is a consequence of the nature of the equations and boundary conditions.

3. The standard (root-mean-square) deviation of the neutron flux is proportional to the squared ratio of the linear core size L to the migration length M and is inversely proportional to $\sqrt{N_{FA}}$, where N_{FA} is the number of FA or other reactor-core elements having a constant deviation of the properties.

4. The higher the quality of the reflector (or the more homogeneous the field), the greater the amplitude of the fluctuations of the neutron flux (Fig. 1a).

In fact, the nonuniformity of the flux deviations, which manifests itself as the dependence of the dispersion $R(\mathbf{r}, \mathbf{r})$ on the coordinate $\mathbf{r}$, is a consequence of the skews of the real neutron fields relative to the results of their physical calculation; these skews are due to the combined action of randomly distributed perturbations. These skews are next described with the aid of a system of functions Φ_k/Φ_0 with random coefficients; the statistical description of these coefficients (variance and the coefficients of the correlation between the coefficients) is contained in the expression for the autocorrelation function of the neutron flux [6].

The form obtained in this approximation for the large-scale correlations in the errors of the calculation makes it possible, when we know the deviations of the calculation from the measurements of the neutron flux in individual fuel assemblies, to establish the computational error and, therefore, the neutron field in all the FA. Inaccuracy of the measurements as well as the inexact knowledge of the reactor properties (concentration of nuclei, cross sections) and the methodological imperfection of the computational program raise the problem of merging diverse sources of information, with an estimation of the inaccuracy of each source, into a single information flow. The inaccuracy of each source of information is described by the corresponding matrix of covariations of the ACF. Before describing the method of merging we point out the principal difference in the descriptions of random fields of neutrons and fields of energy release.

The fluctuations of the energy-release field are comprised of the neutron-flux fluctuations and the macroscopic fission cross section. Accordingly, the autocorrelation function of the energy-release field is the sum of the ACF of the neutron flux, the ACF of the fission

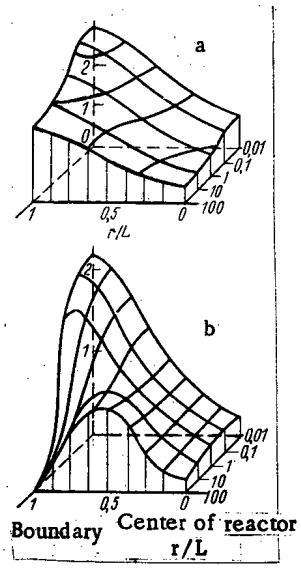

Fig. 1. Some characteristics of random fluctuations of the neutron flux in response to randomly distributed perturbations of the properties of the core in a critical reactor: a) mean-square value of the relative fluctuations of the neutron flux σ_{calc} (rel. units) as a function of the distance r/L to the center of the reactor core (of radius L) and h, the index of the reflector efficiency that is proportional to the logarithmic derivative of the flux at the reactor-core boundary: $L(\mathbf{n}\nabla)\Phi + h\Phi = 0$ (a smaller value of h corresponds to a more homogeneous neutron field); b) correlation of the flux of neutrons with the neutron-generating perturbations of the fission cross section $\langle \delta\Phi(\mathbf{r})\delta\Sigma_f(\mathbf{r})\rangle$ (rel. units) as a function of the parameters r/L and h (the calculations were carried out in the diffusion approximation).

cross section, and the cross correlations of the neutron flux with the fission cross section $S(\mathbf{r}, \mathbf{r}') = \langle \delta\Phi(\mathbf{r})\delta\Sigma_f(\mathbf{r}')\rangle$. As shown by calculations, the amplitude of the cross correlations is proportional to the square of the ratio of the linear reactor size L to the migration length M, whereas the ACF of the neutron flux is proportional to $(L/M)^4$. The relative role of the cross correlations, therefore, is substantial in reactors with a small L/M ratio or with a low sensitivity of the flux to perturbations. It is noteworthy that $S(\mathbf{r}, \mathbf{r})$ as a function of the coordinate in a reactor without a reflector increases toward the periphery of the reactor core while in a reactor with a reflector after some growth it diminishes toward the periphery (see Fig. 1b), thus smoothing out the inhomogeneity of the fluctuations of the energy-release field.

The spread of the properties of FA, in fact, takes place in many parameters, including some not affecting the cross section. The deviations of many properties lead to the growth of the ACF of the neutron flux and, therefore, a reduction of the relative role of the cross correlations $S(\mathbf{r}, \mathbf{r}')$ of the ACF of the cross section in the formation of the ACF of the energy-release field. The latter can, in the first approximation, be replaced by the ACF of the neutron flux in a number of practical calculations (this is done below), although analysis of the other components is important, particularly in the methodological processing of numerical experiments.

Thus, suppose that P and P_{meas} are the vectors of the unknown relative errors in the energy release of the FA. The first vector with N_{FA} components (N_{FA} is the number of FA in the reactor) describes the errors of the calculation, while the second vector with N_{meas} components (N_{meas} is the number of FA with detectors) describes the error of measurement. Suppose that R is the covariation matrix of the errors of calculation while R_{meas} is the covariation matrix for the errors of measurements of the energy release. The details of the method of calculating the matrix elements $[R]_{ij} \approx R(r_i, r_j)$ have been presented in [4], and R_{meas} is usually specified by means of a diagonal matrix.

Until the measurements become equal to the calculations the density of the probability of finding a given combination of vectors P and P_{meas} in the reactor under study is proportional to

$$R_{apri} \sim \exp\left\{-\frac{1}{2}\left[\mathbf{P}^T R^{-1}\mathbf{P} + \mathbf{P}^T_{meas} R^{-1}_{meas}\mathbf{P}_{meas}\right]\right\}, \quad (4)$$

if we postulate a normal distribution law and if we allow for the fact that the errors of measurement do not depend on the errors of calculation.

Once the measurements become equal to the calculations, we know the discrepancy vector

$$\mathbf{Y} = \mathbf{P}_{meas} - \Pi\mathbf{P}, \quad (5)$$

where Π is the projection matrix of dimension $N_{meas} \times N_{FA}$ such that $\Pi\mathbf{P}$ is the vector of errors of calculation in FA with detectors. The a posteriori probability distribution is the a priori distribution (4), considered on the manifold (5) and renormalized on it. The mathe-

matical expectation of P for this distribution will be denoted by X. When the distribution is normal, X is at the same time the most probable value of P, i.e., the vector of most probable relative corrections to the physical calculation of the energy release in the FA. For X we get a system of equations

$$\left.\begin{aligned}\Pi\mathbf{X} &= -R_{\text{meas}}(R_{\text{meas}}+\Pi R\Pi^{\mathrm{T}})^{-1}\Pi R\Pi^{\mathrm{T}}R^{-1}_{\text{meas}}\mathbf{Y}\\ \mathbf{X} &= -R\Pi^{\mathrm{T}}R^{-1}_{\text{meas}}(\mathbf{Y}+\Pi\mathbf{X}).\end{aligned}\right\} \tag{6}$$

Upon finding X from these equations, we can obtain the linear-approximation correction to the calculation. The result will not differ from that given by "statistical interpretation" [1] if in it we use the same covariation matrix R. The term "statistical interpretation" as applied to an inhomogeneous field of energy release, in our opinion, is inappropriate, but the difference between the calculations described above and the method of [1] consists essentially in the use of the resulting matrices R in different ways. In this paper R is calculated by using the harmonic expansion (2).

A search algorithm for the correction vector X is built into the program ÉREBUNI, which uses individual measurements of the power of the FA to correct the physical calculation of the energy-release fields in the $(r-\varphi)$ geometry of reactors, specifically the VVÉR-440 and ÉGP-6 (Bilibinskaya Atomic Heat and Power Plant) reactors.

The effectiveness of the program was checked by numerical experiments. Using the Monte Carlo method, we simulated the errors of the measurements, the systematic errors of the program of physical calculations, and errors due to the random spread of the FA parameters. The discrepancy between the energy-release fields corrected according to the ÉREBUNI program and the conventional true fields was within limits of accuracy of the correction method that were in satisfactory agreement with analytic estimates [7]. These estimates were made in terms of the analysis of spatial harmonic which constitute a deviation of the calculation from the real field of energy release. The contribution of the k-th harmonic (averaged over the reactor) $\overline{R^k}$ to the average variance $\overline{R}$ of the calculation

$$\bar{R}=\sum_k \overline{R^k}=\frac{1}{N_{\text{FA}}}\,\text{Spur}\,R \tag{7}$$

can be treated as the indeterminacy of the calculation of the energy-release field at the k-th harmonic as a consequence of the spread of the FA properties. The error in the recording of the harmonic by detectors is on the order of $\sigma_{\text{meas}}/\sqrt{N_{\text{meas}}}$ (σ_{meas} is the mean-square error of the detector). The accuracy of the result of the correction of the physical calculation for the k-th harmonic depends on the relation between $\sigma_{\text{meas}}/\sqrt{N_{\text{meas}}}$ and $\sqrt{\overline{R^k}}$. In an approximation that is correct for a fairly large number of detectors the ratio $\overline{\sigma^2_{\text{calc}}}/\overline{\sigma^2_{\text{corr}}}$ before and after correction is expressed by the formula

$$\overline{\sigma^2_{\text{calc}}}/\overline{\sigma^2_{\text{corr}}}\approx\sum_k \overline{R^k}/\left|\sum_k \overline{R^k}\,(1+\overline{R^k}N_{\text{meas}}/\sigma^2_{\text{meas}})^{-1}\right|. \tag{8}$$

The next test of the program consisted in reproducing the energy-release fields from the results of physical calculation and a small part (8-16 points out of 269) of measurements with fission chambers, carried out during the physical start-up of the first, second, and third reactors of the Bilibinskaya Atomic Heat and Power Plant. When the results of the reproduction (correction) of one such field from 16 points were compared with the remaining 253 points (fuel channels), we detected that the discrepancy had a variance of 17 $(\%)^2$, while the discrepancy between the uncorrected calculation and the measurements was 37 $(\%)^2$. The results of the reproduction differ from the results obtained in [8] by no more than 1.5%, although in that paper different points were taken as the reference points and there were more of them, 24.

The program was also tested in calculations of different states of the VVÉR-440 reactor of the Armyanskaya Atomic Power Plant [9]. As the "reference" energy-release field we took the results of indirect measurements of the power of 190 fuel assemblies with the aid of individual thermocouples at their exits, although the error of these measurements is fairly high. In the case of reactor states with large initial discrepancies between the uncorrected

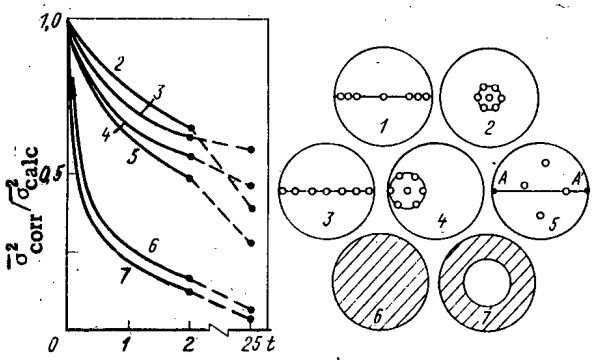

Fig. 2. Estimates of the expected quality of the reproduction of the energy-release fields from the results of physical calculation and measurements in the VVÉR-440 reactor. The diagrams show 6 and 7 shaded regions with 30 uniformly arranged detectors.

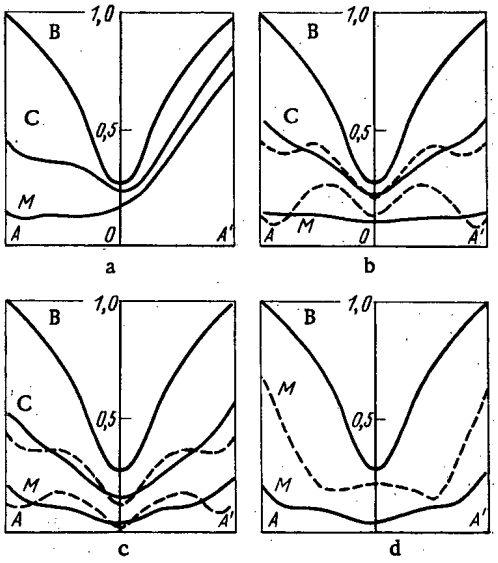

Fig. 3. Distribution of the expected error σ_{corr} (rel. units) of the energy-distribution fields along the line AA' (see scheme 5 in Fig. 2) for several versions of detector arrangement [a) scheme 4 of Fig. 2; b) schemes 3 and 1 (- - -); c) schemes 6 and 7 (- - -); d) schemes 6 and 5 (- - -)] and for different relations between the measuring error σ_{meas} and the error $\overline{\sigma}_{calc}$ of the uncorrected calculation: B) $\sigma_{meas} \gg \sigma_{calc}$; C) $\sigma_{meas} = \overline{\sigma}_{calc}$; M) $\sigma_{meas} = \frac{1}{5}\overline{\sigma}_{calc}$.

calculation and the measurements (when the error due to the spread of the properties of the fuel assemblies plays a large role), from the fact that the corrected and measured energy-release fields become more similar we can see a graphic improvement in the quality of the reproduction of the field as a consequence of the correction made to the physical calculation.

The inhomogeneous distribution of the errors of the physical calculation in the space of the reactor core permits the assumption that there exists a particular arrangement of detectors which gives a smaller error of reproduction of the energy-release fields by the method described. We choose as a criterion of the quality of reproduction the squared error $\overline{\sigma}^2_{corr}$ of reproduction (correction), averaged over the reactor:

$$\overline{\sigma}^2_{corr} = \frac{1}{N_{FA}} \text{Spur } R_x, \tag{9}$$

where R_X is the covariation matrix of the correction vector X (the diagonal elements are the expected squares of the reproduction errors). The matrix R_X, in accordance with the lemma on matrix inversion, can be written as

$$R_X = (R^{-1} + \Pi^T R^{-1}_{meas} \Pi)^{-1} = \\ = R - R\Pi^T (R_{meas} + \Pi R \Pi^T)^{-1} \Pi R. \quad (10)$$

The latest version of the ÉREBUNI program has been supplemented with a module for calculations of the diagonal elements of the matrix R_X for a given way of arranging the detectors. Figure 2 gives the ratio $\bar{\sigma}^2_{corr}/\bar{\sigma}^2_{calc}$ of the reproduction error to the variance of the uncorrected physical condition, for certain ways of arranging the detectors (shown on right) as a function of $t = \bar{\sigma}^2_{calc}/\bar{\sigma}^2_{meas}$, where σ_{meas} is the error of the measurements. Comparison of the different versions of detector arrangement shows that the reproduction error $\bar{\sigma}_{corr}$ is smaller when the detectors are symmetrically arranged with respect to the azimuthal angle and are displaced from the center toward the periphery of the reactor core. The advantage gained from the displacement is especially pronounced for a small number (fewer than 10) of detectors. For example, for $N_{meas} = 7$ the effect of the optimum arrangement is equal to the effect from a 1.5-fold increase in the number of detectors arranged uniformly.

Qualitatively, this conclusion can be explained by the nonuniformity of the representation of different harmonics in the skews of the energy-release fields relative to the computed results. The first, most probable harmonics have a maximum near the boundary of the reactor core. We point out that we are considering skews and contributions of harmonics relative to the fundamental harmonic, i.e., $(\tilde{\Phi}_0 - \Phi_0)/\Phi_0$ and Φ_k/Φ_0. It is advantageous to move the detectors to points corresponding to the maximum of Φ_k/Φ_0 so that the signal/noise ratio (skew for the given harmonic/measuring error) would be maximum for reliable recording of the first harmonics that make the largest contibution to the amplitude of the skew (Fig. 3).

It must be noted that in fact the indeterminacy of the physical calculation is due to not only the error of the input data but also to the systematic error of the computational program. Having an idea of the scale of the systematic error of the program and the most probable points of its occurrence, we can "reproduce" not only the errors of the cross sections and the errors of the detectors but also the systematic errors. With the development of computational capabilities the systematic error will, obviously, become much smaller.

LITERATURE CITED

1. E. V. Filipchuk, P. T. Potapenko, and V. V. Postnikov, Control of the Neutron Field of a Nuclear Reactor [in Russian], Énergoizdat, Moscow (1981).
2. M. Williams, Atomkernenergie, 22, No. 4, 248 (1973).
3. V. A. Karpov, V. G. Nazaryan, and V. V. Postnikov, At. Energ., 40, No. 6, 456 (1976).
4. V. K. Goryunov, At. Energ., 44, No. 4, 357 (1978).
5. E. A. Gomin and S. S. Gorodkov, At. Energ., 46, No. 3, 187 (1979).
6. V. K. Goryunov, At. Energ., 49, No. 5, 321 (1980).
7. V. K. Goryunov and Ya. V. Shevelev, Problems of Atomic Science and Engineering. Series "Nuclear Constants" [in Russian], No. 3 (47), 3 (1982).
8. I. S. Akimov and R. A. Zemtseva, Preprint FÉI-1008, Physics and Power Institute, Obninsk (1980).
9. K. A. Gazaryan et al., in: Reactor Physics Experimentation. Proceedings of the Third All-Union Seminar on Problems of Reactor Physics [in Russian], TsNIIatominform, Moscow (1983), p. 130.

INCORPORATING RELIABILITY IN OPTIMIZING UNITS IN NUCLEAR POWER STATIONS CONTAINING WATER-COOLED–WATER-MODERATED REACTORS

N. E. Buinov, S. M. Kaplun, and L. S. Popyrin

UDC 621.039.019.3:51.001.57

A major topic additional to providing safety and economy in nuclear power stations is to incorporate equipment reliability in the choice of the optimum design for units containing water-cooled–water-moderated (VVÉR) reactors. The criterion for choosing the unit structure is the minimum reduced cost C for the system and the reserve power in the electrical power system (EPS), with the latter required to compensate for the deficiency in power production due to failure and repairs in the unit equipment:

$$C = C_0 + C_u = \sigma\left[(K_0 + K_u) + \sum_{t=1}^{T} (L_{ot} + L_{u\,t})(1+p)^{-t}\right]. \quad (1)$$

Here C_o is the reduced cost without allowance for unplanned repairs; C_u is the reduced cost for backup to the EPS and for unplanned repairs; K_o is the capital investment in the unit, including a structural redundancy; L_{ot} is the loss during operating year t without allowance for unplanned repairs; K_u is the capital investment in the backup EPS power; T is the calculated working period; and σ and p are normative efficiency and reduction coefficients. The values of K_o and L_{ot} are determined by the usual method [1]. The annual losses due to lack of reliability in the unit are

$$L_{u\,t} = L_{Bt} + L_{Pt} + L_{St} + L_{Ct}, \quad (2)$$

where L_{Bt} is the loss due to overconsumption of fuel in the EPS and in the unit during failure, L_{Pt} are other working losses due to the backup power in the EPS, L_{St} are the losses due to unplanned shutdown and startup in the unit, and L_{Ct} are the losses involved in restoring failed equipment.

The following are the components of the annual losses due to complete and partial failures in unit equipments:

$$L_{Bt} = \sum_{s=1}^{S_t} \sum_{j=1}^{J_t} [(N_{tj} - N_{ts}) P_{tj} \tau_{ts} (b_{Rt} p_{Rt} - b_{tj} p_t)] + \sum_{s=1}^{S_t} N_{ts} \tau_{ts} (b_s - b_{ts}) p_t, \quad (3)$$

for $N_{tj} \leqslant N_{ts}$

$$L_{Bt} = \sum_{s=1}^{S_t} \sum_{j=1}^{J_t} N_{tj} P_{tj} \tau_{ts} (b'_s - b_{tj})\, p_t;$$

$$L_{Pt} = \frac{\alpha_R k_R}{8760\, RPU_R} \sum_{s=1}^{S_t} \sum_{j=1}^{J_t} (N_{tj} - N_{ts}) P_{tj} \tau_{ts}; \quad (4)$$

$$L_{St} = \sum_{s=1}^{S_t} n_{ts} \overline{L}_{ns}; \quad (5)$$

$$L_{Ct} = \sum_{m=1}^{M} n_{mt} \tau_{mt} \overline{L}_m. \quad (6)$$

Translated from Atomnaya Énergiya, Vol. 57, No. 3, pp. 157-161, September, 1984. Original article submitted July 11, 1983; revision submitted February 22, 1984.

0038-531X/84/5703-0593$08.50

Here S_t is the number of complete and partial failures in a unit in year t; J_t is the number of load levels, which is adapted to the mode of operation; N_{tj} is the power output at load level j; N_{ts} is the power of the unit in state of failure s; P_{tj} is the probability or relative annual duration of load level j; τ_{ts} is the mean recovery time on failure s; b_{Rt} and p_{Rt} are the specific consumption and specific prices for the fuel for the backup power; b_{tj} and p_t are the specific fuel consumption at load level j and the specific costs of the fuel in the unit; b_s and b_{ts} are the specific fuel consumption in the unit in emergency and planned reduction of the load to N_{ts} (b_s' for $N_{tj} \leqslant N_{ts}$); α_R is the overall coefficient for assigning capital investment to the backup power; k_R is the specific capital investment in the backup power; RPU_R is the reserve power use factor; n_{ts} is the number of failures of type s in year t; $\bar{L}_{ns}$ is the specific loss due to startup and shutdown on complete failures of the unit or when parts of it are switched out; M is the number of types of equipment; n_{mt} is the number of failures in equipment m; τ_{mt} is the mean recovery time for equipment of type m; and L_{mt} is the mean hourly cost for emergency repair of equipment of type m.

We can take as a general parameter for the reliability the coefficient π representing the provision of the planned energy production, which incorporates the complete and partial failures as well as the load graph:

$$\pi = 1 - \frac{\Delta E}{E_0}; \quad \Delta E = \sum_{s=1}^{S_t} \sum_{j=1}^{J_t} (N_{tj} - N_{ts}) P_{tj} \tau_{ts}, \tag{7}$$

ΔE is the energy deficiency due to the complete and partial failures in the unit and E_o is the planned energy production by the unit in accordance with the load graph (neglecting failures).

To calculate the structural reliability in a unit, we use a scheme composed of M systems joined in sequence. Each system may have L_m subsystems that perform identical functions and which share the total production (power) of system m in equal parts. An individual subsystem l_m includes Z_l units, in which there are X_z working components and Y_z backup ones. For a unit in a nuclear power station containing water-cooled–water-moderated reactors, the following thermomechanical equipment components may be assumed: reactor, steam generator, main circulation pump (MCP), pipelines, turbine, feed and condensate pumps, and so on. The numbers and connections of the elements are determined by their functions in the system.

One starts calculating the reliability parameters of a unit with those of the elements, and the possible changes in these parameters during the working period may be approximated as a power law in years of service. This enables one to assume constant parameters for the fluxes of failures and repair during a year for each element. The reliability of the z units is determined in accordance with the connection structure, and analytical relationships for total failures have been given for this purpose in [2]. The form of failure, complete or partial, in item z is determined by the number of elements $\bar{x}_z$ failing in it and by the technical minimum unit power N_{tm}:

$$\text{if } (X_z + Y_z) > x_z > Y_z \text{ and } N_{zx} \geqslant N_{tm}, \text{ then we have a partial failure;}$$

$$\text{if } (X_z + Y_z) > \bar{x}_z > Y_z \text{ and } N_{zx} < N_{tm} \text{ or } \bar{x}_z = (X_z + Y_z), \text{ then we have a complete failure.} \tag{8}$$

Here N_{zx} is the power of a unit on the failure of $\bar{x}_z$ elements in item z. The reliability parameters for subsystem l_m are found from the scheme for the series connection of z_l items separately for the complete and partial failures. The equipment power and the reliability parameters for system m on failure of $\bar{l}_m$ out of L_m technologically parallel subsystems may be defined as follows if the items are identical in reliability:

$$N_{\bar{l}_m} = \gamma_{l_m} N (L_m - \bar{l}_m)/L_m, \quad \tau_{\bar{l}_m}(t) = \tau_{l_m}(t);$$
$$\omega_{\bar{l}_m}(t) = 2^{\bar{l}_m - 1} \omega_{l_m}(t) \tau_{l_m}(t)^{l_m - 1} C_{L_m}^{\bar{l}_m} / C_{L_m - 1}^{\bar{l}_m - 1}, \tag{9}$$

where N is the installed power of a unit; γ_{l_m} is the safety factor on output for subsystem l_m; $\omega_{l_m}(t)$, $\tau_{l_m}(t)$ are the fault flux parameter and the mean recovery time for subsystem l_m; $C_{L_m}^{\bar{l}_m}$ and $C_{L_m}^{\bar{l}_m - 1}$ are the numbers of combinations from L_m taken $\bar{l}_m$ at a time and from L_m^{-1} taken

TABLE 1. Initial Data on Equipment Reliability

Element or part of station	Power, MW	Parameter estimates					
		mean		pessimistic		optimistic	
		$\omega\times10^3$, h^{-1}	τ, h	$\omega\times10^3$, h^{-1}	τ, h	$\omega\times10^3$, h^{-1}	τ, h
Reactor	1000	0,2	135	0,25	150	0,1	100
	2000	0,3	150	0,4	200	0,15	125
MCP	250	0,025	100	0,04	120	0,02	60
	500	0,04	120	0,06	150	0,025	100
Steam generator	250	0,09	200	0,12	225	0,06	150
	500	0,13	225	0,15	250	0,09	200
Main pressurized equipment	250	0,025	60	0,04	80	0,015	40
	500	0,035	100	0,05	150	0,025	60
Turbine	500	0,4	100	0,5	130	0,35	70
	1000	0,6	130	0,75	150	0,45	100
	2000	0,7	140	0,85	165	0,55	110
Feed pump	500	0,15	25	0,2	35	0,1	20
	1000	0,21	30	0,3	40	0,15	25
Condensate pump	250	0,12	10	0,18	15	0,09	5
	500	0,18	15	0,25	20	0,12	10
	1000	0,2	20	0,3	25	0,15	15
Low-pressure heater	500	0,045	10	0,06	15	0,03	5
	1000	0,06	15	0,08	20	0,04	10
High-pressure heater	500	0,04	10	0,055	15	0,03	5
	1000	0,055	15	0,07	20	0,04	10

TABLE 2. Mean Estimates of the Differences in Capital Investment in Units for Various Forms of Structure

Power, MW	Number of loops and turbines	Capital investment difference, million rubles	
		with MPE	without MPE
1000	4+2*	0*	−1,4
	4+1	−5,9	−7,3
	2+2	−5,8	−7,5
	2+1	−11,7	−13,4
2000	4+2†	—	0†
	4+1	—	−14,6

*Taken as the initial form for a unit containing a VVÉR-1000.
†Taken as the initial form for a unit containing a VVÉR-2000.

τ_m^{-1} at a time correspondingly. The form of failure in the unit when $\bar{\tau}_m$ subsystems fail may be determined from the relation between the parameters N_{τ_m} and N_{tm} by analogy with the above expressions. The reliability parameters in the unit may be found from the scheme for the series-connected systems. The calculations give the reliability parameters for all the hierarchic levels in the unit for each year of operation t.

At the end of 1982, there were over 150 water-cooled power reactors working in the world, whose total service life exceeded 2000 reactor-years. The conditions of use vary widely as do the standard dimensions and the designs, which means that the information on the reliability and cost is inhomogeneous and ambiguous [3-6]. Therefore, the initial data for theoretical researches on reliability may be specified as the average and the limits to the ranges corresponding to the average pessimistic and optimistic evaluations (Table1). The initial cost

parameters were varied from + 40% to −10% of the mean estimates. Various conditions for emergency repair of the first circulation loops were also considered: shutting down the unit for repair immediately after fault is observed (mode I), shutting down the unit for repair in accordance with the management service during the period of falling load in the EPS (mode II), and repairing the individual components of the switched-out loop with its main pressurizing equipment (MPE) if possible without shutting down the reactor (mode III).

In the calculated example, forms of scheme were drawn up for units containing water-cooled–water-moderated reactors of power 1000-2000 MW, which differed in the number of loops in the first circuit, the presence or absence of MPE, in the number of turbines, and correspondingly in the capital investment (Table 2). The transition from a double unit to a single one containing a VVÉR-1000 gives an economy in the reduced costs on account of a reduction in capital investment of an average 1.5 million rubles per year. In the case of the VVÉR-2000, C_o is reduced on average by 3.7 million rubles per year on going from a double unit to a single one. On the other hand, the reliability parameters of a single unit are lower than those of a double one because of the larger number and longer duration of the complete failures, which increases the cost for maintaining a reliable energy supply in the EPS, namely C_u (Table 3). From the value of C for the overall reduced costs, one can say that forms of system containing two turbines are economically more efficient than single units because ΔE_t is reduced by 10-25% (Table 3), with the corresponding reduction in the necessary emergency backup in the EPS. This result agrees with the conclusion for units containing water–graphite reactors [6].

The optimum number of circulation loops is dependent to a considerable extent on the mode of transfer to repair conditions and on the presence or otherwise of MPE. If the repairs are conducted in modes I and II, no matter whether there is MPE, the forms of units containing VVÉR-1000 reactors with two loops are more efficient than forms containing four loops because of the reduction in costs not only due to equipment failures but also to capital investment. The improved reliability in a unit containing two loops is explained by the reduced number of equipment items liable to complete failure. If, on the other hand, the MPE provides for sealing off a disconnected loop and ensures conditions for safe repair of the failed circulation loops in course (mode III), then the reduction in number of complete failures in the unit in a scheme with four loops reduces the power deficiency by 8-10% by comparison with the two-loop scheme. Correspondingly, the savings in overall reduced costs for a four-loop scheme containing MPE are from 0.4-1.1 million rubles a year.

Eliminating the MPE from a four-loop first circuit in a VVÉR-1000 gives a saving in capital investment of up to 1.5 million rubles, together with a relative reduction in the deficiency in energy production in mode I by 5-8% or by 4-6.5% in mode II, which reduces the reduced costs by 1.0-2.5 and 0.5-1.7 million rubles a year, respectively. The lower economy in mode II occurs because the power loss from the unit on shutdown for repair is less than that when a loop in the MPE is shut down.

We not only determined the costs with various estimates for the initial data but also found the optimum levels of equipment reliability improvement (Fig. 1). The following relationship applies between the reliability-change coefficient β_i and the costs of the elements:

$$Q_i = Q_{0i}\beta_i^{\alpha_i} = Q_{0i}(\omega_{0i}\tau_{0i}/\omega_i\tau_i)^{\alpha_i}, \quad (10)$$

where Q_{oi} and Q_i are the costs of equipment type before and after raising the reliability, while ω_{oi}, ω_i, τ_{oi}, and τ_i are the fault-flux parameters and the mean recovery times, and α_i is a coefficient given values from 0-0.6 in our calculations. Equation (10) was used to determine the limiting permissible capital investment δk_{re} going to reliability enhancement. According to Fig. 1, the optimum reliability level is attained for a single unit containing a VVÉR-2000 on raising β_i by more than a factor of 2.5, while the permissible increase in the capital investment is 20-40% of the original equipment cost.

Table 3 shows that the forms of units with two turbines are more efficient than single units with the various reliability estimates; on the other hand, there are uncertainties in the data, so we examined the necessary increase in the reliability in a single unit required to make it more efficient than a double one. The calculations showed that this requires a reduction in the fault-flux parameter for the turbine equipment in a single unit containing a VVÉR-1000 of 20-50% in accordance with the element reliability estimates and the value

TABLE 3. Comparison of Reliability and Reduced Costs for Forms of a Unit Scheme Containing VVÉR-1000 and VVÉR-2000 without MPE (Mode I)

Power, MW	No. of loops and turbines	Reliability estimates	ΔE_t^*, %	π^*, %	C_u, million rubles/yr	C, million rubles/yr
1000	4+2	Average	13,5	86,5	23,2	127,3
	4+1		16,2	83,8	26,7	129,6
	2+2		12,6	87,4	21,8	124,3
	2+1		15,3	84,7	25,6	126,5
	4+2	Pessimistic	18,9	81,1	32,2	136,3
	4+1		21,6	78,4	35,2	137,8
	2+2		17,6	82,4	30,4	132,9
	2+1		20,5	79,5	33,7	134,6
	4+2	Optimistic	7,3	92,7	12,8	116,9
	4+1		9,2	90,8	15,5	118,1
	2+2		7,4	92,6	13,0	115,5
	2+1		9,3	90,7	15,6	116,5
2000	4+2	Average	22,0	78,0	73,6	269,3
	4+1		24,8	75,2	78,7	270,7
	4+2	Pessimistic	29,8	70,2	97,6	293,3
	4+1		33,7	67,3	104,5	296,5
	4+2	Optimistic	13,6	86,4	45,9	241,6
	4+1		14,5	85,5	50,8	242,8

*In the fourth year of operation with a 3-yr repair cycle the repair durations for a unit containing a VVÉR-1000 were 1080, 1440 and 1080 h a year and those for VVÉR-2000 were 1180, 1460, and 1180 h a year.

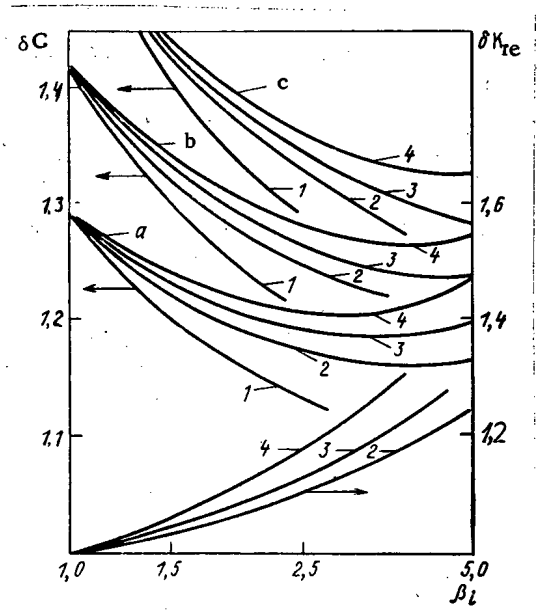

Fig. 1. Dependence of the relative reduced costs δC and capital investment δk_{re} in a single unit containing a VVÉR-2000 on the reliability-change coefficient β_i with the following estimates for the reliability: optimistic (a), average (b), and pessimistic (c) with the values of α = 0 (1); 0.4 (2); 0.5 (3); 0.6 (4); δC is given relative to the value of C_o before optimization.

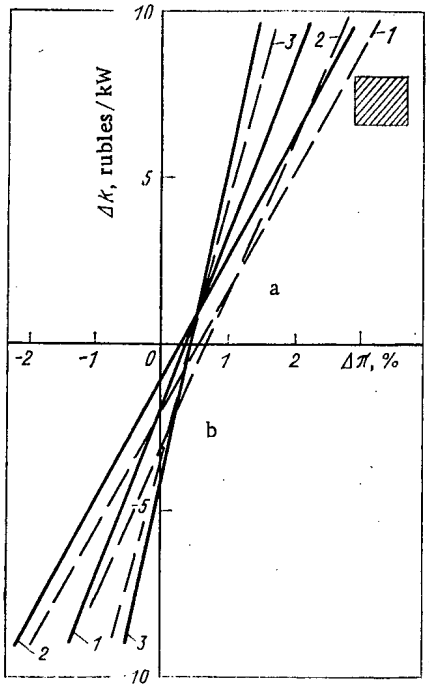

Fig. 2. Equal-performance limits for a single unit (a) and a double unit (b) containing VVÉR-2000 with the optimistic reliability estimate (1), the average estimate (2), and the pessimistic one (3) in relation to the differences between them in providing the planned output $\Delta\pi = \pi_d - \pi_m$ and as regards capital investment $\Delta k = k_d - k_m$, (the subscript m corresponds to a single unit, and subscript d to a double one): ——) mode I; - - - -) mode II; the hatched rectangle shows the relation between Δk and $\Delta\pi$ for the average estimates for the reliability and equipment cost.

of α. The additional specific capital investment required to improve the reliability should not exceed 7.7-1.7 rubles/kW, which appears feasible.

At present, there are discussions on the numbers of cylinders for turbines of power 500 or 1000 MW and above, as well as on simplifying regeneration systems while simultaneously increasing the heat output to users and the desirability of other changes in turbines that affect the cost, reliability, and efficiency. As regards the economy in direct use of metal and labor, turbines of higher power have potential advantages, and the same applies as regards the cost of the control and monitoring equipment. Theoretical studies enable one to estimate the effects from these improvements, as well as from changes in the parameters of the nuclear power station as a whole and of the EPS, which influence the numbers of turbines and other items in a unit. A boundary zone of equal efficiency has been identified for single and double units for various estimates of the equipment reliability (Fig. 2). Figure 2 shows the relation between reliability and capital investment for double and single units, which enables one to determine the effectiveness of various designs intended to raise the reliability in VVÉR-2000 systems. Similar relationships have been derived for units containing VVÉR-1000.

The following conclusions are drawn:

1) It is important to consider equipment reliability in defining the schemes for nuclear power station units;

2) zones of equal efficiency have been defined for structural forms of units containing VVÉR reactors, as well as the zones of higher efficiency subject to alterations in reliability, equipment cost, and other factors;

3) it has been shown to be economically desirable to increase the reliability of a single unit containing VVÉR reactors by making additional capital investments that enable one to reduce the costs for providing EPS backup and equipment repair;

4) an economic comparison of different forms shows that it may be desirable to use two circulation loops in a unit containing a VVÉR-1000 subject to the condition that the required reactor safety is provided.

LITERATURE CITED

1. L. S. Popyrin, Mathematical Simulation and Optimization for Thermal Power Systems [in Russian], Énergiya, Moscow (1978).
2. B. A. Kozlov and I. A. Ushakov, Handbook on Calculating Reliability for Automatic and Electronic Equipment [in Russian], Sov. Radio, Moscow (1975).

3. A. I. Klemin, Statistical Engineering Calculations in the Design of Nuclear Reactors [in Russian], Atomizdat, Moscow (1973).
4. S. M. Kaplun, Optimizing Reliability in Power Systems [in Russian], Nauka, Novosibirsk (1982).
5. Yu. V. Smirnov, D. D. Sokolov, and I. D. Sokolova, The Nuclear Industry in Foreign Countries [in Russian], Atomizdat, Moscow (1980).
6. I. Ya. Emel'yanov, A. I. Klemin, Yu. I. Koryakin, et al., "A comparative analysis of reliability and economy in nuclear power station units containing one and two turbine systems," At. Energ., 53, No. 2, 67-70 (1982).

EFFECTS OF IRRADIATION ON THE ELASTOPLASTIC DEFORMATION OF Zr + 1% Nb FUEL PIN CLADDING

V. A. Matushkin, A. A. Medvedev,
Yu. V. Miloserdin, B. D. Semenov,
Yu. K. Bibilashvili, and I. S. Golovnin

UDC 621.039.548.3

It is extremely important to have information on the mechanical properties of structural materials under actual working conditions in order to improve the performance of nuclear reactors. In particular, in order to choose the optimum conditions for running the reactor up to power one needs experimental results obtained at very low neutron fluences (up to 10^{24} m^{-2}). Also, such data are of some value in researching radiation damage accumulation. In this connection, we have examined the effects of reactor irradiation on the resistance to elastoplastic strain in standard fuel-pin sheaths of diameter 9.15 × 0.65 mm made of Zr + 1% Nb alloy.

In accordance with the standard method [1-3], the tubular specimens underwent cyclic sign-varying torsion with a constant strain amplitude of ± 0.7%. The small tube thickness enabled us to analyze the results by means of standard relationships for the shear deformation γ and the tangential stress τ:

$$\gamma = \varphi \frac{R}{l}; \quad \tau = \frac{M}{\pi (R^2 + r^2)(R - r)},$$

where φ is the angle of torsion in the working part of the specimen of length l, R and r are the outside and inside radii of the cylindrical tube, and M is the torsional moment.

The plastic strain γ_c was determined as the difference between the total γ and the elastic strain:

$$\gamma_c = \gamma - \frac{\tau}{G},$$

where G is the shear modulus.

The tests were performed with TsIRK apparatus [4] as follows. Initially the elastoplastic strain in the fuel-pin sheath was examined under laboratory conditions over a wide range in strain rate: 8×10^{-4}-8×10^{-9} sec^{-1} at 295-780°K. At each temperature, we used 20-30 strain cycles with a rate $\alpha = 8 \times 10^{-4}$ sec^{-1}. The cyclic-strain diagram after temperature change stabilized within 3-5 cycles. In some cycles, the material was kept at constant load (in creep testing) for short times (up to 2×10^4 sec) or under monotonically decreasing load. Such tests enable one to estimate virtually all the parameters required to forecast the accumulation of plastic strain in a given state of stress [1]: the temperature dependence of the elastic moduli, the yield point, the sensitivity to the strain rate, and the change in deformation resistance during steady conditions under load [5, 6].

After this, the apparatus together with the specimen was placed in the core of an IRT-2000 reactor. The flux densities for the thermal neutrons and fast ones (E > 0.1 MeV) were $1.2 \cdot 10^{17}$ and $1.8 \cdot 10^{16}$ $m^{-2} \cdot sec^{-1}$, respectively. The tests under irradiation were performed at 540-

Translated from Atomnaya Énergiya, Vol. 57, No. 3, pp. 162-165, September, 1984. Original article submitted August 1, 1983; revision submitted March 21, 1984.

0038-531X/84/5703- 0599$08.50

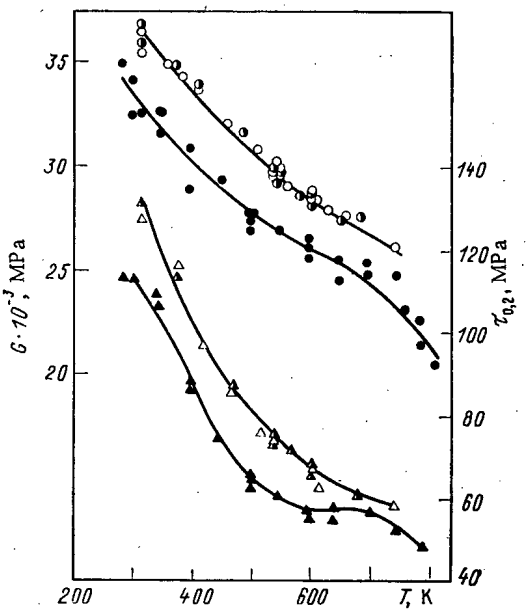

Fig. 1. Temperature dependence of the shear modulus G(●, ○) and of the yield point $\tau_{0.2}$(Δ, ▲): ●, ▲) before irradiation; ○, Δ) $\Phi = 1.5 \times 10^{23}$ m^{-2}; ▲, ◑) after irradiation.

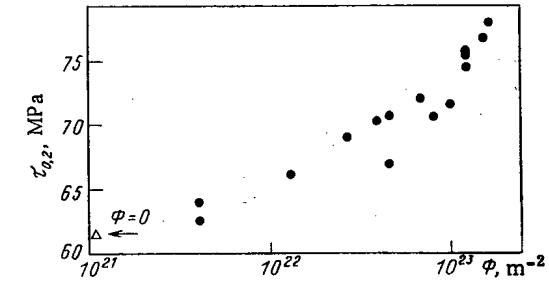

Fig. 2

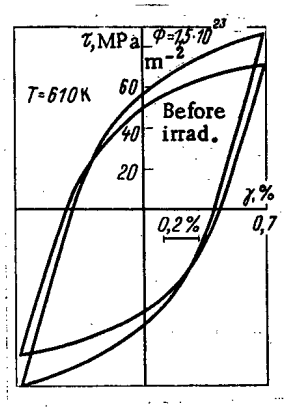

Fig. 3

Fig. 2. Dependence of the yield point for Zr + 1% Nb alloy on thermal-neutron fluence at 540°K.

Fig. 3. Cyclic-deformation diagrams for Zr + 1% Nb.

770°K. During the reactor shutdown, the temperature fell to 320°K. During 95% of the time, the irradiation was under conditions of self-heating at 540°K.

The graph of the temperature dependence of the cyclic shear modulus (Fig. 1) shows that irradiation to a thermal-neutron fluence $\Phi = 1.5 \times 10^{23}$ m^{-2} increases the shear modulus by 10-13% at all temperatures, with the change in modulus occurring at $\Phi = 10^{21}$ m^{-2} and persisting in the range 10^{21}-10^{23} m^{-2}. Also, the results obtained with the reactor working and after it had been shut down are described by a single temperature dependence, which shows that this low flux density has no effect on the elastic modulus.

The cyclic yield point $\tau_{0.2}$ was determined from the steady-state diagrams for sign-varying deformation in the range 300-780°K. Figure 1 also shows the temperature dependence of the yield point obtained before irradiation, during irradiation, and during reactor shutdown. The increase in the yield point was determined only by the neutron fluence and was independent of the flux density. Figure 2 shows the effect of the fluence on the yield point at 540°K.

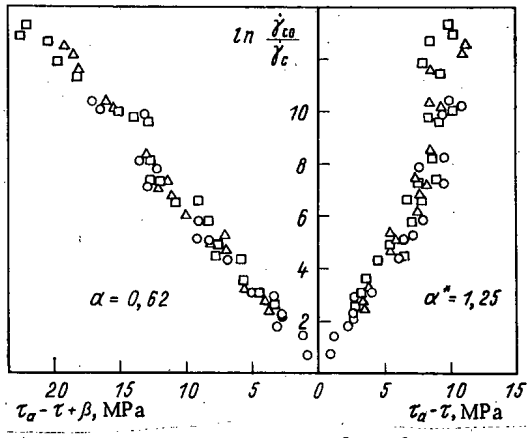

Fig. 4. Dependence of ln ($\dot{\gamma}_{c\alpha}/\dot{\gamma}_c$) on the difference in the effective stresses during irradiation at 540°K: ○) creep at τ = 81 MPa; △, □) relaxation at τ_0 = 60 and 41 MPa, respectively.

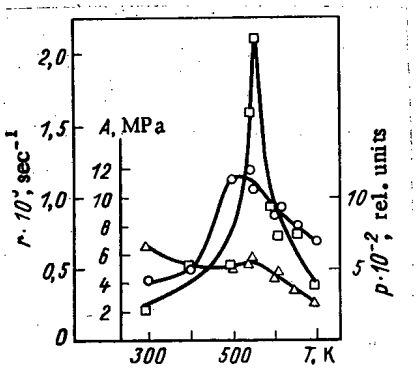

Fig. 5

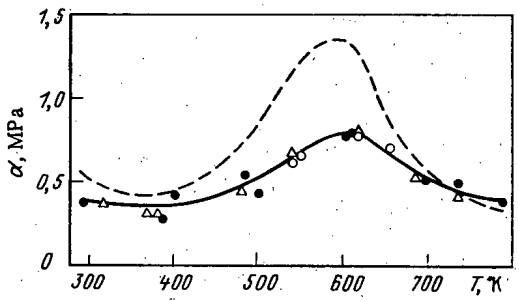

Fig. 6

Fig. 5. Temperature dependence of the parameters r(□), p(△), and A(○) from (4).

Fig. 6. Dependence of α on temperature with allowance for dynamic strain aging (——) and without such allowance (- - -): ●) before irradiation; ○) during irradiation; △) after irradiation; - ---) $\alpha^* = d\ln\frac{\dot{\gamma}_{c\alpha}}{\dot{\gamma}_c}/d(\tau_a - \tau)$; —) $\alpha = d\ln\frac{\dot{\gamma}_{c\alpha}}{\dot{\gamma}_c}/d(\tau_a - \tau + \beta)$.

The increases in shear modulus and plastic-deformation resistance on irradiation substantially affect the diagram for cyclic sign-varying strain (Fig. 3). To estimate the effects of irradiation on the accumulation of plastic strain, over 1000 creep and stress-relaxation tests were performed. Orovan's relation was used in processing the results:

$$\dot{\gamma}_c = b\rho_m V(\tau - \tau_i),$$

where b is Burgers vector; ρ_m is the mobile-dislocation density; $V(\tau - \tau_i)$ is the mean speed of the mobile dislocations, which is a function of the effective stresses $\tau_e = \tau - \tau_i$; τ is the applied stress; and τ_i is the inverse internal stress, which is dependent on the accumulated plastic strain and on the loading history.

If we assume that the mobile-dislocation density and the internal stresses are dependent only on the accumulated plastic strain at the given fluence, flux density, and temperature, then one can derive a relationship between the plastic strain rate $\dot{\gamma}_c$ at the stress $\tau(\gamma_c)$ and the rate $\dot{\gamma}_{c\alpha}$ under conditions of strain rate α:

$$\frac{\dot{\gamma}_{c\alpha}}{\dot{\gamma}_c} = \frac{V[\tau_a(\gamma_c) - \tau_i(\gamma_c)]}{V[\tau(\gamma_c) - \tau_i(\gamma_c)]}, \quad (1)$$

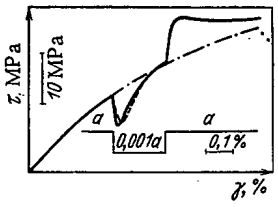

Fig. 7. Strain diagram for Zr +1% Nb on changing the strain rate a by a factor 10^3 at T = 593°K: ——) experiment; - - -) calculation from (3) and (4).

where $\tau_a(\gamma_c)$ is the resistance to strain with rate a.

For an exponential relationship between the mean speed of the mobile dislocations and the effective stress we get

$$\frac{\dot{\gamma}_{ca}}{\dot{\gamma}_c} = \exp\{\alpha[\tau_a(\gamma_c) - \tau(\gamma_c)]\}.$$

The plastic-strain rate at a constant rate of displacement in the loading tie is defined by

$$\dot{\gamma}_{ca} = a\Big/\Big[1 + \frac{d\tau_a}{d\gamma_c}\Big(\frac{1}{G} + \frac{1}{c}\Big)\Big], \tag{2}$$

where G is the equipment rigidity and $d\tau_a/d\gamma_c$ is the current plasticity modulus.

Then the coefficient α defining the sensitivity of the material to strain rate ($\alpha = \frac{d \ln \dot{\gamma}_c}{d\tau}\Big|_{T,\gamma_c}$) can be found from the slope of the experimental curve constructed from the creep-test data or from stress-relaxation results in $\ln(\dot{\gamma}_{ca}/\dot{\gamma}_c) - (\tau_a - \tau)$ coordinates (Fig. 4). The agreement between these results indicates that the initial assumptions are correct. Then knowing α and the strain diagram, one can calculate the rate of plastic strain accumulation from

$$\dot{\gamma}_c = \Big[a\Big/1 + \frac{d\tau_a}{d\gamma_c}\Big(\frac{1}{G} + \frac{1}{C}\Big)\Big]\exp\{\alpha(\tau - \tau_a(\gamma_c)\}. \tag{3}$$

However, the dependance of $\ln(\dot{\gamma}_{ca}/\dot{\gamma}_c)$ on $\tau_a - \tau$ is substantially nonlinear in the range 500-600°K (Fig. 4), which is due to dynamic strain aging, which has a considerable effect on the behavior of Zr +1% Nb at the working temperature.

The increase in strain resistance after a temporary reduction in the strain rate or partial unloading due to dynamic strain aging may be related to the increase in the internal stresses by the value β [6]. Then to retain the given plastic strain rate it is necessary to increase the applied stresses by $\Delta\tau = \beta$. Therefore, one can judge the changes in the internal stresses from the changes in the applied ones under conditions of variable-rate strain.

The results show that the degree of strain aging is dependent on time and on the plastic strain. With an infinitely small increment in the internal stresses, one can write the following approximation for this material [6]:

$$d\beta = r(A - \beta)\,dt - p\beta\,d\gamma_c, \tag{4}$$

where r, A, and p are parameters to be determined from experiment which are dependent on temperature (Fig. 5). A notable result from these studies is that irradiation does not affect the dynamic strain aging parameters.

The change in the inverse stresses on aging during creep or stress relaxation must be incorporated in determining the sensitivity to strain rate: the coefficient α is calculated from the slope of the curve in $\ln(\dot{\gamma}_{ca}/\dot{\gamma}_c) - (\tau_a - \tau + \beta)$ coordinates (Fig. 4). In accordance with Fig. 6, the data obtained before irradiation, during it, and afterwards lie on a common curve, which shows that the sensitivity of Zr +1% Nb to strain rate remains unchanged within the limits of the fluence and neutron flux density used.

Joint consideration of (3) and (4) enables one to describe the fairly complicated phenomena observed in tests at variable strain rates and under the corresponding working conditions in fuel-pin sheaths when the reactor power varies. Figure 7 compares the calculations with experimental data obtained under conditions of nonstationary loading (with the strain rate reduced by a factor of 1000).

These results indicate that one can use (3) to forecast the accumulation of plastic strain under conditions of brief nonstationary loading at high temperatures and low fluences. In practical calculations, allowance must be made for the changes in τ_i and α due to the dynamic strain aging and for the changes in G and τ_α caused by the irradiation conditions. Additional experiments are required to establish whether these formulas can be used for more prolonged irradiation and higher flux densities.

LITERATURE CITED

1. B. D. Semenov, Methods of Examining Creep and Relaxation in Refractory Materials under Sign-Varying Torsion over a Wide Temperature Range: Ph. D. Thesis [in Russian], MIFI, Moscow (1975).
2. Yu. V. Miloserdin, V. N. Chechko, and B. D. Semenov: Proceedings of the All-Union Symposium on Few-Cycle Fatigue at Elevated Temperatures [in Russian], Issue 1, ChPI, Chelyabinsk (1974), p. 123.
3. Yu. V. Miloserdin, V. N. Chechko, and B. D. Semenov, Inventor's Certificate No. 532032, Byull. Izobret. No. 38 (1976).
4. A. S. Glinskii et al., Reactor Tests on Materials [in Russian], Énergoatomizdat, Moscow (1983).
5. Yu. V. Miloserdin et al., Techniques in Radiation Experiments [in Russian], Issue 9 (1981), p. 116.
6. V. A. Matushkin et al., Probl. Prochn., No. 6, 80 (1981).

DAMAGE SUMMATION IN ANNEALING AND REPEATED IRRADIATION OF PRESSURE-VESSEL STEEL

V. A. Nikolaev, V. I. Badanin, and A. M. Morozov

UDC 621.039.531

Reducing heat treatment is a means of increasing the working life of pressure vessels of water-cooled–water-moderated reactors (VVÉR), but its use requires a knowledge of the laws of radiation embrittlement in materials under conditions of repeated irradiation in order to provide a reliable forecast of viability on further use. Since it is far from always desirable or possible to bring about complete recovery of the properties of the material by reducing heat treatment, it is important to establish how the residual damage sums with the radiation damage produced by repeated irradiation. The available information is very restricted because the corresponding studies are very complicated [1, 2].

In the early experiments [1], it was found that the residual shift in the embrittlement temperature ΔT_{res} (50°C), persists in A350-LF1 steel after irradiation to a neutron fluence of 3×10^{23} m^{-2} and annealing at 307°C, and this should be borne in mind in estimating the total shift ΔT_t after repeated irradiation. It is possible to do this on the assumption that the material has already accumulated some damage at the start of the repeated irradiation, this damage corresponding to an equivalent neutron fluence F_e, which causes a radiation embrittlement effect of ΔT_{res}. This approach is less conservative than the method of independent (arithmetic) summation of ΔT_{res} with the shift due to the neutron fluence on repeated irradiation (ΔT_{F_2}), and so if it is to be used in calculations one requires a reasonably reliable experimental basis for it, the more so since ambiguous results were obtained in a series of experiments on the irradiation of welded joints in A533-B steel: a difference from the results from repeated irradiation after annealing at 399°C, which confirmed the results of [1], while the changes in T_t resulting from annealing at 343°C and subsequent irradiation agreed best with the view that the damage sums independently [3].

In this connection, experiments were performed on repeating the irradiation of Soviet reactor steel following variable intermediate-annealing temperature and determination of

Translated from Atomnaya Énergiya, Vol. 57, No. 3, pp. 165-167, September, 1984. Original article submitted October 13, 1983; revision submitted January 31, 1984.

0038-531X/84/5703-0603$08.50

ΔT_{res}. We examined 15Kh2MFA steel made commercially with phosphorus and copper contents of 0.013 and 0.15%, respectively. An abbreviated program was also used in testing 15Kh2NMFA steel (0.012% phosphorus, 0.12% copper). As it was necessary to irradiate a large number of specimens simultaneously under identical conditions in order to determine T_t, the embrittlement temperature, for 15Kh2MFA steel, we used impactor specimens of size 5 × 5 × 27.5 mm. The 15Kh2NMFA steel was tested in the form of standard specimens.

The cassettes containing the specimens were placed in ampules of identical internal diameter and were irradiated in the core of the VVR-M reactor. The cassettes were inserted in the ampules as sliding fits and the irradiation temperature was not more than 250°C. The temperatures of the specimens during the first irradiation were monitored with 8 Chromel—Alumel thermocouples. On repeated irradiation, the specimens were sealed in by means of a conical fitting ground into the head of the ampule and the edges were rolled over by remote control. In that case, it was impossible to insert thermocouples, and diamond indicators were used to monitor the temperature.

The initial irradiation of the 15Kh2MFA specimens was performed to a neutron fluence of $F_1 = 7.5 \cdot 10^{23}$ m^{-2} ($E \geq 0.5$ MeV). The irradiation temperature varied over the height of the ampule over the range 180-200°C at the start of the exposure and up to 215 ± 15°C in the closing stage. The rise in the embrittlement temperature ΔT_{F_1} under these conditions was 100°C, which corresponds to an irradiation embrittlement coefficient of $A_{F_1} = \Delta T_{F_1}/(F_1 \cdot 10^{-22})^{1/3} = 24$. Annealing for 100 h at 240, 275, or 325°C produced reductions in the shift in T_t correspondingly of 80, 50, and 20°C, i.e., the degrees of recovery were 20, 50, and 80%.

The repeated exposure was given to previously irradiated specimens either with or without annealing as above, as well as to control specimens, which had not previously been irradiated. In the latter, the irradiation to a fluence of $F_2 = 8.7 \cdot 10^{23}$ m^{-2} raised T_t by 130°C, which corresponds to $A_{F_2} = 29$. The value of A_{F_2} is higher than A_{F_1} evidently because of the lower temperature in the repeated irradiation (100-120°C).

Specimens annealed at 240, 275, and 325°C showed additional increases in T_t of 70, 70, and 100°C, respectively. The smallest shift in T_t on repeated irradiation (50°C) occurred in the material that had not been annealed. Therefore, the embrittlement of 15Kh2MFA steel on repeated irradiation, which is characterized by the additional shift in T_t, is the less the more the material has been embrittled after the preliminary treatment: irradiation or annealing after irradiation (Fig. 1).

The first exposure of the 15Kh2NMFA steel specimens was at T_F = 160-180°C with a neutron fluence F_1 of 8.3×10^{23} m^{-2}, which gave $\Delta T_{F_1} = 160$°C; annealing the specimens at 350°C for 100 h resulted in $\Delta T_{res} = 20$°C. After repeated exposure ($F_2 = 9 \cdot 10^{23}$ m^{-2}) ΔT_F for the un-

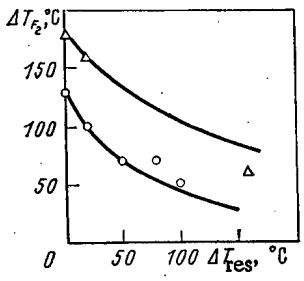

Fig. 1

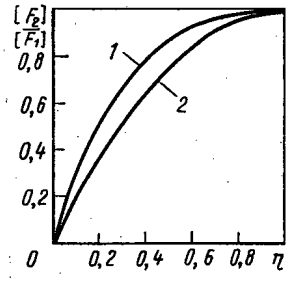

Fig. 2

Fig. 1. Dependence of the rise in viscous—brittle transition temperature ΔT_{F_2} on repeated irradiation on the preceding shift ΔT_t due to preliminary irradiation and incomplete annealing. The curves have been constructed from (4): ○) steel 15Kh2MFA, fluence 8.7×10^{23} m^{-2}; Δ) steel 15Kh2NMFA, neutron fluence 9×10^{23} m^{-2}.

Fig. 2. Dependence of the increase in permissible neutron fluence on the degree of recovery in T_t on annealing steels 15Kh2MFA (1) and 15Kh2NMFA (2).

annealed specimens increased to 220°C, i.e., by 60°C. In specimens that had been annealed, the additional shift in T_t was 160°C, as against 180°C in the control specimens. Therefore, the experiments indicate unambiguously that there is nonadditive summation of the residual damage (after annealing) and the damage caused by repeated irradiation.

We now transfer to considering the damage summation principle and first consider the behavior of 15Kh2MFA steel under conditions of stepwise change in irradiation temperature from T_1 to T_2, where $T_1 > T_2$, where consequently there is no annealing of the defects formed at T_1 during the second stage of irradiation. We assume formally that the value of ΔT_{F_1} corresponds to F_e at T_2, i.e., $F_e = (\Delta T_{F_1}/A_{F_2})^3$. Then the total shift is

$$\Delta T_c = A_{F_2}(F_e + F_2)^{1/3} = (A_{F_1}^3 F_1 + A_{F_2}^3 F_2)^{1/3}. \quad (1)$$

The justification for summing the damage in accordance with (1) can be checked by means of the above experiments with 15Kh2MFA steel: $\Delta T_c = (24^3 \cdot 75 + 29^3 \cdot 87)^{1/3} = 147$°C with the experimental value $\Delta T_c = 150$°C.

The summation for $T_1 > T_2$ was checked in independent experiments, whose detailed description falls outside the scope of this paper. We mention only one result, which was obtained for the metal in a welded joint in 15Kh2MFA steel. The specimens of this material were originally irradiated at 290 ± 10°C to a fluence of 4.4×10^{23} m^{-2} and then additionally to a fluence of 2.7×10^{23} m^{-2} at 225 ± 10°C. The increment ΔT_t due to that irradiation was 140°C, whereas (1) gives $\Delta T_c = 152$°C.

A similar result was obtained for 15Kh2NMFA steel, for which, however, the change in T_t satisfies a dose dependence of the form

$$\Delta T_F = C_F F^{1/2}, \quad (2)$$

where C_F is a coefficient dependent on the irradiation temperature that characterizes the radiation stability of the steel. Statistical processing was applied to data from 17 experiments in which the fluence varied from 2×10^{23} to 3.9×10^{24} m^{-2}, which showed that with irradiation temperatures of 200 ± 20°C and 240 ± 10°C the power-law dependence of the embrittlement for this steel applies with powers of m = 0.446 and 0.532, respectively. In this connection, the summation formula for 15Kh2NMFA steel was similar to (1), but A_F should be replaced by C_F, while the powers 1/3 and 3 should be replaced by 1/2 and 2. In the above experiment, $C_{F_1} = 17.5$, $C_{F_2} = 19$, and the calculated value of ΔT_c was 240°C, while the actual value was 220°C.

We now consider the damage summation on partial recovery during annealing ($\Delta T_{res} > 0$) and repeated irradiation. By analogy with (1), we get for 15Kh2MFA steel that

$$\Delta T_c = (\Delta T_{res}^3 + A_{F_2}^3 F_2)^{1/3}. \quad (3)$$

The values of ΔT_c calculated from this formula with ΔT_{res} of 20, 50, and 80°C as given by experiment were correspondingly 128, 130, and 137°C, which agree with the experimental values (120, 120, and 150°C) within the error with which ΔT_t is determined.

If the dose dependence of the radiation embrittlement is described in general by a power law with power m, then the summation formula becomes

$$\Delta T_c = (\Delta T_{res}^{1/m} + C_{F_2}^{1/m} F_2)^m. \quad (4)$$

Calculation from (4) for 15Kh2NMFA steel (m = 1/2, $\Delta T_{res} = 20$°C, $F_2 = 9 \cdot 10^{23}$ m^{-2}, $C_{F_2} = 19$) gives $\Delta T_c = 182$°C while the experimental value is 180°C.

These relationships imply important conclusions on the calculation of the limiting permissible neutron fluence under conditions of irradiation after annealing. Consider a pressure vessel made of 15Kh2MFA steel for which the established limiting permissible fluence is $[F_1] = ([\Delta T_t]A_F)^3$, where $[\Delta T_t]$ is the limiting permissible shift in T_t allowed by the working conditions. If $[F_1]$ has been attained and the vessel is annealed with a degree of recovery in the properties of the material $\eta = \{[\Delta T_t] - \Delta T_{res}\}[\Delta T_t]$, then in accordance with (3) the permissible fluence for the subsequent operation is

$$[F_2] = \frac{[\Delta T_t]^3 - \Delta T_{res}^3}{A_F^3} = [F_1]\{1-(1-\eta)^3\}. \quad (5)$$

Figure 2 shows the dependence of $[F_2]/[F_1]$ on η as expressed by (5). We see that to increase $[F_1]$ by 80% it is sufficient to have $\eta = 0.4$, i.e., 40% recovery in the properties of the material. As to increase η requires a corresponding increase in the annealing temperature, one assumes that recovery of the properties by 40-60% is an optimal specification for the annealing. For structures made of 15Kh2NMFA steel, the power in (5) varies by a factor of 2, as previously, and the corresponding curve is flatter (Fig. 2).

LITERATURE CITED

1. U. Potapovs, J. Hawthorne, and C. Serpan, Nucl. Appl., 5, No. 6, 389 (1968).
2. L. Steele, At. Energy Rev., 7, No. 2, 3 (1969).
3. J. Hawthorne, in: Irradiation Embrittlement, Thermal Annealing and Surveillance of Reactor Pressure Vessels, IAEA, Vienna (1979), p. 181.

EFFECT OF CHEMICAL COMPOSITION AND ANNEALING CONDITIONS ON THE RADIATION EMBRITTLEMENT OF THE METAL OF LOW-ALLOY WELDED SEAMS

V. A. Nikolaev, A. M. Morozov, V. I. Badanin, A. S. Teshchenko, and R. P. Vinogradov

UDC 621.039.531:621.791.053

The metallurgical factors determining radiation embrittlement of low-alloy reactor steels have been studied in sufficient detail. However, for the metal of welded joint, mainly determining the operating efficiency of the structures on the whole, data about the mechanisms of the effect of chemical composition and heat treatment on radiation embrittlement are quite few [1-3]. This has served as the basis for the study of radiation embrittlement of the metal of welded seams as a function of their annealing conditions and the contents of certain alloying and impurity elements.

In order to explain the role of alloying elements in the radiation embrittlement of the metal of seams, the effect of the contents of nickel and manganese, which improve the structure of the metal weld, its strength, and resistance to brittle fracture [3], was studied, but, judging by the data for the base metal [4-6], they can have an unfavorable influence on the radiation stability. As the content of impurity elements (phosphorus and copper) is an important factor controlling the radiation embrittlement of steel and the metal of welded seams [1-3, 7], it was advantageous to study in detail the effect of these elements on the embrittlement of the metal of specific seams.

Material and Investigation Procedure. The effect of chemical composition was studied on the metal of laboratory welded seams, obtained by the use of experimental batches of wire of Cr–Mn–Ni–Mo composition, which is the basis of Sv-08KhGNMTA wire [7] and which is intended for the automatic welding of the pressure vessels of water-cooled/water-moderated power reactors. In the metal of the seams investigated, the phosphorus content varied within the limits of 0.008-0.022%, copper 0.03-0.35%, nickel 0.76-2.16%, and manganese 0.47-0.95%. In each individual series of compositions the content of one element was varied as a rule, the contents of the others being almost unchanged.

Grade É-12 (0.18% Cu, 0.01% P) and 03ZhR (0.01% Cu, 0.004% P) irons were used in smelting the metal of the experimental compositions. The fusions, with a mass of 160 kg, were carried out in an open induction furnace. The elements being varied were added in the furnace (nickel, manganese) or in the ladles (copper, phosphorus) in proportion with the casting of the metal in ingots of mass 16 kg. Wire with a diameter of 5 mm was obtained from these ingots by forging and subsequent drawing. Welded samples were prepared under grade 48NF-18M flux (Technical Specification 5.965-4011-72); plates of 15Kh2NMFA steel with a content of 0.017%

Translated from Atomnaya Énergiya, Vol. 57, No. 3, pp. 167-172, September, 1984. Original article submitted October 13, 1983.

 0038-531X/84/5703-0606$08.50

TABLE 1. Chemical Composition, Cooling Conditions after Annealing and Irradiation, and Increase under Irradiation of the Critical Temperature of Brittleness T_c of the Metal of the Welded Seams Investigated

Series and composition No.	Content of varied elements, mass%				Cooling	Irradiation		T_c, °C
	Mn	Ni	P	Cu		neutron fluence, cm^{-2}	temperature, °C	
1—1	1,0	1,5	0,008	0,04	In the furnace to 300°C, then in air	$4,3 \cdot 10^{19}$	270—340	20
1—2	1,0	1,5	0,012	0,04		$4,3 \cdot 10^{19}$	270—340	20
1—3	1,0	1,5	0,015	0,04		$4,3 \cdot 10^{19}$	270—340	30
1—4	1,0	1,5	0,020	0,04		$4,3 \cdot 10^{19}$	270—340	40
1—5	1,0	1,5	0,015	0,32		$4,3 \cdot 10^{19}$	270—340	80
1—6	1,0	1,5	0,020	0,35		$4,3 \cdot 10^{19}$	270—340	90
2—1	0,63	1,28	0,011	0,07	In water	$2,5 \cdot 10^{19}$	320—340	70
2—2	0,63	1,28	0,015	0,07		$2,5 \cdot 10^{19}$	320—340	80
2—3	0,63	1,28	0,018	0,07		$2,5 \cdot 10^{19}$	320—340	90
2—4	0,63	1,28	0,022	0,07		$2,5 \cdot 10^{19}$	320—340	100
3—1	0,63	1,28	0,010	0,07	In water	$2,5 \cdot 10^{19}$	320—340	60
3—2	0,63	1,28	0,010	0,10		$2,5 \cdot 10^{19}$	320—340	80
3—3	0,63	1,28	0,010	0,135		$2,5 \cdot 10^{19}$	320—340	120
4—1	0,75	1,30	0,011	0,03	In the furnace to 300°C, then in air	$2,6 \cdot 10^{19}$	290—310	40
4—2	0,75	1,30	0,011	0,10		$2,6 \cdot 10^{19}$	290—310	50
4—3	0,75	1,20	0,011	0,18		$2,6 \cdot 10^{19}$	290—310	70
4—4	0,75	1,20	0,011	0,27		$2,6 \cdot 10^{19}$	290—310	90
5—1	0,47	0,91	0,012	0,19	In the furnace to 300°C, then in air	$2,6 \cdot 10^{19}$	290—310	60
5—2	0,47	1,70	0,012	0,19		$2,6 \cdot 10^{19}$	290—310	80
5—3	0,50	0,76	0,012	0,17		$2,4 \cdot 10^{19}$	270—300	50
5—4	0,50	1,42	0,012	0,17		$2,4 \cdot 10^{19}$	270—300	70
5—5	0,50	2,16	0,012	0,17		$2,4 \cdot 10^{19}$	270—300	90
6—1	0,47	1,20	0,012	0,19	In the furnace to 300°C, then in air	$2,6 \cdot 10^{19}$	290—310	60
6—2	0,64	1,20	0,011	0,19		$2,6 \cdot 10^{19}$	290—310	60
6—3	0,75	1,20	0,011	0,18		$2,6 \cdot 10^{19}$	290—310	70
6—4	0,82	1,20	0,012	0,19		$2,5 \cdot 10^{19}$	300—310	80
6—5	0,83	1,20	0,011	0,19		$2,5 \cdot 10^{19}$	300—310	80
6—6	0,85	1,20	0,012	0,19		$2,5 \cdot 10^{19}$	300—310	90
6—7	0,95	1,20	0,011	0,19		$2,5 \cdot 10^{19}$	300—310	90
7—1	0,60	1,1	0,007	0,26	In the furnace to 300°C, then in air	$2,8 \cdot 10^{19}$	290—310	40
7—2	0,63	1,0	0,004	0,26		$2,8 \cdot 10^{19}$	290—310	40

phosphorus and 0.14% copper and with a thickness of 50 mm were used. Welding was carried out in the following conditions: I_{weld} = 600-650 A, U_{arc} = 38-40 V, V_{weld} = 24 m/h, reverse polarity, and temperature of heating up of the plate before welding was 150-200°C. The chemical composition of the metal of the welds investigated is given in Table 1.

The heat treatment of the samples was high tempering with the following conditions: heated to 650°C and held for 10 h. Most of the welded samples (see Table 1, No. 1, 1-6; No. 4, 1-4; No. 5, 1-5; No. 6, 1-7; No. 7, 1-2), in accordance with a realistic regime of heat treatment of the articles, were cooled in the furnace to 350°C* (rate of cooling 20°C/h), and then in air. The materials of two series of compositions, with a variable phosphorus and copper content, after annealing were cooled in water in order to study the effect of impurity elements with a high cooling rate of the welds.

The tendency of the materials to radiation embrittlement was estimated by the values of ΔT_c — the shift of the ductile—brittle transition temperature T_c caused by irradiation. The values of T_c were determined by the impact viscosity serial curves, using notched samples with a size of 5 × 5 × 27.5 mm (radius of the bottom of the notch was 0.25 mm and the depth 1 mm). The testing temperature, at which the impact viscosity amounted to one-half of the maximum value, was used for T_c.

The samples were irradiated in the core of the VVR-M reactor by the usual procedure [4]. The temperature was measured with a Chromel—Alumel thermocouple, spot-welded to the samples.

*As in the Russian original; the temperature given in Table 1 is 300°C — Publisher.

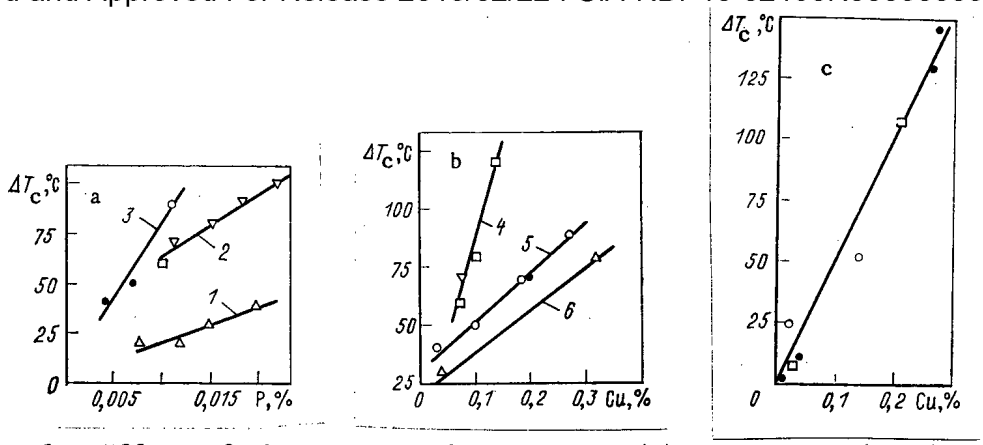

Fig. 1. Effect of the content of phosphorus (a) and copper (b, c) on the increase in T_c of the metal of welded seams of Cr–Mn–Ni–Mo composition, by the action of neutron irradiation. a: 1) compositions 1–1 to 1–4 (Δ), neutron fluence $4.3 \cdot 10^{19}$ cm^{-2} at 270-340°C; 2) compositions 2–1 to 2–4 (▽), 3–1 (□), $2.5 \cdot 10^{19}$ cm^{-2} at 320-340°C; 3) compositions 4-4 (○), 7–1, 7–2 (●) $(2.6$ to $2.8) \cdot 10^{19}$ cm^{-2} at 290-310°C; b: 4) compositions 3–1 to 3–3 (□), 2–1 (▽), neutron fluence $2.5 \cdot 10^{19}$ cm^{-2} at 320-340°C; 5) compositions 4–1 to 4–4 (○), 6–3 (●), $2.6 \cdot 10^{19}$ cm^{-2} at 290-310°C; 6) compositions 1–3, 1-5 (Δ), $4.3 \cdot 10^{19}$ cm^{-2} at 270-340°C; c: ●) 1.95-2.01% Ni; □) 1.45-1.64% Ni, neutron fluence with energy E > 1 MeV $2.8 \cdot 10^{19}$ cm^{-2} at 288°C [1, 2]; ○) 1.65-1.75% Ni, neutron fluence with energy E > 1 MeV $3.5 \cdot 10^{19}$ cm^{-2} at 288°C [1, 2].

There was no possibility of regulating the temperature of the samples during irradiation because, during the reactor run, a monotonic increase in temperature was observed within the limits of 20-40°C. In view of the fact that in this situation the temperature conditions of the final stage of exposure [8] set the determining value for radiation damage to the material, as the principal characteristic of the irradiation regime we assumed the maximum values of the temperature of the samples.

The fluence of neutrons with energy $E \geq 0.5$ MeV was determined on the basis of the power output of the reactor during the time of irradiation, preliminary measurements of the flux density at the site of location of the samples, and additional monitoring by irradiated activation detectors together with the samples. The $^{54}Fe(n, p)^{54}Mn$ reaction was used, with a cross section of $\bar{\sigma} = 92$ mb (1 b = 10^{-28} m^2) for neutrons with energy in excess of 0.5 MeV of the energy spectrum of the VVR-M reactor core.

Results of the Investigation. The experimental data about the effect of irradiation on the increase in T_c for a different phosphorus concentration in the metal of the welded seams, with a copper content of 0.04-0.07% and different cooling rates after annealing, are given in Table 1 and also in Fig. 1a. The data presented were obtained for irradiation at a maximum temperature of 340°C. It follows from Fig. 1a that with increase in the phosphorus content, the values of ΔT_c increase almost linearly. In this case, for the material cooled in water (curve 2), despite the somewhat lower neutron fluence, markedly greater variations of T_c were obtained than for materials cooled in the furnace (curve 1). An even sharper intensification of embrittlement with increasing phosphorus content was found for the metal of welds containing 0.26-0.27% copper and subjected to slow cooling after annealing (curve 3). If the high values of ΔT_c in this case can be partially explained by the lower irradiation temperature ($\sim$ 310°C), then the steeper slope of curve 3 confirms the intensification of the effect of phosphorus in the presence of copper.

The effect of the copper content on radiation embrittlement of the metal of the welds investigated is described in Fig. 1b. On the curves of the concentration relation, constructed on the results of tests of individual series of compositions, the points are plotted corresponding to the experimental data for materials with identical cooling conditions and with a similar content of other elements and with similar irradiation conditions. It can be seen that for all materials the shift of ΔT_c increases linearly with increase of the copper concentration from 0.03 to 0.3%. For materials having been slowly cooled after annealing, the curves of the concentration relationship have a lesser slope and, in addition, they are

disposed lower, even in the case of irradiation at a lower temperature. With copper concentrations < 0.05%, a tendency to merging of the curves is observed. For metal with slow cooling after annealing, a neutron fluence of $\sim 2.5 \cdot 10^{19}$ cm^{-2}, and an irradiation temperature of 300-310°C, an increase in the copper content by 0.2% causes an increase in ΔT_c by approximately 50°C, while in the same conditions an increase in the phosphorus content by 0.005% led to an increase in ΔT_c by approximately 40-45°C. Thus, the effect of copper on embrittlement of the welds is more than a factor of 10 weaker than the effect of an equal amount of phosphorus.

For comparison with the experimental data obtained, Fig. 1c shows the results of a study of radiation embrittlement of the metal of experimental welded seams of similar composition (2.5Cr—Mn—Ni—Mo) with a copper content varying within the limits of 0.01-0.27% and with a phosphorus content of 0.007-0.012% [1, 2]. After annealing, the welded samples were cooled at the rate of 56°C/h. Samples of these welds were irradiated at 288°C. It follows from a comparison of Figs. 1c and 1a that with a concentration of < 0.05% copper in the seams, the values of ΔT_c almost coincide with those obtained experimentally. With a copper concentration of > 0.1%, the published experimental points [1, 2] in conjunction with the intermediate values of the rate of cooling after annealing are disposed between the curves obtained for the materials having been cooled after annealing either in water or in the furnace (one should also bear in mind the slight difference in the irradiation temperature of the welded materials).

In comparing the effect of copper on the radiation embrittlement for the seam metal and steel 15Kh2MFA [4, 5] at an irradiation temperature of 340-350°C, a definite similarity can be noted in the behavior of these materials, shown in the linear dependence of ΔT_c on the copper content within limits of up to 0.3% and with a phosphorus concentration of $\geq 0.01\%$. When the irradiation temperature is reduced, the effect of the influence of copper increases. Judging by the experimental data obtained for welded seams, an increase of the cooling rate also shows the same effect.

The effect of the nickel concentration on the radiation embrittlement of the metal of the welded seams, with a phosphorus content of 0.010-0.012% and 0.17-0.19% of copper, subjected to slow cooling after annealing, is shown in Fig. 2a. The data given relate to an irradiation temperature of 300-310°C. It can be seen that with a change in the weld metal of the nickel concentration from 0.76 to 2.16%, the value of ΔT_c is almost doubled (from 50 to 90°C). Comparison of the results obtained with the data of [4-6] concerning the effect of nickel on the radiation embrittlement of the base metal of 15Kh2MFA steel showed that for the metal of the welded seams and for deformed steel, the nature of the radiation embrittlement versus the nickel concentration is almost identical. The linear dependence with almost

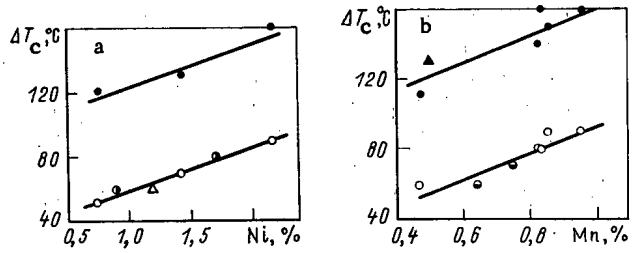

Fig. 2. Effect of the content of nickel (a) and manganese (b) on the increase in T_c of the metal of welded seams of Cr—Mn—Ni—Mo composition by the action of neutron irradiation: a) compositions 5—1 to 5—5, 6—1 (see Table 1): ◑, Δ) neutron fluence $2.6 \cdot 10^{19}$ cm^{-2} at 290-310°C; ○) $2.5 \cdot 10^{19}$ cm^{-2} at 270-300°C; ●) $3.8 \cdot 10^{19}$ cm^{-2} at 50-80°C; b) compositions 6—1 to 6—7, 5—4: ◒ neutron fluence $2.6 \cdot 10^{19}$ cm^{-2} at 300-310°C; ○) $2.5 \cdot 10^{19}$ cm^{-2} at 300-310°C; ●, ▲) $3.8 \cdot 10^{19}$ cm^{-2} at 50-80°C.

the same angle of slope is maintained even in the case of a reduction of the irradiation temperature to 50-80°C. Similar results were obtained when studying the effect of nickel in the case of the metal of welded seams of Cr—Mn—Ni—Mo composition [2].

Manganese, similarly to nickel, intensifies the tendency of the seam metal to radiation embrittlement, which is demonstrated in Fig. 2b. In this figure, the set of points corresponding to the experimental values of ΔT_c for the material of almost one series, obtained with an irradiation temperature of $\sim$ 310°C, shows that with increase in the manganese concentration approximately from 0.5 to $\sim$ 1%, an increase in ΔT_c is observed from 60 to 90°C. Irradiation at 50-80°C leads to stronger radiation embrittlement of the materials investigated, but the nature of the dependence of ΔT_c on the manganese concentration is maintained. Similar observations were obtained also for Cr—Ni—Mo—V steel [5, 6]. As confirmation of the negative effect of manganese, the data on the embrittlement of welded seam metal of Cr—Mn—Ni—Mo composition [2] can be considered also.

From a comparison of the ΔT_c curves of metal of the seams investigated versus the manganese and nickel concentrations, it follows that manganese exerts a stronger influence on embrittlement than the same amount of nickel, although it cannot be excluded that the result is characteristic only for the metal of the melt being considered.

Discussion. Consideration of the experimental data obtained indicates that for the metal of welded seams of studied composition, in the main the same regularities of the effect of alloying and impurity elements on radiation embrittlement are qualitatively observed as for the principal metal — chrome—molybdenum steel. Consequently, there are grounds for assuming the mechanisms of this effect also to be identical.

Relative to the role of phosphorus in the intensification of radiation embrittlement of steel and alloys of iron, the opinion is expressed in [9] that atoms of this element, owing to its capability of forming loose complexes with vacancies or mixed dumbbell-type pairs with interstitial atoms, segregate on imperfections of the crystal structure of ferrite, in particular on accumulations of point defects or on the grain boundaries. In consequence of the low surface energy of phosphorus and the deformation of the lattice in these zones of segregation, the interatomic bonds are weakened and embryo microcracks can originate most easily here. If the irradiation temperature is sufficiently high for annealing the defects (above 300-350°C), the embrittlement caused by the presence of phosphorus in its principal appearances is similar to thermal brittleness. The difference, in essence, reduces to the acceleration of the diffusion redistribution of phosphorus under the action of superequilibrium vacancies. The similarities of these two phenomena concern also the effect of alloying elements. Nickel and manganese intensify the segregation processes, first and foremost in consequence of the reduction of solubility of phosphorus in ferrite [10], but in radiation embrittlement their role is not limited to this. Judging by the fact that with increase in concentration of these elements in steel and alloys, a marked increase in radiation hardening is observed in the case of irradiation at a temperature in excess of 300°C, and the atoms of nickel and manganese in some way participate in the formation of a defect structure. Definite hypotheses have been expressed concerning the mechanism of their interaction with defects [11], but reliable arguments still have not been found.

The effect of copper on embrittlement likewise is explained by the increase in radiation hardening [5, 12]. The cause of this effect is associated in [12] with the heterogeneous origin of vacancy accumulations at complexes of vacancy—copper atoms, owing to which the volume concentration of defects is increased, resolvable in the electron microscope. Certain data, characterizing the change of physical properties of iron—copper alloys in conditions of irradiation [11], coincide with this concept. According to this concept, the increase in sensitivity of steel and the weld metal to the presence of copper, with increase in the phosphorus content, can be traced as a consequence of the increase in the volume concentration of intercrystallite defect zones, enriched with phosphorus.

It cannot be excluded that welded seams, in preserving the characteristic of the structure of cast metal, such as crystallization nonuniformity of distribution of the elements, have certain specific properties of behavior by comparison with forged steel. Both phosphorus and copper show a tendency to liquidate in the interdendritic layers of cast steel [13], in connection with which it is possible to suppose that these elements, entering into competition, mutually change the volume concentration of individual structural components of the weld metal.

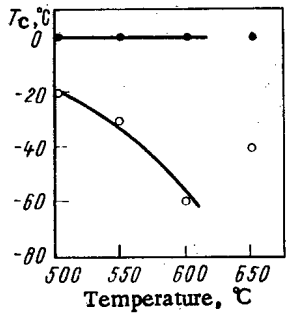

Fig. 3. Dependence of T_c of the metal of welded seams of Cr–Mn–Ni–Mo composition on the temperature of final annealing: ○) initial state; ●) after irradiation up to a neutron fluence of $5 \cdot 10^{19}$ cm^{-2}.

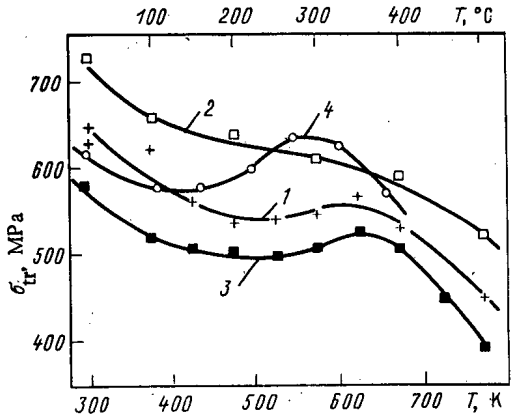

Fig. 4. Dependence of σ_{tr} on the temperature of testing: 1) metal of a welded seam of Cr–Mn–Ni–Mo composition (wire Sv-08KhGNMTA); 2) steel 15Kh2MFA; 3) steel 10KhN1M; 4) steel A-302-B.

The marked dependence of the radiation embrittlement of the weld metal on the rate of cooling of the samples after annealing is interpreted most naturally as the result of a change in the ferrite of the concentration of limitedly soluble elements, affecting the radiation tendency to damage. Thus, it was established that previous prolonged irradiation (500–1000 h) maintained at 450–500°C, causing an increase in T_c for steel, is inclined to thermal brittleness, and at the same time it reduces its sensitivity to embrittlement with subsequent irradiation [14]. This fact was described by the partial transfer of phosphorus atoms from the solid solution at the boundaries of the former austenitic grains during aging, owing to which the corresponding fraction of phosphorus atoms is excluded from the processes of interaction with radiation defects. It is slightly probable, however, that in the weld metal containing less than 0.020% of phosphorus, the grain-boundary segregation processes derived an appreciable development during slow cooling of the samples ($\sim$ 15 h) after annealing. The experiment, moreover, did not reveal any significant difference in the angle of slope of the curves of the dependence of embrittlement on the concentration of phosphorus in the case of a change of the cooling rate, whereas in the case of a deficit of phosphorus in the solid solution, such a difference should be expected.

The circumstance that for rapidly cooled welds the maximum angle of slope is observed for the curves of the dependence of embrittlement on the content of copper gives the basis for supposing a possible responsibility of this element for the observed effect. The limit of solubility of copper in iron does not exceed 0.15% by mass at 450°C [15], and in alloyed ferrite it can only be less. The separation of excess copper from the solid solution during slow cooling of the welds from 500–350°C, in principle, is capable of weakening the tendency of the metal to radiation embrittlement. This assumption, admissible in relation to welds with a copper content of > 0.1%, does not explain, however, the reason for the sensitivity to the rate of cooling of the welds containing 0.04–0.07% copper (see Fig. 1a). Meanwhile, the nonrandomness of this result coincides with the data of a special experiment carried out on the metal of a welded sample, performed with commercial wire grade Sv-08KhGNMTA and heat treated in industrial conditions in the following regime: annealing 650°C, 16 h; cooling in the furnace to 350°C, then in air. The contents of phosphorus and copper in the weld metal amounted to 0.013 and 0.05%, respectively. This sample was divided into four parts, three

of which were subjected to additional annealing according to different conditions: 600°C, 10 h; 600°C, 10 h + 500°C, 10 h; 550°C, 10 h. The samples in all cases were cooled in water. As a result of the additional heat treatment, the initial value of T_c (−40°C) varied within limits of ± 20°C, and in proportion with the reduction of temperature of the final annealing, an increase in T_c was observed. After irradiation up to a neutron fluence of $5 \cdot 10^{19}$ cm^{-2} at 300-330°C, the values of T_c were found to be identical, independently of the conditions of the previous annealing. The minimum shift of ΔT_c (20°C) is appreciable for metal subjected to stepwise annealing with a concluding temperature of 500°C, and the maximum shift of ΔT_c (60°C) — for metal after annealing at 600°C (Fig. 3). Intermediate values of ΔT_c were obtained for metal after regular heat treatment, i.e., after annealing at the highest temperature (650°C), but with cooling in the furnace.

Thus, even with a low content of copper, a change of cooling conditions after annealing changes somewhat the sensitivity of the welds to radiation embrittlement.

A change of the cooling rate after annealing can also change the concentration in the solid solution of implanted atoms (carbon, nitrogen). The effective influence of these elements on the increase in radiation hardening and embrittlement of alloys of iron, and also low-alloy steels, is well known. Although until recently there is no single universally accepted hypothesis for explaining the mechanism of the effect of implanted atoms on the formation of defects in alloys based on iron [16, 17, 11], the role of these elements in radiation embrittlement is quite important. It is understood, owing to the alloying of the metal of welding wire with carbide- and nitride-forming elements, in the first place chromium, that the concentration of carbon and nitrogen in the ferrite of the welds after high annealing cannot be so high as in technical iron or carbon steel. Nevertheless, concerning the presence of dissolved implanted elements in the weld metal, the nonmonotonicity can be confirmed of the change with temperature of the transient tensile strength σ_{tr} (Fig. 4). The extreme dependence of the strength and plasticity of iron and steel in the range 200-400°C reflects the phenomenon of dynamic deformation aging (blue brittleness), to the cause of which is attributed blocking of the loose dislocations by atoms of implanted impurity, mainly atoms of nitrogen [18]. A comparison of the metal of the weld with the studied composition and certain structural steels shows (Fig. 4) that steel of grade 15Kh2MFA, alloyed in addition to chromium with such a strong carbide- and nitride-forming element as vanadium, manifests the minimum tendency towards deformation aging, and for foreign steel A302-B (C—Mn—Mo composition), according to the data of [19], this effect is expressed in the greatest degree. The metal of welds made with wire of grade Sv-08KhGNMTA, occupies an intermediate position and is similar to steel 10KhN1M, which has a similar system of alloying.

LITERATURE CITED

1. U. Potapovs and J. Hawthorne, Nucl. Appl., 6, 27 (1969).
2. J. Hawthorne, E. Fortner, and S. Grant, Welding J., 49, No. 10, 453 (1970).
3. V. V. Ardentov et al., Welding Materials for the Mechanized Welding of Reactor Pressure Vessels of Nuclear Power Stations of Increased Power [in Russian], Automatic Welding, No. 6, 51 (1981).
4. V. A. Nikolaev and V. I. Badanin, At. Energ., 37, No. 6, 491 (1974).
5. V. A. Nikolaev and V. I. Badanin, in: Radiation Effects of the Change of Mechanical Properties of Structural Materials and Methods of Their Investigation [in Russian], Naukova Dumka, Kiev (1977), p. 75.
6. V. I. Badanin and V. A. Nikolaev, Metalloved. Term. Obrab. Met., No. 9, 21 (1979).
7. V. I. Badanin et al., Inventor's Certificate No. 528161, Byull. Izobret., No. 34, 30 (1976).
8. L. Steele and J. Hawthorne, New Information on Neutron Embrittlement and Embrittlement Relief of Reactor Pressure Vessel Steels, ASTM STP 380, 283 (1965).
9. V. A. Nikolaev, V. V. Rybin, and V. I. Badanin, in: Effect of Impurities on the Radiation Embrittlement of Low-Alloyed Steel. Physics of Brittle Failure. Collection of Reports of the Third All-Union Conference, Kiev [in Russian], Institute of Problems of Material Behavior of the Academy of Sciences, Ukrainian SSR, Pt. 2 (1976), p. 89.
10. Phase Diagrams of Metal Systems, Issue 15 [in Russian], All-Union Institute of Scientific and Technical Information, Moscow (1970), p. 226.
11. V. A. Nikolaev, Problems of Nuclear Science and Technology. Series: Physics of Radiation Damage and Radiation Material Behavior [in Russian], No. 2 (13) (1980), p. 47.

12. F. Smidt and H. Watson, Metal. Trans., 3, 2065 (1972).
13. Yu. A. Nekhendzi, Cast Steel [in Russian], Metallurgizdat (1948).
14. V. I. Badanin and V. A. Nikolaev, At. Energ., 41, No. 3, 209 (1976).
15. A. E. Vol, Structure and Properties of Binary Metallurgical Systems [in Russian], Vol. 2, Moscow (1962), p. 749.
16. E. Little and D. Harries, Metal. Sci. J., 27, 701 (1970).
17. G. Seidel, Phys. Status Solidi, 25, 175 (1968).
18. A. Cottrell, Philos. Mag., 44, 829 (1953).
19. L. Steele, Neutron Irradiation Embrittlement of Reactor Pressure Vessel Steels, IAEA, Vienna (1965).

EROSION OF Fe—Cr—Ni ALLOYS AND VANADIUM ALLOYS DURING BOMBARDMENT WITH HELIUM IONS

B. A. Kalin, I. I. Chernov, V. L. Yakushin,
V. I. Badanin, I. P. Kursevich,
V. A. Nikolaev, and V. N. Kulagin

UDC 621.039.531

Austenitic heat-resistant alloys and alloys of refractory metals, in particular vanadium, are considered to be prospective structural materials for thermonuclear reactors. It has been established that these materials are subjected to considerable erosion in consequence of helium blistering, and it is well known that the nature and degree of damage to the surface by blistering depends on the alloying and purity of the starting material. Because of this, a comparative investigation was carried out of the erosion of a number of trinary Fe—Cr—Ni alloys with fcc lattices and alloys of vanadium with bcc lattices, by bombardment with helium ions with energies of up to 40 and 100 keV at a temperature of 290-970°K and an ion dose of $(8-50)\cdot10^{21}$ m^{-2}. The chemical composition and heat treatment of the alloys are given in Tables 1 and 2. All the alloys are homogeneous solid solutions with dispersed se-

TABLE 1. Chemical Composition, Treatment, and Certain Mechanical Properties (at 290°K) of Vanadium Alloys*

Item No.	Material	Treatment	Melt	Mass fraction of elements, %					σ_u, MPa	δ, %	H_μ, MPa
				V	Ti	C	H	others			
1	VÉL-2	CD	I	Base	—	0,02	$1\cdot10^{-3}$	0,01Al	335	—	1550±120
2	VTsU	TO-1	I	Same	—	0,4	$5\cdot10^{-3}$	0,03Fe 2,5Zr	410	20	1080±100
3	V—7Nb	TO-2	I	» »	—	0,017	$3\cdot10^{-3}$	0,01Y 7,0Nb	540	18	2040±180
4	V—14Nb	TO-2	I	» »	—	0,017	$3\cdot10^{-3}$	14,0Nb	635	17	2590±230
5	V—8Cr	TO-2	I	» »	—	0,016	$3\cdot10^{-3}$	8Cr	515	18	1870±150
6	V—5Ti	TO-2	I	» »	5,0	0,017	$4\cdot10^{-3}$	—	445	15	1780±180
7	V—15Ti	TO-2	I	» »	15,0	0,017	$4,5\cdot10^{-3}$	—	770	9	2020±200
8	V (technical)	TO-2	L	» »	—	0,035	$2\cdot10^{-4}$	—	—	—	1890±180
9	V—10Ti	TO-2	L	» »	10	0,046	$1,2\cdot10^{-4}$	—	—	—	1990±190
10	V—20Ti	TO-2	L	» »	20	0,034	$2,9\cdot10^{-4}$	—	—	—	2020±200
11	V—30Ti	TO-2	L	» »	30	0,033	$1,7\cdot10^{-4}$	—	—	—	2170±220
12	V—40Ti	TO-2	L	» »	40	0,037	$4\cdot10^{-4}$	—	—	—	2320±230

*CD — cold deformation; TO-1 and TO-2 — annealing at 1470 and 1370°K during 1 h, respectively; I, L — industrial and laboratory melts.

Translated from Atomnaya Énergiya, Vol. 57, No. 3, pp. 173-178, September, 1984. Original article submitted December 8, 1983.

0038-531X/84/5703-0613$08.50

TABLE 2. Chemical Composition, Treatment, and Microhardness (at 290°K) of Fe–Cr–Ni Alloys

Material	Thermal treatment	Mass fraction of elements, %			H_μ, MPa
		Fe	Cr	Ni	
Kh20N15	1270 K, 1h	Base	20	15	1435±145
Kh20N25	1270 K, 1h	Same	20	25	1295±130
Kh20N35	1270 K, 1h	» »	20	35	1300±130
Kh20N45	1270 K, 1h	35	20	45	1315±130
Kh20N55	1270 K, 1h	25	20	55	1320±130
Kh20N80	1270 K, 1h	—	20	80	1335±135
Ni(99.98%)	1070 K, 1h	—	—	Base	—

TABLE 3. Coefficients of Erosion of Vanadium Alloys, Irradiated with He^+ Ions, 10^{-2} atom/ion

Material	$E = 40$ keV, $D = 2 \cdot 10^{22}$ m^{-2}					$E = 100$ keV, $D = 5 \cdot 10^{22}$ m^{-2}
	370–420 K	570 K	670 K	770 K	870 K	
VÉL-2	10±3	14±4	18±5	19±5	14±4	14±3
VTsU	27±7	29±7	11±3	6±2	~ 0	19±5
V–7Nb	27±7	56±14	—	3±1	~ 0	59±15
V–14Nb	18±5	40±10	39±10	0,3±0,1	~ 0	24±6
V–8Cr	31±8	58±15	33±8	15±4	~ 0	105±30
V–5Ti	28±7	95±24	110±27	60±15	~ 0	77±19
V–15Ti	5±2	40±10	35±9	33±8	15±4	33±8

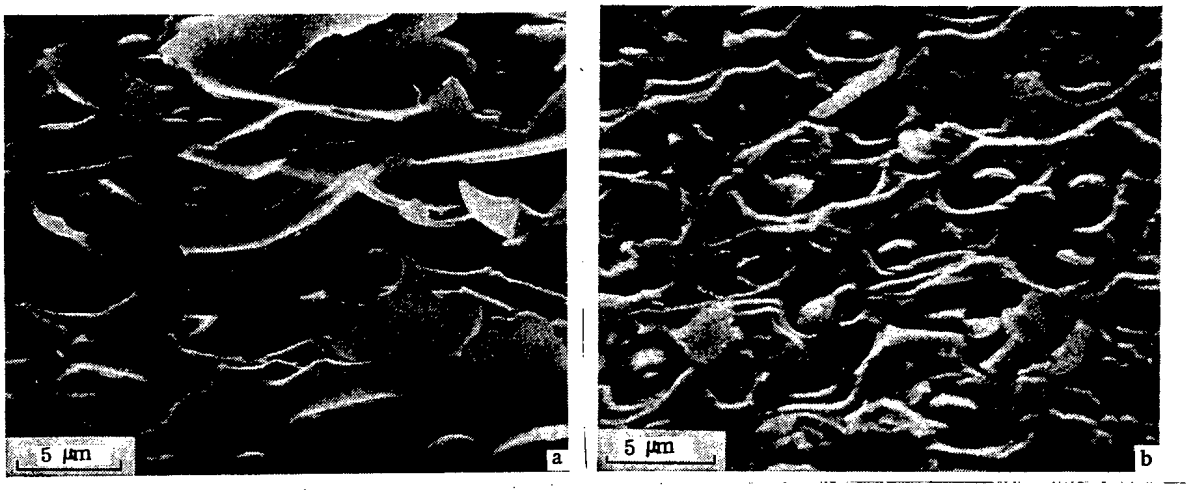

Fig. 1. Surface erosion of V-8Cr alloy, irradiated at 420°K with He^+ ions with energy 40 keV up to a dose of $2 \cdot 10^{22}$ m^{-2} (a) and at 770°K with He^+ ions with energy 100 keV up to a dose of $5 \cdot 10^{22}$ m^{-2} (b).

gregation of the carbide phase. The bombardment of the electropolished samples was conducted in the ILU-3 ion accelerator [1] by the cassette method: 8 targets with a size of 4.5 × 8 mm were clamped with a cover in the cells of a metal cassette and irradiated by horizontal scanning with a beam of helium ions. The procedure ensured completely identical bombardment conditions of all samples. The surface of the irradiated samples was investigated on an RÉM-200 scanning electron microscope. The coefficient of erosion was calculated from an electrom-microscope photograph of the surface, using the well-known procedure [2].

Vanadium Alloys. The results of the electron-microscope investigation of industrial alloys of vanadium, irradiated with He^+ ions with energy 40 and 100 keV, are shown in Table 3, and typical photographs of the surface topography are shown in Fig. 1. Analysis of the results allowed a number of the special features of erosion of the samples investigated to be explained.

The temperature dependence of the erosion of the alloys is found to be identical and is characterized by a maximum. As seen from Table 3, in the case of the alloying of vanadium with Zr and C (VTsU alloy), Cr, Nb, and Ti, the temperature range of intensive scaling is extended and moves into the region of lower temperature; the coefficient of erosion S also is increased in comparison with that observed for pure vanadium of the electron-beam melt (VÉL-2). In consequence of the effect of alloying additives on the temperature corresponding to the maximum scaling, the nature and degree of damage to the surface with identical irradiation

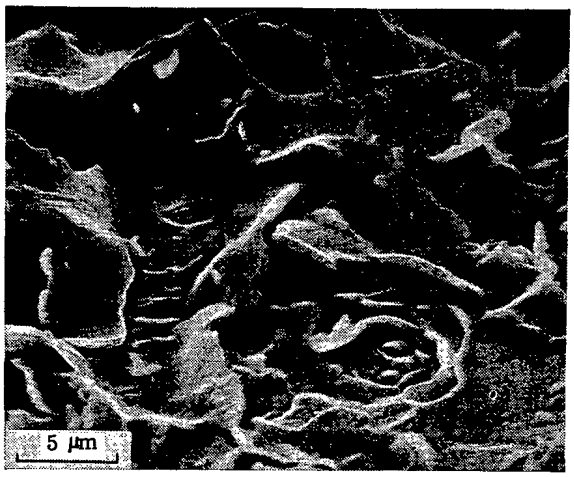

Fig. 2. Surface erosion of vanadium VTsU, irradiated at 770°K with He^+ ions with energy 100 keV up to a dose of $5 \cdot 10^{22}$ m^{-2}.

TABLE 4. Dependence of the Coefficient of Erosion in Consequence of Scaling of Fe–Cr–Ni Alloys on the Nickel Content and the Temperature, during Irradiation with He^+ Ions with Energy 40 keV up to a Dose of $1 \cdot 10^{22}$ m^{-2}, 10^{-2} atom/ion

Material	T, °K				
	290	470	670	770	970
Kh20N15	28±6	59±12	69±14	21±4	0
Kh20N25	32±6	72±14	88±18	⩽5	0
Kh20N35	21±4	38±8	55±11	~0	0
Kh20N45	10±2	13±3	34±7	~0	0
Kh20N55	18±4	42±8	58±12	<1	0
Kh20N80	24±5	48±10	60±12	<1	0
Ni	(18±4)*	(32±6)†	5±1	<1	0

*At T = 370°K.
†At T = 570°K.

conditions are different. As seen from Table 3 and Fig. 1, at 370-420°K two-layer scaling of the surface takes place and the alloys V–8Cr, V–5Ti, V–7Nb, and VTsU have maximum values; at 570-670°K, the alloys V–Ti, V–Cr and V–Nb are characterized by maximum erosion, and the alloy VTsU by minimum erosion. At a temperature of 770°K, the alloys V–Nb and VTsU have the maximum erosion. High-temperature undamaged blisters are observed on the majority of alloys investigated at T ⩾ 870°K; however, in the case of VÉL-2 and V-15Ti, even more scaling is observed (see Table 3).

As a result of the irradiation of the alloys with He^+ ions with energy 100 keV up to a dose of $5 \cdot 10^{22}$ m^{-2} at 770°K, a change of nature and degree of erosion was detected (see Table 3): for the alloy V–8Cr, four layers of scaling with blisters in deep craters (see Fig. 1b); for the alloy V–5Ti, six layers; and for the alloy V–7Nb, three layers. The minimum erosion is observed for the alloys of vanadium VTsU (Fig. 2) and VÉL-2.

The data presented confirm the complex dependence of the erosion stability of the alloys on the composition, temperature of irradiation, and energy of the ions, in view of which a systematic investigation was conducted of the erosion of vanadium alloys with mass fractions of titanium from 0 to 40% (see Table 1, items 8-12).

The results of the electron-microscope investigation of the irradiated V–Ti alloys are presented in Figs. 3 and 4. Damage to the surface of the alloys varies in a complex way in proportion with increase of the titanium content (see Fig. 3); the coefficient of erosion

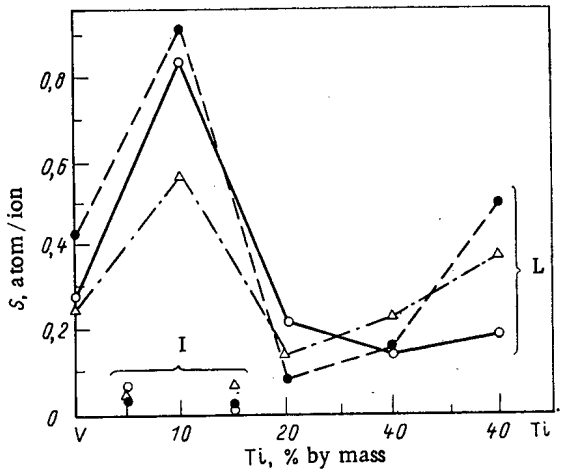

Fig. 3

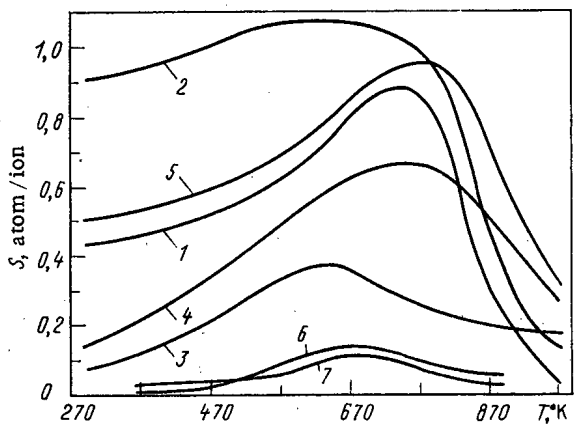

Fig. 4

Fig. 3. Dependence of the coefficients of erosion of alloys of V—Ti, melts L and I, on the titanium content, as a result of irradiation with He^+ ions with energy 40 keV and $T_{irr} \leq 370°K$, with doses of $8 \cdot 10^{21}$ m^{-2} (○); $1 \cdot 10^{22}$ m^{-2} (●) and $1.5 \cdot 10^{22}$ m^{-2} (Δ).

Fig. 4. Temperature dependence of the coefficients of erosion of alloys of melts L (1-5) and I (6, 7), irradiated with He^+ ions with energy 40 keV, up to a dose of $1 \cdot 10^{22}$ m^{-2}; 1) vanadium, technical; 2) alloy V—10Ti; 3) V—20Ti; 4) V—30Ti; 5) V—40Ti; 6) V—5Ti; 7) V—15Ti.

decreases at first and then increases. The increased erosion of the alloy V-10Ti, apparently, is caused by the increased concentration of carbon (see Table 1). The relation between the coefficients of erosion of the alloys and vanadium is maintained over a wide temperature range (see Fig. 4), approximately up to 770°K, which confirms the stable effect of titanium. At a temperature in excess of 770°K, erosion of the alloy is reduced sharply and with increase in the titanium content the range of scaling is increased on the side of higher temperature. With a low carbon concentration (I melt), the erosion of alloys with a mass fraction of titanium of 5 and 15% is reduced considerably, as this follows from Figs. 3 and 4 and Table 3.

According to the electron-microscope photographs, the increase in the coefficient of erosion of vanadium alloys as a result of alloying is caused by scaling (flaking of large sections of the surface), and the reduction of the coefficient of erosion is explained by flaking of the domes of individual blisters, and a reduction of the carbon content suppresses the flaking and stimulates the formation of blisters. Thus, alloying of vanadium with substitution elements (Nb, Cr, and Ti), strengthening the solid solution, increases the temperature range of intensive scaling, and in the system of V—Ti alloys, alloys with 20-30% of titanium have the maximum erosion.

Fe—Cr—Ni Alloys. The results of the electron-microscope investigation of samples of these alloys are presented in Tables 4 and 5 and in Fig. 5.

All the alloys investigated were subjected to radiation erosion at $T < 770°K$. The dependence of the coefficient of erosion on the nickel content in the alloys has a nonlinear nature (see Table 4): alloys with a mass fraction of nickel of 35-45% (see Fig. 5a) and pure nickel are subject to the minimum erosion, and alloys with a mass fraction of 15-25% and 80% (see Fig. 5b) are subject to the maximum erosion. The same regularity is observed for all temperature values investigated. At 670°K the first pores appear in pure nickel along the boundaries ($S \approx 0.05$ atom/ion), while for Fe—Cr—Ni alloy the maximum erosion is observed ($S = 0.88$ atom/ion). No pores were detected on the surface of the alloys right up to a temperature of 970°K, and at $T \geq 770°K$ high-temperature blisters are observed, the parameters depending on the content of nickel in the alloys (see Table 5). The distribution of these blisters by size is characterized by two peaks, and with increase in the nickel content in the alloys up to a mass fraction of 45%, the density of fine blisters ($d \leq 0.5$ μm) is reduced. At 770°K the coarsest, most frequently ruptured blisters with the least density are observed in alloy Kh20N15, and the coefficient of erosion amounts to 0.21 atom/ion (see Table 4).

TABLE 5. Parameters of the Blisters in Fe–Cr–Ni Alloys Irradiated at 770°K with He^+ Ions with Energy 40 keV up to a Dose of $1 \cdot 10^{22}$ m^{-2}

Alloy	d_{max}, μm	$\rho \cdot 10^{-10}$, m^{-2}		
		ρ ($d \leq 0,5$ μm)	ρ ($d > 0,5$ μm)	ρ_{tot}
Kh20N15	4,9	21,9	8,5	30,4
Kh20N25	3,3	8,8	17,7	26,5
Kh20N35	2,7	3,3	21,6	24,9
Kh20N45	3,2	0	22,3	22,3
Kh20N55	3,5	0	24,9	24,9
Kh20N80	3,6	0	24,6	24,6

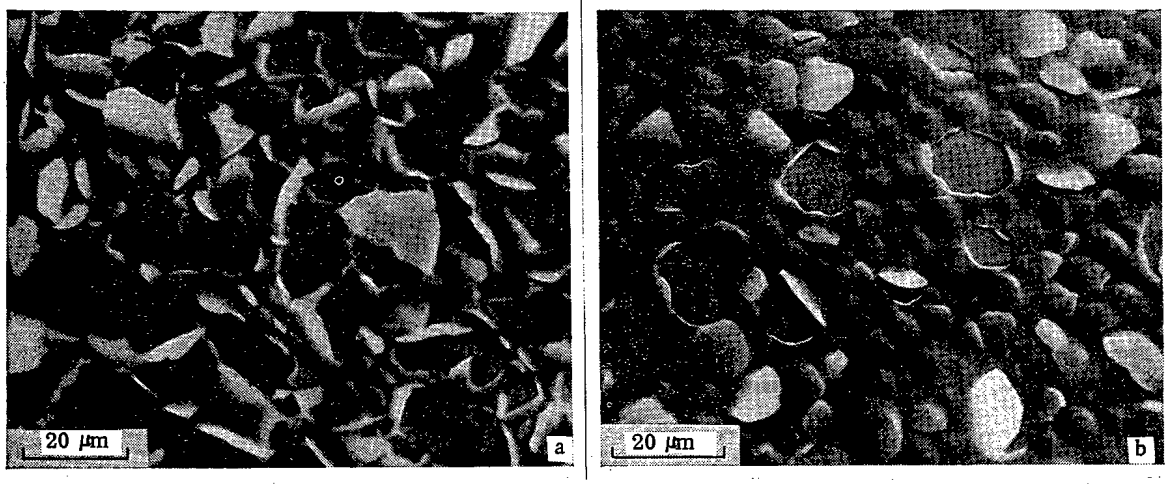

Fig. 5. Surface erosion of alloys Kh20N45 (a) and Kh20N15 (b), irradiated at 470°K with He^+ ions with energy 40 keV up to a dose of $1 \cdot 10^{22}$ m^{-2}.

With increase in the nickel content, the density of the coarse blisters ($d > 0.5$ μm) is increased, their sizes are reduced, and the coefficient of erosion does not exceed 0.05 atom/ion. In the alloy Kh20N15, flaking of the surface ceases at a higher temperature than in other alloys and pure nickel.

Discussion of Results. The majority of researchers relate the degree of surface damage with the mechanical properties of the materials and their structure [3-6]. Therefore, it is advantageous to carry out the analysis of the results obtained in the light of these concepts.

The materials investigated, according to their crystal structure, can be divided into two groups: with bcc and fcc lattices; however, they all are solid solutions of alloying substitution and implantation elements. The set of experimentally obtained data and the results of previous investigations [6-9] confirm the existence of two general tendencies. First, with identical irradiation conditions the materials with the bcc lattice (for example, refractory metals and their alloys) are less damaged by erosion than austenitic steels and alloys with an fcc lattice. Hence it follows that the process determining the blistering depends not only on the mechanical properties but also on the characteristics of the crystal structure of the material. Second, the irradiation erosion of the solid solutions is intensified with increase in the number and content of alloying elements. For example, complexly alloyed steels and nickel and vanadium alloys are characterized by large erosion in comparison with less alloyed solid solutions [7-9] (see Table 3). Therefore, it can be supposed that the high short-duration and long-duration durability and high resistance to stress relaxation intensify the surface radiation damage.

If the surface damage is determined by the properties of the material, then a monotonic change of the coefficient of erosion would be expected, as the mechanical properties of the alloys, in particular the tensile strength usually increase in proportion with increase in concentration of the alloying elements up to 50% approximately. However, the experiments

TABLE 6. Change of Electron Configuration, Electron Density (ρ_e), and Average Size of the Ions ($\bar{r}_i$) in Alloys

Composition of alloy by mass, %	Electron configuration	Characteristic valence	ρ_e, electrons/atom	$\bar{r}_i$, nm
V	$3d^34s^2$	5	5,00	0,0400
95V—5Ti	—	—	4,95	0,0412
90V—10Ti	—	—	4,90	0,0424
85V—15Ti	—	—	4,85	0,0436
80V—20Ti	—	—	4,80	0,0448
70V—30Ti	—	—	4,70	0,0472
60V—40Ti	—	—	4,60	0,0496
Ti	$3d^24s^2$	4	4,00	0,0640
92V—8Cr	—	—	5,08	0,0396
Cr	$3d^54s^1$	6	6,00	0,035—0,058
93V—7Nb	—	—	5,00	0,0420
86V—14Nb	—	—	5,00	0,0441
Nb	$4d^45s^1$	5	5,00	0,0690
Fe	$3d^64s^2$	3	3,00	0,0650
80Fe—20Cr	—	—	3,00	0,0664
65Fe—20Cr—15Ni	—	—	2,85	0,0675
55Fe—20Cr—25Ni	—	—	2,75	0,0682
45Fe—20Cr—35Ni	—	—	2,65	0,0689
35Fe—20Cr—45Ni	—	—	2,55	0,0696
20Fe—80Ni	—	—	2,20	0,0720
Cr	$3d^54s^1$	3	3,00	0,0600
Ni	$3d^84s^2$	2	2,00	0,0600

confirm the deviation from the expected monotonic change of the coefficient of erosion in proportion with increase of the alloying elements (see Tables 3 and 4 and Fig. 3) in solid solutions with bcc and fcc lattices.

It may be supposed that a change of erosion with a change of concentration of the alloying additives must correlate with a corresponding change of state of the solid solutions and their properties, in particular the structure of the outer electron shells and the sizes of the ions [10]. The resistance of metals to plastic deformation depends on the nature of the packing of the atoms and the electron density, but the resistance to damage is determined predominantly by the electron density, i.e., by the binding energy. If we suppose that the number of collectivized electrons is proportional to the characteristic valence of the elements occurring in the alloys, then a definite similarity can be traced of the change of electron density and the sizes of the ions in the systems V—Ti and Fe—Cr—Ni. It is shown in Table 6 how the electron density in the calculation per atom of alloy and the average radius of the ions in the alloy vary:

$$\bar{r}_i = \sum r_{M_i} C_i / 100,$$

where r_{M_i} is the radius of the ion of the i-th metal M with the characteristic valence, and C_i is the concentration of metal atoms. It can be seen from Table 6 that in both systems the electron density calculated per single atom is reduced in proportion with the increase of the content of one of the alloying components in the alloy, and the average size of the ions and, consequently, the interatomic distance increase. Thus, two parameters are varied simultaneously, which are responsible for the monotonic reduction of the thermodynamic and strength characteristics.

In consequence of the characteristics of the interaction of the electron shells of the atoms in alloys of the systems V—Ti, V—Nb, V—Cr, and Fe—Cr—Ni, the concentration curve of the high-temperature strength is characterized by two maxima, displaced to the side of both pure components (for example, vanadium and the alloying element), and this effect appears around the recrystallization temperature and is temperature-dependent. The presence of the maximum of strength in the region of a small concentration of alloying elements can be explained qualitatively, first, by the marked difference between the coefficients of erosion of alloys similar in composition and, second, by the change of ratio between the coefficients of erosion with increase of irradiation temperature (see Table 3). When analyzing the diagram of the change of tensile strength and the limit of plasticity of alloys of the systems

V—Ti, V—Nb, and V—Cr, it was established [11] that the change of mechanical properties corresponds to the concepts concerning the existence of the two maxima. With the addition of chromium and titanium, the strength is increased markedly and the plasticity is reduced, and particularly sharply by alloying with chromium. This corresponds to the maximum values of erosion of the alloys (see Table 3). Alloying with small additions of titanium, however, causes a reverse change of σ_u and δ. The introduction of refining titanium (5% by mass) into the vanadium causes a sharp increase of σ_u and a reduction of δ, in complete accordance with the nature of the change of erosion of alloys with a low carbon content (melt I), when the erosion minimum is observed with a mass fraction of 5% titanium. However, an increase in the carbon concentration (melt L) sharply changes the erosion pattern (see Figs. 3 and 4), in that the erosion maximum for a mass fraction of 10% titanium and a mass fraction of 0.046% of carbon evidently is caused by the significant strength of the alloy and by the reduction of its plasticity in consequence of the formation of dispersed carbides of titanium. Alloying of vanadium with titanium and carbon promotes an increase in the energy of activation of creep by the increase of the high-temperature strength and, as a consequence of this, erosion at 970°K increases because of the widening of the range of flaking in the high-temperature region in the series V → V—10Ti → V—20Ti → V—30Ti → V—40Ti. The monotonic change of strength and of the coefficient of erosion is observed with a relatively identical content of the implanted impurities (see Table 1). On the whole, it is necessary to note the extremely strong influence of implantation impurities (especially carbon) on the change of the coefficients of erosion of alloys with a bcc lattice.

The implantation impurities also play a special role in fcc metals [8], having increased octahedral vacancies and characterized by an increased solubility of carbon. The effect of the implanted impurities in the solid solution is determined by the elastic dilation of the fcc lattice because of the difference in the sizes of the cation and the vacancies [12]. It was established [8, 13] that with increase in the content of implantation impurities and, first and foremost, carbon, nitrogen, and boron, the erosion of austenitic materials is intensified, whereas a decrease in their concentration in consequence of double vacuum remelting or heat treatment of the alloys in casting leads to a reduction of the surface scaling. An important mechanism for the intensification of erosion was also discovered [8] in consequence of the distribution of implantation impurities throughout the depth of the target and their buildup in the surface layer during ion bombardment, as a result of which the strength is increased significantly and the plasticity of the irradiated layer is reduced. Based on these concepts, it is easier to explain the increased erosion in trinary Fe—Cr—Ni alloys with a mass fraction of nickel > 45%. An increase in the content of Ni reduces the ability of austenitic alloys to carbide formation and increases the amount of unbound carbon in the solid solution; moreover, diffusion of the carbon is accelerated, which must promote segregation of the carbon in the surface layer during ion irradiation. Thus, with an identical total content of carbon, Fe—Cr—Ni alloys with a mass fraction of nickel of more than 45% under the influence of both these factors must be characterized by increased erosion.

In conclusion, it should be noted that the experimentally obtained coefficients of erosion as a result of irradiation with He^+ ions characterize the special features of surface damage in the final stage of blister formation and, in conjunction with the results of earlier investigations [6, 8, 13], confirm unambiguously that the well-known correlation of the coefficients of erosion with the mechanical characteristics is possible only for materials with identical structural-phase state, and these characteristics must be obtained for the surface layer. Unambiguous conformity between radiation erosion and the mechanical macroproperties of the material is hardly possible, since with ion irradiation deformation and damage take place in a thin surface layer, and the diameters of the blisters usually are less than the grain size.

LITERATURE CITED

1. V. M. Gusev, N. P. Busharov, and S. M. Naftulin, "The 100-keV ILU ion accelerator with ion separation by mass," Prib. Tekh. Eksp., 4, 19-25 (1969).
2. A. D. Gurov, B. A. Kalin, N. M. Kirilin, et al., "Temperature dependence of erosion of stainless steels during ion irradiation," At. Energ., 40, No. 3, 254-255 (1976).
3. W. Bayer, J. Nucl. Mater., 76-77, 3-5 (1978).
4. Yu. V. Martynenko, "Theory of blistering," Preprint IAÉ-3145, Moscow (1979), p. 40.
5. M. Rich et al., in: Proceedings of an International Symposium on Plasma-Wall Interaction, Pergamon Press, New York (1977), pp. 391-400.

6. B. A. Kalin, D. M. Skorov, and V. L. Yakushin, Investigation of Radiation Erosion of Structural Materials during Irradiation with Helium Ions. Problems of Nuclear Science and Technology. Series Physics of Radiation Damage and Radiation Material Behavior [in Russian], No. 2(13) (1980), pp. 72-81.
7. B. A. Kalin, N. M. Kirilin, A. A. Pisarev, et al., "Temperature dependence of the erosion of alloys of vanadium and niobium during irradiation with helium ions," At. Energ., 42, No. 1, 13-15 (1977).
8. E. E. Goncharov, M. I. Guseva, B. A. Kalin, et al., "Effect of thermal treatment and alloying on the radiation erosion of austenitic stainless steels and alloys," At. Energ., 53, No. 4, 243-250 (1982).
9. B. A. Kalin, D. M. Skorov, and V. L. Yakushin, "Investigation of the methods of increasing the lifetime of the primary wall of a thermonuclear reactor," in: Reports of the Second All-Union Conference on Engineering Problems of Thermonuclear Reactors [in Russian], Vol. 4, D. V. Efremov Scientific-Research Institute of Electrophysical Equipment, Leningrad (1982), pp. 61-68.
10. V. K. Grigorovich, Flame-Resistance and Phase Diagrams [in Russian], Metallurgiya, Moscow (1969), p. 324.
11. Yu. V. Efimov, V. V. Baron, and E. M. Savitskii, Vanadium and Its Alloys [in Russian], Nauka, Moscow (1969), p. 254.
12. V. K. Grigorovich and E. N. Sheftel', Dispersion Hardening of Refractory Metals [in Russian], Nauka, Moscow (1980), p. 304.
13. N. M. Beskorovainyi, B. A. Kalin, V. N. Kulagin, et al., "Effect of alloying, thermal treatment and aging in casting on the radiation erosion of stainless steels of type 16-15," Poverkhnost'. Fiz.- Khim. Mekh., No. 10, 83-90 (1983).

RESONANCE EFFECTS IN THE INTERACTION OF 0.2-0.8-MeV NEUTRONS WITH ^{56}Fe NUCLEI

A. A. Sarkisov, I. N. Martem'yanov,
A. M. Boguslavskii, V. N. Ivanov,
and G. N. Ivanov

UDC 539.17

Calculations of individual components of nuclear reactors and radiation shields require detailed knowledge of the energy and angular distributions of neutrons described by the transport equation. The solution of this equation involves poorly known values of the parameters $\langle\sigma_{tot}\rangle$, $\langle\sigma_s\rangle$, $\langle 1/\sigma^k_{tot}\rangle$, $\langle\sigma_s\omega_l\rangle\left\langle\frac{\sigma_s\omega_l}{\sigma^k_{tot}}\right\rangle$, $f_{tot}(0)$, and $f_s(0)$, which characterize the structure of the neutron total and partial interaction cross sections of elements which comprise the reactor and shield. The symbol $\langle\ \rangle$ denotes the average over the energy range considered.

Preliminary estimates of a number of physical characteristics (group-averaged cross sections, asymptotic relaxation length, average logarithmic decrement, etc.) for iron show 20-30% differences in the values calculated with and without taking account of resonance shielding of the cross sections. Thus, the asymptotic relaxation length of 1-2-MeV neutrons in iron, calculated from experimental data with allowance for the effect of shielding in the P_4 approximation, is 7.9 ± 0.7 cm. The value of this same quantity calculated without taking account of the resonance structure of the cross sections is 6.1 cm [1].

Results of studies of the structure of the neutron total scattering cross section of iron in the ranges 1.5-10 MeV, 1-2 MeV, and 2.5-5.24 MeV are given in [2-4]. In the present article we report on measurements in the 0.2-0.8-MeV energy range made by using a horizontal channel of the IR-100 research reactor [5]. The equipment was arranged according to the principle of central geometry, with the extraction of the neutron beam through a collimating system. The total collimation length of 4.1 m and a diameter of 0.046 m ensured "good" geometry.

Translated from Atomnaya Énergiya, Vol. 57, No. 3, pp. 179-182, September, 1984. Original article submitted July 28, 1983.

0038-531X/84/5703-0620$08.50

We took account of the effect of shielding in the transmission of neutrons through extended layers of shielding materials by using the method of resonance filters proposed by M. N. Nikolaev. Resonance neutrons were removed from the beam by extended filters made of the material under investigation. A thin scatterer was also made of the same material. Cylindrical filters 0.05 m in diameter were made of 98% ^{56}Fe, and the scatterers were a set of thin-walled shells 0.05 m high and of various wall thicknesses. This permitted the experimental determination of the effect of multiple neutron scattering. By placing the scatterer "in the beam" and "outside the beam," the background effects could be determined.

The following quantities were measured directly in the experiment on filtered neutron beams: N(t), the rate of counting neutrons which passed through a filter of thickness t without interaction and entered the detector at the location of the scatterer; N(t, μ), the rate of counting neutrons which passed through the filter and were scattered through an angle $\Theta = \cos^{-1}\mu$; N(0), the counting rate in the direct beam with no filter or scatterer present. Neutrons were recorded with a 30 × 30 mm stilbene scintillation counter with n–γ pulse-shape discrimination. For an n–γ separation efficiency of almost 100%, the energy threshold of the apparatus was ∿ 100 keV, and the degree of discrimination against gamma rays was 10^{-4}. Measurements were performed for filter thicknesses of 0, 0.02, 0.06, 0.10, 0.14, 0.18, and 0.22 m and at 10 angles for which the cosine of the scattering angle varied from 0.9 to –0.9 in 0.2 steps.

The important characteristics of the medium, taking account of the resonance structure of the cross sections, are expressed in terms of the parameters N(t), N(t, μ), and N(0):

the scattering cross section for neutrons which passed through a filter of thickness t and after scattering remained within the limits of the group being studied:

$$\langle\sigma_s(t,\ \mu)\rangle = \frac{R^2}{4\pi n}\,\frac{N(t,\mu)}{N(t)}\ ; \tag{1}$$

the group-averaged integral microscopic scattering cross section for neutrons transmitted through a filter of thickness t; this is found by integrating Eq. (1) over the cosine of the scattering angle from –1 to + 1;

the total transmission function for a filter thickness t:

$$T(t) = \frac{N(t)}{N(0)}\ ; \tag{2}$$

the group-averaged microscopic total cross sections for the interaction of neutrons with nuclei for a filter thickness t, neglecting resonance shielding:

$$\langle\sigma_{tot}\rangle = \lim_{t\to 0}\frac{d}{dt}\left\{\frac{\int_{2,5}^{5,24} dE\eta(E)\varphi(E)\exp[-\Sigma_{tot}(E)t]}{\int_{2,5}^{5,24} dE\eta(E)\varphi(E)}\right\}, \tag{3}$$

where $\varphi(E)dE$ is the neutron spectrum at the exit of the horizontal channel, and $\eta(E)$ is the detector sensitivity function.

TABLE 1. Average Microscopic Neutron Total Interaction and Scattering Cross Sections of Iron for Various Filter Thicknesses, b*

Energy range, MeV	Filter thickness, m						
	0	0,02	0,06	0,10	0,14	0,18	0,22
				Total cross sections			
0,8–0,4	3,3±0,7	3,1±0,1	3,0±0,1	2,8±0,2	2,7±0,2	2,5±0,2	2,4±0,3
0,4–0,2	3,03±0,09	2,9±0,2	2,8±0,2	2,6±0,2	2,5±0,2	2,3±0,3	2,2±0,3
				Scattering cross sections			
0,8–0,4	3,30±0,06	3,10±0,08	2,9±0,1	2,8±0,1	2,6±0,2	2,5±0,2	2,4±0,2
0,4–0,2	3,00±0,09	2,90±0,10	2,8±0,1	2,5±0,2	2,4±0,2	2,3±0,3	2,2±0,3

*1 b = 10^{-28} m^2.

TABLE 2. Subgroup Parameters for Iron Samples

Energy range, MeV	j	a_j^i	σ_{tot}^j, b
0,8—0,4	1	0,68±0,03	3,89±0,08
	2	0,32±0,03	1,58±0,02
0,4—0,2	1	0,83±0,04	3,49±0,07
	2	0,17±0,04	1,25±0,02

TABLE 3. Microscopic Characteristics of the Structure of Total Cross Sections for Iron Samples

Energy range, MeV	$\langle 1/\sigma_{tot}\rangle$, b	$\langle 1/\sigma_{tot}^2\rangle$, $\frac{1}{b^2}$	$\langle\sigma_{tot}\rangle$, b	$\bar{\sigma}_{tot}$, b	$f_{tot}(0)$
0,8—0,4	0,43±0,2	0,24±0,01	3,33±0,07	1,78±0,02	0,53±0,4
0,4—0,2	0,40±0,01	0,233±0,008	3,05±0,04	1,70±0,01	0,56±0,4

TABLE 4. Group Characteristics of the Resonance Structure of the Neutron Differential Scattering Cross Sections of Iron

Energy range, MeV	$\langle\sigma_s\omega_l\rangle$			$\langle\sigma_s\omega_l/\sigma_{tot}^k\rangle$		
	$l=0$	$l=1$	$l=2$	$l=0$	$l=1$	$l=2$
			$k=1$			
0,8—0,4	1,88±0,3	0,170±0,009	0,018±0,002	1,06±0,02	0,095±0,007	0,010±0,001
0,4—0,2	1,58±0,03	0,130±0,008	0,014±0,001	0,93±0,02	0,076±0,006	0,008±0,001
			$k=2$			
0,8—0,4	1,06±0,02	0,999±0,008	0,014±0,002	0,59±0,01	0,045±0,007	0,006±0,001
0,4—0,2	0,93±0,01	0,078±0,007	0,009±0,001	0,55±0,01	0,045±0,006	0,005±0,001

The values of the group-averaged total and scattering cross sections are shown in Table 1 as functions of the filter thickness. The averaging was performed over the energy ranges taken in BNAB-78. The cross sections clearly diminish with increasing filter thickness. In the experimental determination of the effective cross sections the neutron energy intervals were chosen from the results of the calibration of the spectrometer by using a set of OSGI standard gamma sources and changing the light output by the method of "known cross sections" [6].

Our values of the group-averaged neutron microscopic total interaction cross sections of iron are about 13% larger than the values in [7], which were obtained by using filters of thickness zero and 19.95 cm. For the range 0.4-0.2 MeV the experimental results are in satisfactory agreement with the BNAB-78 values. For the range 0.8-0.4 MeV our values of the total and scattering cross sections are 13% smaller than the BNAB-78 values.

Analysis of the total transmission functions and their approximation by a sum of exponentials, the choice of the initial approximations, and the determination of the statistical weight of the experimental points made it possible to determine the parameters a_j^i and σ_{tot}^j of the total cross section for the groups considered. In the energy range ΔE of a group the parameter a_j^i determines the fraction of the whole group i occupied by the subgroup j, and the σ_{tot}^j are the subgroup microscopic cross sections. The analysis was performed by the method of least squares and linearization of the approximating function with iterations [8]. The results of the studies of the subgroup parameters are listed in Table 2.

We resolved the total transmission function into two exponentials, whereas in [8] three were used. The transmission curve deviates from exponential in the energy range considered.

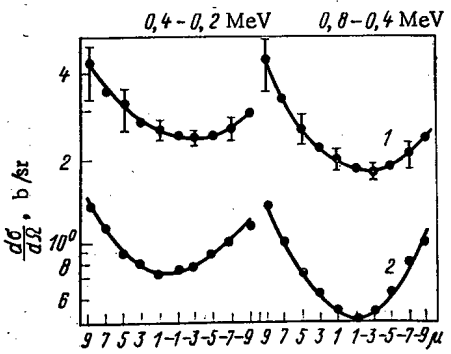

Fig. 1. Angular distributions of unfiltered neutrons, and difference angular distributions of unfiltered and filtered 0.8-0.2-MeV neutrons scattered by ^{56}Fe as measured behind 14-cm-thick extended shields.

The experimental data permitted a determination of the group characteristics of the resonance structure of the neutron total interaction cross sections:

the moments of the total cross section taking account of shielding

$$\left\langle \frac{1}{\sigma_{tot}^k} \right\rangle = \frac{1}{(k-1)!\,\rho N(0)} \int_0^{t_{max}} dt\, t^{k-1} N(t). \tag{4}$$

Since the effect of resonance shielding in the cross sections is determined mainly by the first and second moments, we took k = 1 and 2 in the calculations;

the average neutron total interaction cross sections taking account of resonance shielding

$$\bar{\sigma}_{tot} = \frac{\langle 1/\sigma_{tot} \rangle}{\langle 1/\sigma_{tot}^2 \rangle}; \tag{5}$$

the shielding factors of resonances in the total cross sections

$$f_{tot}(0) = \frac{\overline{\sigma_{tot}}}{\langle \sigma_{tot} \rangle}. \tag{6}$$

The results of the study of the group characteristics of the total cross sections are listed in Table 3.

From the experimental data we determined the group parameters which characterize the resonance structure of the differential scattering cross sections:

the spherical harmonics of the scattering cross section:

$$\overline{\langle \sigma_s \omega_l \rangle} = \frac{R^2}{n} \frac{1}{N(0)} \int_{-1}^{+1} d\mu N(t, \mu) P_l(\mu); \tag{7}$$

the constants, taking account of shielding in the total and scattering cross sections:

$$\left\langle \frac{\sigma_s \omega_l}{\sigma_{tot}^2} \right\rangle = \frac{R^2}{n} \frac{1}{(k-1)!\,N(0)} \int_0^{t_{max}} dt\, t^{k-1} x \int_{-1}^{1} d\mu N(t, \mu) P_l(\mu); \tag{8}$$

the shielding factors of the scattering cross section:

$$f_s = \frac{1}{\langle \sigma_s \rangle} \frac{\langle \sigma_s/\sigma_{tot} \rangle}{\langle 1/\sigma_{tot} \rangle}, \tag{9}$$

where $P_l(\mu)$ is the Legendre polynomial of order l, and the $\langle \omega_l \rangle$ are the moments of the scattering indicatrix.

All the expressions given take account of corrections for multiple scattering in the filter and scatterer. These corrections were determined by modeling with the Monte Carlo method. The characteristics of the scattering cross section are listed in Table 4. The shielding factor for the scattering cross section is 0.75 ± 0.01 in the range 0.8-0.4 MeV and 0.78 ± 0.02 in the range 0.4-0.2 MeV. The errors in the determination of all values are 5-7%.

Using the experimental data and Eq. (1), we obtained the neutron differential scattering cross sections of iron in the energy ranges studied (Fig. 1, curve 1). The figure shows the statistical errors for the experimental points. The errors of certain values for scattering into the forward hemisphere correspond to errors in the determination of values from Eqs. (2)-(9); for scattering into the backward hemisphere the errors are ± 10-20%. The angular distributions plotted from the experimental data in the energy ranges considered are satisfactorily approximated by second-order Legendre polynomials [9].

In determining the shielding of the neutron differential scattering cross sections it is convenient to consider the difference angular distributions for unfiltered and filtered beams, rather than the distribution for filtered beams. These are shown by curves 2 in Fig. 1 for a 14-cm-thick iron filter. These curves have a pronounced diffraction character. The values of this difference for angles symmetrical with respect to $\theta = \pi/2$ differ by more than a factor of 1.5, which is clearly beyond the limits of experimental error. The change of shape of the resonance angular distribution for filtered and unfiltered beams shows the presence of shielding in the neutron total and differential scattering cross sections.

Our results shown in Table 1-4 and Fig. 1 confirm the presence of shielding in the neutron total and differential scattering cross sections of iron, which is clearly related to the change of shape of the filtered as compared with the unfiltered neutron spectrum. The quantitative data obtained permit the refinement of the effective interaction cross sections of iron, which is an important structural material, and taking account of resonance effects by introducing corrections for the shielding of cross sections in multigroup and subgroup calculations of nuclear reactors and radiation shields.

LITERATURE CITED

1. D. L. Broder et al., in: Problems of the Physics of Reactor Shielding [in Russian], No. 2, Atomizdat, Moscow (1966), p. 88.
2. L. P. Abagyan et al., USSR Paper 357 at the Third Geneva Conf. [in Russian], Atomizdat, Moscow (1964).
3. A. G. Guseinov et al., in: Bulletin of the Nuclear Data Center [in Russian], No. 6, Atomizdat, Moscow (1969), p. 407.
4. A. G. Guseinov et al., At. Energ., 52, 118 (1982).
5. L. V. Konstantinov et al., At. Energ., 29, 453 (1970).
6. V. I. Kukhtevich, L. A. Trykov, and O. A. Trykov, Single-Crystal Scintillation Spectrometer with an Organic Phosphor [in Russian], Atomizdat, Moscow (1971).
7. Yu. A. Egorov, Yu. V. Pankrat'ev, and V. D. Tolstykh, in: Radiation Safety and Shielding of Nuclear Power Plants [in Russian], No. 1, Atomizdat, Moscow (1975), p. 110.
8. M. N. Nikolaev and V. F. Khokhlov, in: Bulletin of the Nuclear Data Information Center [in Russian], No. 4, Atomizdat, Moscow (1967), p. 420.
9. M. N. Nikolaev and O. N. Babazayants, Anisotropy of the Elastic Scattering of Neutrons [in Russian], Atomizdat, Moscow (1972).

APPLICATION OF GAMMA SPECTROMETRY IN INTEGRATED EXPERIMENTS ON REACTOR PHYSICS

A. V. Bushuev and V. N. Ozerkov

UDC 621.039.51

The physical parameters of a nuclear reactor (multiplication factor, breeding factor, and others) are determined by the ratios of the rates of different neutron reactions. The required accuracy of their measurements, depending on the characteristics of the reactor under study, is estimated by means of calculations of the sensitivity of the critical load (or the doubling time, parameters of the outer loop) to errors in the experimental results.

Experiments are performed on the subcritical and critical assemblies with flux densities of 10^5-10^{10} neutrons/(cm^2·sec) and recently in power reactors with $\varphi = 10^{12}$-10^{15} neutrons/(cm^2·sec). A special task of these studies is to analyze the nuclide content of the spent nuclear fuel, which gives information on the contribution of different processes over the operating time of the reactor. In order to obtain the required volume of information, complexes of different instruments and techniques, each of which had limited application, were used.

Often investigations of one reaction interfere with other reactions, occurring simultaneously and creating a background for the measurements. In order to decrease the background, laborious chemical procedures are used. Many of the problems enumerated above can be solved by the method of gamma spectrometry. The possibilities for its application have increased especially after the development of the semiconducting detectors, which have a high resolution with satisfactory photon-detection efficiency. Other favorable factors are the refinement of nuclear data (quantum yields of radiation and others) and the development of efficient programs for processing the instrumental spectra on a computer. In this paper, we analyze the possibilities of gamma spectrometry in studies of neutron processes in nuclear reactors.

Measurements of the Ratios of Neutron Reaction Rates. The procedure for determining the ratio of reaction rates includes the following stages: irradiation of the sample in a fixed region of the reactor, measurement of the instrumental spectrum of the gamma radiation of the irradiated sample, computer processing of the spectra in order to determine the intensity of production of separate reaction products and their content in the sample, and calculation of the ratio of the reaction rates from the content of their products:

$$R_i = \frac{S}{I_\gamma \varepsilon \tau}\left(\frac{1}{Y_i}\right) \times \frac{\exp(\lambda T)\lambda A}{[1-\exp(-\lambda \Delta T)][1-\exp(-\lambda \tau)]\, P m_0 K_1 K_2 N_0}. \quad (1)$$

Here S is the area of the photopeak created by the gamma rays of the product-monitor of the reaction rate; I_γ is the quantum yield of the recorded radiation; ε is the detection efficiency; λ is the decay constant of the reaction product; τ is the duration of the measurement; T is the time interval from the end of the irradiation to the beginning of the measurements; ΔT is the duration of irradiation; A is the atomic mass of the isotope; m is its weight content in the sample; P is the mass of the sample; N_0 is Avogadro's number; K_1 is the correction for absorption of detected quanta within the sample; K_2 is the correction for the "dead" time of the apparatus used; Y is the probability of formation (output) of the fragment-monitor of the fission reaction rate (this cofactor appears in measurements of the fission reaction rate).

Expression (1) explicitly contains the measured quantities and the external data: nuclear ($I\gamma$; λ; Y) and nonnuclear (ε, P, m, K_1, K_2).

If the error in the external data is large, then a different method for solving the problem can be used. This variant is based on weighing the samples in the flux of neutrons with a standard spectrum for which the reaction cross sections are well known (most often in the

Translated from Atomnaya Énergiya, Vol. 57, No. 3, pp. 182-186, September, 1984. Original article submitted November 11, 1983.

0038-531X/84/5703-0625$08.50

flux of thermal neutrons). In this case, expression (1), to within corrections for the dead time, for the change in the yield of fragments, depending on the neutron spectrum, and so on, assumes the form

$$R_i = (S_i/S_{th})\, R_{th}. \qquad (2)$$

The experimental results can be affected by a perturbation of the neutron field when the sample is placed in the reactor or into the thermal neutron flux. This source of error is minimal if for studies of reactions occurring in the fuel, samples prepared from the same fuel are used (usually these are tablets consisting of enriched uranium dioxide). Such samples have adequate strength with a thickness of 1 mm and greater, and their diameter is selected to equal the diameter of the fuel element. The following difficulties appear when using these samples for the measurements:

1. The radioactive nuclei — products of the neutron reactions — can be nonuniformly distributed over the radius of the irradiated samples. Special measures must be adopted in order to obtain identical efficiency of detection of quanta emitted from different sections of the surface of the sample [1].

2. A significant part of the detected gamma quanta can be absorbed inside the sample. The corresponding correction is determined either by a computational method, or the results of measurements of the absorption coefficient for gamma quanta in the real geometry are used.

3. Calibration of the sample perturbs the thermal-neutron field. The corresponding correction is obtained by a calculation with the help of the Monte Carlo method or from special experiments.

In the studies of lattice of thermal reactors, the standard set of parameters to be determined includes the modified conversion factor (MCF), ρ^{28}, δ^{28}, δ^{25} and the spectral indices, including $\sigma_f^{239}/\sigma_f^{235}$. Thus, in the experiments, it is necessary to determine the rates of the reactions $^{238}U(n, \gamma)$, $^{235}U(n, f)$, $^{238}U(n, f)$ and $^{239}Pu(n, f)$, as well as the cadmium ratios for the first two reactions. It is advantageous to use ^{239}Np as a monitor for the rate of the reaction $^{238}U(n, \gamma)$ and the fission products ^{143}Ce, ^{140}La, and others as monitors for the rates of the fission reactions.

We compare below the errors in the enumerated parameters achieved (first value) in gamma-spectroscopic measurements and the allowable (second value) values [2], %:

MCF . . . 1,26; 2—3
ρ^{28} 1,5; 2,5
δ^{25} 2,5; 2,5
δ^{28} 2,2; 5,0

The error in the ratios of the average cross sections presented below correspond to the smallest error among the errors obtained with the help of expressions (1) and (2).

The parameters ρ^{28} and δ^{25} (Table 1) are usually determined either by the cadmium screen method (a) or the indicator method 1/v (b). Unfortunately, the method of gamma spectrometry

TABLE 1. Components of the Errors in the γ-Spectrometrical Determination, %

Parameter	Correction for perturbation of the field	Error in the measurements	Error in the constants
MCF	0*	1,0	0,77
ρ^{28} a	0,5	1,0	0
b	0,5—1,0	1,0	0
δ^{25} a	0,5	1,0	1,5—2,0
b	0,5—1,0	1,0	1,5—2,0

*If in determining the MCF a sample identical in size and composition to the regular fuel tablets is used, the perturbation of the neutron field is absent.

TABLE 2. Nuclear Data for the Monitors of the Rates of (n, γ) and (n, 2n) Reactions on the Nuclides Th, U, Np, and Pu [3]

Reaction	Radionuclide-monitor	Half-life	Radiation energy, keV	Quantum yield, %
^{232}Th (n, γ)	^{233}Pa	27,0±0,1 day	311,9	38,6±0,5
^{236}U (n, γ)	^{237}U	6,75±0,01 day	208	21,7±0,2
^{238}U (n, γ)	^{239}Np	2,355±0,004 day	277,8	14,1±0,4
^{237}Np (n, γ)	^{238}Np	2,117±0,002 day	984	23,8
^{232}Th (n, 2n + γ, n)	^{231}Th	25,51±0,01 h	84,2	6,5±0,4
^{238}U (n, 2n + γ, n)	^{237}U	6,75±0,01 day	59,5	33,5

TABLE 3. Yield of Fission Products of Th, U, Np, and Pu [4], %

Fission product	Yield per neutron-induced fission act									
	thermal neutrons			fast neutrons						
	^{235}U	^{239}Pu	^{233}U	^{232}Th	^{233}U	^{235}U	^{236}U	^{238}U	^{237}Np	^{239}Pu
^{143}Ce	5,94±0,05	4,47±0,03	5,89	6,87	5,59	5,72±0,08	5,72±0,08	4,6±0,13	4,92±0,16	4,34±0,12
^{140}La	6,34±0,06	5,56±0,06	6,41	7,89	6,29	6,03±0,07	5,76	6,01±0,01	5,58	5,29±0,07

(as practically all competing methods) does not permit measuring in low-flux reactors the rate of radiative capture reactions for ^{235}U and ^{239}U.

The enumerated reactions, together with the radiative capture reaction in ^{235}U, make the main contribution to the neutron balance and determine the criticality of the thermal reactor. Useful information on the formation of the isotopic composition of plutonium can be obtained from measurements of the fission reaction rates for ^{240}Pu, ^{241}Pu, and others. In solving a number of problems associated with the external fuel cycle, it is of great interest to study the reactions ^{236}U(n, γ), ^{237}Np(n, γ), and ^{238}U(n, 2n + γ, n), leading to the accumulation of ^{236}Pu, ^{238}Pu, and ^{232}U, on whose concentrations the selection of the technology and the refabrication regime of spent fuel depend.

In studying uranium–thorium lattices, the experimental program includes measurements of the rates of radiative capture reactions as well as rates of the reaction (n, 2n + γ, n) in ^{232}Th and the fission reactions in ^{232}Th and ^{233}U. The required information on the rate monitors for these reactions is presented in Tables 2 and 3.

Table 4 summarizes the results of the analysis of the errors in the measurements of the ratios of the rates of a number of important reactions occurring in fast reactors.* Information on the allowable error in their determinations is also presented there.

Thus it has been established that gamma-spectroscopic measurements can yield information on most of the important neutron reactions occurring in the fuel of a nuclear reactor with the required accuracy. We note especially the usefulness of studying the Doppler effect accompanying the resonance absorption of neutrons in this manner [5]. With the help of gamma-spectrometrical techniques, it is possible to study the neutron reactions not only in the fuel, but also in other reactor components: in structural materials, in some heat carriers (Na), and others. Gamma-spectrometrical measurements with collections of resonant, threshold, and other indicators give information on the spatial-energy distribution of the neutron field, including a detailed picture of the neutron field in a unit cell, in nonuniform lattices, etc. [6].

Determination of the Depth of Fuel Burnup. The distribution of fission products over the active zone of the reactor characterizes the energy liberation field, and their concen-

*It should be noted that the accuracy of measurements of the rates of threshold reactions in the experiments in thermal reactors is lower than in fast reactors, due to their lower probability for the (n, f) reactions.

TABLE 4. Total Errors in Measurements of Some Functionals in a Fast Reactor, Their Components, and the Permissible Error, %

Functional	$\Delta\left(\frac{I_\gamma}{I_{\gamma f}^{235}}\right)$	$\Delta\left(\frac{\varepsilon_i}{\varepsilon_f^{235}}\right)$	$\Delta\left(\frac{Y_i}{Y_f^{235}}\right)$	$\Delta\left(\frac{p_i}{p^{235}}\right)$	$\Delta\left(\frac{K_1}{K_1^{235}}\right)$	$\Delta\left(\frac{K_2}{K_2^{235}}\right)$	$\sqrt{\Sigma\Delta_i^2}$	Permissible error
$\langle\sigma_c^{236}\rangle/\langle\sigma_f^{235}\rangle$	1,1	2,5	1,1	0,7	0,5	0,5	3,1	3,6
$\langle\sigma_f^{236}\rangle/\langle\sigma_f^{235}\rangle$	0,01		1,1	0,7		0,5	1,3	2,8
$\langle\sigma_c^{237}/\sigma_f^{235}\rangle$		2,5	1,1	0,7	0,5	0,5	2,9	3,6
$\langle\sigma_f^{237}\rangle/\langle\sigma_f^{235}\rangle$	0,01		1,1	0,7		0,5	1,3	2,8
$\langle\sigma_c^{238}\rangle/\langle\sigma_f^{235}\rangle$	2,8	2,5	1,1	0,7	0,5	0,5	4	3,6
$\langle\sigma_{(n,\,2n+\gamma,\,n)}\rangle/\langle\sigma_f^{235}\rangle$		2,5	1,1	0,7	0,5	0,5	2,9	10,2
$\langle\sigma_f^{239}\rangle/\langle\sigma_f^{235}\rangle$	0,01		1,78	0,7		0,5	2	2,8
$\langle\sigma_c^{232}\rangle/\langle\sigma_f^{235}\rangle$	1,3	2,5	1,1	0,7	0,5	0,5	3,2	3,6
$\langle\sigma_f^{232}\rangle/\langle\sigma_f^{235}\rangle$	0,01		1,1	0,7		0,5	1,4	2,8
$\langle\sigma_{(n,\,2n+\gamma,\,n)}^{232}\rangle/\langle\sigma_f^{235}\rangle$	6,2	2,5	1,1	0,7	0,5	0,5	6,8	10,2
$\langle\sigma_f^{233}\rangle/\langle\sigma_f^{235}\rangle$	0,01		1,1	0,7		0,5	1,3	2,8
$\langle\sigma_f^{238}\rangle/\langle\sigma_f^{235}\rangle$	0,01		2,0	0,7		0,5	2,2	2,8

tration in the fuel characterizes the depth of fuel burnup. In determining the total number of fission events by the gamma-spectroscopic method, the emission from ^{137}Cs and some other fission products is usually used [7]. The errors of the gamma-spectroscopic determination of burnup are due to the statistical error in the measurements, the error in determining the detection efficiency, the uncertainty in the value of the average yield of the fission product, and the corrections for its burnup and decay.

In measurements with samples of a solution of the fuel, the spectrometer is usually calibrated with the help of a collection of radioactive sources. In these cases, the error in the determination of the efficiency ε is determined by the inaccuracy in the nominal data for the sample sources (1%). In experiments with fuel elements or fuel assemblies, the gamma spectrometer is calibrated based on destructive tests or with help of a special standard fuel element of a standard fuel assembly. The upper limit of the error ε is given by the uncertainty in the certified data for the spent fuel element or fuel assembly in nondestructive measurements and is equal to $\sim$ 3%.

The value of the average yield, as a rule, is determined from a mass-spectrometrical analysis [8] or by a computational method. The uncertainty of the yield of products in fissioning of ^{235}U makes the determining contribution to the error in the average value of the yield Y_{av} of the product–monitor with a burnup depth of less than 40 kg/ton U. The yield of ^{137}Cs with fissioning of uranium in thermal and fast reactors is known to within 0.8 and 2.9%. The errors in the corrections with burnup and decay of the monitor are equal to 0.1-0.4 and 0.1-0.2%, respectively.*

The information presented permits estimating the minimal error in the gamma-spectroscopic determination of the fuel burnup depth of thermal and fast reactors. It is equal to 1.4-3.1 and 3.1-4.2%, respectively.

Determination of Plutonium Accumulation. The intense gamma emission of the uranium fission products initiates x-ray emission of heavy nuclei, whose measurement can give information on their content in the spent fuel of a power reactor. The number of corresponding x-ray quanta is proportional to the content of the element in the spent fuel and the excitation probability.

For the detection, it is most convenient to use the x-ray emission in the K_α series. For elements with Z = 92-95, the energy difference between the K_α lines is equal to 1.5 keV, and in order to distinguish them in the total emission spectrum of the fuel element, a spectrometer with high energy resolution ($\sim$ 700 eV at an energy of 122 keV) is required.

*The correction for the burnup of the monitor is significant. For a fuel burnup depth of 40 kg/ton U in a fast reactor, this correction and the correction for the decay of ^{137}Cs over the operating time do not exceed 5%.

The analysis for the plutonium content is compatible with the procedure of gamma scanning in determining the burnup depth. The elemental ratio Pu/U in the fuel elements of a fast reactor is determined in this manner [9]. Attempts have been made to determine with the same method the accumulation of plutonium in the fuel elements of water-moderated–water-cooled power reactors. Due to the nonuniform plutonium accumulation over the radius of the fuel elements of thermal reactors and the weak penetrability of the recorded quanta, corrections for the difference in the concentration of plutonium in the surface layer and at the center of the fuel element must be introduced into the experimental results.

The error in the determination of tha ratio Pu/U consists of the random error in the measurements and the error in the correction for the different efficiencies of detection of the K_α quanta of uranium and plutonium and for the difference in their excitation probabilities. With a plutonium accumulation of $\sim$ 15-25 kg/ton U, the random error exceeds 2%. The correction for the difference in the detection efficiency can be determined from special measurements with standard sources, and the correction for the differences in the excitation probabilities can be determined computationally. Due to the closeness of the energies of the recorded quanta, these corrections do not exceed several percent, so that the random error makes the main contribution to the error in the determination of the plutonium accumulation.

Determination of the Isotopic Ratios in Plutonium Samples. The gamma-spectrometric determination of the content of individual isotopes in solutions and samples of plutonium is based on the detection of gamma quanta in the energy range 30-60 keV, which includes the most intense lines of ^{238}Pu, ^{239}Pu, ^{240}Pu, and ^{241}Am. For such measurements, Si(Li) spectrometers with a resolution of 500 eV for radiation energies of 60 keV are used. It is important to take into account the absorption of low-energy gamma radiation within the sample. The effective thickness of the sample can be determined from the results of intensity measurements of two or several gamma lines of a single isotope (for example, 38.6 and 51.6 keV for ^{239}Pu). The thickness obtained is then used to calculate the corrections for absorption.

The isotopic ratios can be determined by two methods. The first involves the direct determination of the quantitative content of separate isotopes from the intensity of their emission. The second method is based on a comparison of the intensities of lines in the spectra of the sample under study and a standard sample whose composition is known. In the first case, the uncertainties of the nuclear constants used make the main contribution to the error; in the second method, the error in the certified data of the standard makes the main contribution. The necessary condition for gamma-spectroscopic measurements is that the fission products must be removed from the plutonium sample. Their admissible content is no more than 10^{-3} %.

Determination of the Content of ^{232}U in Uranium and ^{236}Pu in Plutonium. The concentration of ^{232}U in uranium samples and ^{236}Pu in plutonium samples can be determined from the intensity of the gamma quanta of ^{208}Tl with energies of 583 or 2615 keV, which are emitted with the highest probability. The error in the determination of the activity of ^{208}Tl is due to the random error in the measurements and the errors in the determination of the effectiveness of the contribution of the background emission of ^{208}Tl, present in the structural materials.

The accuracy of the analysis of the ^{232}U (^{236}Pu) content is increased if thorium is specially removed from the samples under study. Otherwise, it is necessary to know the concentration of ^{228}Th at the moment that the sample is prepared.

The aggregate of the data on the achieved error of the gamma-spectroscopic determination of the characteristics of spent fuel is shown in Table 5. The table also shows for comparison information on the admissible error in these characteristics for a fast power reactor. According to the data in Table 5, the accuracy of gamma-spectrometric measurements in most cases satisfies the requirements. An exception is the determination of the burnup depth, where the error in the values of the yield of ^{137}Cs with fissioning of ^{235}U in a fast reactor must be reduced by a factor of 3. (In the destructive tests on thermal reactors, the required accuracy is almost achieved.)

Thus gamma spectrometry yields important data on the composition of spent fuel. Measurements can give extensive information on the isotopic fields and the energy liberation fields in a reactor with all of their structural and operational peculiarities. Many types of analyses can be performed under operational conditions.

TABLE 5. Error in the Gamma-Spectrometric Determination of the Characteristics of Spent Fuel, %

Error	Burnup depth	Pu accumulation	Concentration of nuclides				
			^{232}U	^{236}Pu	^{238}Pu	^{240}Pu	^{241}Pu
Achieved	3	2	20	20	5	4	4
Admissible	1	1,66	30	30	20	5	4

It is expedient to combine extensive gamma-spectrometric measurement with separate high-accuracy analyses based on traditional (mass and α-spectrometry) methods. It should be noted, however, that in some cases gamma spectrometry is not only more productive, but it can also compete with traditional methods with respect to accuracy (for example, in the analysis of plutonium samples for the content of ^{238}Pu, ^{240}Pu).

Thus the use of gamma spectrometry based on the application of semiconducting gamma- and x-ray detectors makes it possible to obtain, with satisfactory accuracy, information on a number of very important neutron reactions occurring in nuclear reactors and on the concentration of some radionuclides in the spent fuel. A complex analysis of these data makes it possible to estimate some parameters that cannot be measured directly. For example, $^{239}\alpha$ can be determined from measurements of the isotopic composition of plutonium, the burnup depth, and the functional $\langle\sigma_f^{239}\rangle/\langle\sigma_f^{235}\rangle$; the functional $\langle\sigma^{237}_{n,2n}\rangle/\langle\sigma^{237}_{n,\gamma}\rangle$ can be determined from measurements of the ^{238}Pu and ^{236}Pu contents.

LITERATURE CITED

1. A. V. Bushuev and L. N. Yurova, At. Energ., 27, No. 5, 458 (1969).
2. A. V. Bushuev and A. F. Kozhin, in: Proceedings of the Third All-Union Seminar on the Problems in Reactor Physics [in Russian], TsNIIatominform, Moscow (1983), p. 53.
3. IAEA-TECDOC-232, Vienna, p. 123 (1980).
4. J. Cuninghame, in: Proc. of Meeting on Fission Product Nuclear Data, Petten, Paper 10 (1973).
5. A. V. Bushuev et al., At. Energ., 50, No. 6, 387 (1981).
6. N. D. Golyaev et al., Problems in Atomic Science and Technology. Series on Nuclear Constants [in Russian] (1982), No. 3(47), p. 62.
7. A. A. Trunov, At. Tekh. Rubezhom, No. 6, 18 (1980).
8. A. V. Bushuev et al., At. Energ., 53, No. 5, 322 (1982).

PENETRATION OF RADIOACTIVE INDUSTRIAL WATERS FROM THE NORTH SEA INTO CENTRAL REGIONS OF THE BALTIC

S. M. Vakulovskii and A. I. Nikitin

UDC 551.464.6.02

We know that the radiation conditions in the Baltic are affected by the arrival of water from the North Sea, polluted by radioactive industrial effluent carrying high levels of ^{137}Cs [1, 2]. The expedition launched in 1980 by the Institute for Experimental Meteorology observed ^{134}Cs in the mouth of the Baltic itself [3, 4].

We should bear in mind that the influences of other sources of local radioactive pollution (the effluent from nuclear power stations on the shores of the Baltic) are only observed in the direct vicinity of the power stations themselves and then chiefly from the pollution of bioindicators. There are presently no reports of ^{134}Cs being found in sea water caused by the effluent from the Baltic nuclear power stations.

As our criterion of penetration of radioactive effluent water into the center of the Baltic, we used the content of ^{134}Cs in the bottom waters of troughs (Arkonsk, Bornholm, Gdansk, and Gottland) lying in the path of the North Sea waters, since this serves as a radioactive indicator of the presence of polluted water. The radionuclides from the samples of bottom waters comprising several thousand liters were concentrated, since the content of ^{134}Cs is of an extremely low order. The method of sample extraction and the means of concentration have already been described in [3, 5].

Table 1 gives the results obtained for ^{137}Cs and ^{134}Cs (soluble fraction). The average content of ^{137}Cs in suspension in the bottom waters comprised 0.06 Bk/m^3. This result was obtained by measuring combined samples totalling 15,900 liters. The presence of ^{134}Cs was observed in the bottom waters of all stations. The minimum concentrations observed by means of a semiconductor spectrometer with a DGDK-80 detector were set by the speed of measurement and the volume of the sample. For example, where the measurement time was 480 min and the volume of sample 3000 liters, the minimum concentration of ^{134}Cs that could be measured was $\sim 0.04\ Bk/m^3$. We should bear in mind that the presence of a radioactive indicator, such as ^{134}Cs, characteristic only of the North Sea, in the waters of the Baltic can be used to solve the water-dynamics problem and to identify water within the Baltic Sea.

TABLE 1. Content of ^{134}Cs and ^{137}Cs in Samples of Sea Water Taken from the Baltic in June 1983

Region of sea (trench)	Station No.	Depth of sea, m	Level of sample, m	Volume of sample, liters	Salinity, ‰	Concentration, Bk/m^3		Content of industrial ^{137}Cs		
						^{137}Cs	^{134}Cs	Bk/m^3	% of total concentration	% of rise in bottom-water concentration
Arkonsk	80	46	0	1250	7,8	12	—	—	—	—
			45	3000	12,0	22	0,32	5,5	25	55
Bornholm	62H	90	0	730	7,5	12	—	—	—	—
			88	3000	15,0	20	0,24	4,2	21	53
Gdansk	55	102	0	1210	6,1	11	—	—	—	—
			100	3035	11,2	18	0,15	2,9	16	41
Gottland	46	130	0	300	7,3	11	—	—	—	—
			100	4560	9,0	15	0,11	2,1	14	52
	37	240	0	600	7,1	13	—	—	—	—
			170	2300	11,2	18	0,12	2,6	14	51

Translated from Atomnaya Énergiya, Vol. 57, No. 3, pp. 186-188, September, 1984. Original article submitted February 21, 1984.

0038-531X/84/5703-0631$08.50

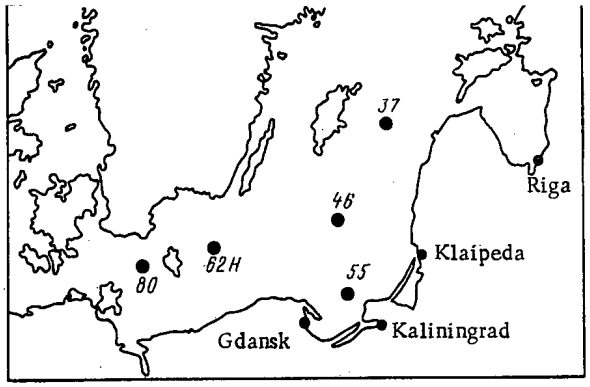

Fig. 1. Locations of sampling stations.

These investigations showed that radioactive pollution present in the North Sea waters has penetrated the system of deep-water trenches of the Baltic as far as the Gottland trench. The greatest degree of ^{134}Cs and ^{137}Cs pollution of bottom waters is found in the Arkonsk trench (Station 80 in Fig. 1), adjacent to the Strait. The concentration of ^{134}Cs in the Gdansk trench (Station 55) is half that in the Arkonsk, while that in the Gottland trench (Stations 46 and 37) is only a third of the Arkonsk level. This is due both to the dilution of the waters and to the decay of the ^{134}Cs as it moves through the sea. As a rule, increased levels of salinity correspond to higher concentrations of ^{134}Cs. An exception is the Arkonsk trench, where the salinity proved to be lower (at 12 $^{0}/_{00}$) than in the Bornholm trench (15 $^{0}/_{00}$) despite the higher concentration of ^{134}Cs.

We should note that a smaller concentration of ^{137}Cs was observed in the surface waters of the areas under investigation in 1983 than in 1980: a reduction from 14-18 Bk/m^3 [3, 4] to 11-13 Bk/m^3. Such a comparison is difficult to make in the deep waters, since the salinity of the bottom waters was higher in 1980 than in 1983. This tendency for the concentration of ^{137}Cs to fall in the surface waters has been confirmed by West German studies [6], which found in December 1981 that the intermediate levels in the concentration of ^{137}Cs were 13-15 Bk/m^3. Investigations carried out in Poland and East Germany, however, did not note any reductions in the concentration of ^{137}Cs in 1981 [7].

By utilizing data on the concentrations of ^{134}Cs in the bottom waters, we are able to estimate the proportion of industrial ^{137}Cs in the total content of radionuclides present in the bottom waters from the ratio of $^{137}Cs/^{134}Cs$ in the effluent. Reference [8] gives an average value of 5.8 $\pm$ 0.6 for this ratio for the point of effluent (Windscale) during 1970-1978. We used a correction factor found earlier [3] for the decay of ^{134}Cs over the time of travel (3.3 years) from the point of entry of the effluent to the Baltic (Arkonsk trench). The time of propagation of the water into the Baltic can be estimated on the basis of data on changes in salinity in the trenches during the period of high encroachment of North Sea water [9]. We can infer from these data that the transfer of water masses from the Arkonsk trench to the Bornholm, Gdansk, and Gottland trenches takes about 1, 4, and 8 months, respectively. The concentration of industrial ^{137}Cs, calculated from this ratio in the effluent, taking account of the decay of ^{134}Cs during the journey, is also given in the table.

We can see that the proportion of industrial ^{137}Cs within the total content of radionuclides in the bottom waters is significant and reaches a level of $\sim$ 25% in the Arkonsk trench. The level of industrial ^{137}Cs tends to fall with distance from the mouth of the Baltic, as we would expect, reaching about 14% in the waters of the Gottland trench. These data also enable us to estimate the contribution made by industrial pollution to the increase in the concentration of ^{137}Cs in the bottom waters in excess of the surface concentration. We can see that $\sim$ 50% of this increase is due to industrial pollution. This value remains practically constant with distance from the mouth of the Baltic to the central region.

We have therefore been able to establish that ^{134}Cs entering the Baltic as the result of emissions from radioactive waste disposal plant at Windscale [Sellafield] is contained in the bottom waters of the Baltic trenches in measurable amounts. Further investigations by the use of this radioactive tracer of North Sea water can determine the extent to which radioactive effluents penetrate to other parts of the Baltic.

LITERATURE CITED

1. Environmental Radioactivity in Denmark in 1978, Riso Report No. 403 (1979).
2. D. B. Styro et al., At. Energ., 55, No. 4, 238 (1983).
3. S. M. Vakulovskii et al., Meteorol. Gidrol., No. 9, p. 72 (1983).
4. L. Lazarev et al., in: Proceedings of Research Coordination Meeting on the Studies of the Radioactive Materials in the Baltic Sea, JI-RC-241, IAEA (1982).
5. S. M. Vakulovskii et al., in: Trudy Instituta Eksperiment. Meteorologii, No. 6(107) [in Russian], Gidrometeoizdat, Moscow (1983), p. 47.
6. H. Kautsky and H. Eicke, Deutsche Hydrographische Zeischrift, 35, No. 5, p. 211 (1982).
7. Investigation of Radioactivity in the Baltic Sea during 1981, Serial Reference on Point II-7.4.1.5 of the Comecon Plan for Nuclear Power in 1981-1985 [in Russian], Leningrad (1983).
8. D. Jeffries, A. Steele, and A. Preston, Deep-Sea Res., 29, No. 6A, p. 713 (1982).
9. P. Khupfer, The Baltic, a Small Sea with Big Problems [in Russian], Gidrometeoizdat, Leningrad (1982).

UNDERGROUND LOW-BACKGROUND-LEVEL LABORATORY FOR RADIOGEOCHEMICAL INVESTIGATIONS

Yu. A. Surkov, O. P. Sobornov,
O. P. Shcheglov, G. Sh. Shengelaya,
K. K. Daneliya, and T. G. Khundzhua

UDC 539.1.074.3

When low levels of radioactivity are being determined in small samples of material, the analytical capabilities of the low-background-level gamma spectrometer used in above-ground laboratories are limited by the contribution that cosmic rays make to the background level of the detector. The sensitivity of gamma spectrometers can be increased by reducing the background levels, and this can be achieved by creating underground low-background-level laboratories, such as are described in [1-5]. These laboratories can also be used for a wide range of physical investigations. In view of their suitability for long-term experiments, there is a need to create new laboratories built to a high specification.

The low-background-level underground laboratory "Saberio" was built in the Soviet republic of Georgia, in an old stope tunnel passing through low-activity limestone for a distance of 430 m (Fig. 1). The height of the tunnel entrance above mean sea level is 140 m and its downwards slope is 10%.

A low-background-level chamber weighing 3500 kg was set into the tunnel at a distance of 350 m from its mouth, under a layer of rock equivalent in its protective properties to 180 m of water equivalent (mwe). It was located in an equipment room linked to the surface laboratory by power, telephone, and coax lines 650 m in length.

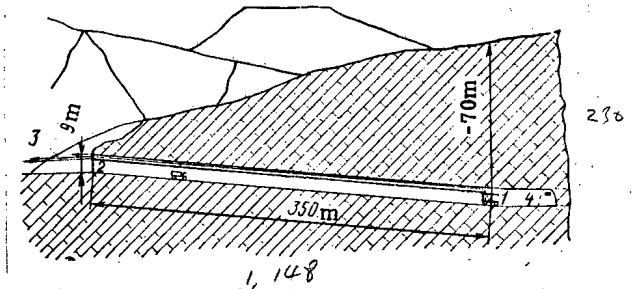

Fig. 1. Layout of Saberio station: 1) underground laboratory; 2) entrance to stope tunnel; 3) communication line with surface laboratory; 4) ventilation opening.

Translated from Atomnaya Énergiya, Vol. 57, No. 3, pp. 188-191, September, 1984. Original article submitted December 29, 1983.

0038-531X/84/5703-0633$08.50

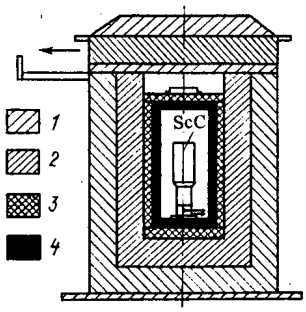

Fig. 2. Sectional arrangement of passive protection for detector: 1) steel; 2) lead; 3) copper; 4) tungsten.

TABLE 1. Background Count Rate for NaI(Tl) Detector in Various Underground Laboratories, min^{-1}

Laboratory and depth, mwe	Thickness of passive protection, g/cm^2	E, MeV							
		0,3–3,4	0,5–0,8	1,0–1,4	1,35–1,55	1,7–2,0	2,5–3,4	3,4–5,0	5,0–7,0
Baksan, 660	353	17,0 (23,1) *	4,76 (6,79)	1,78 (4,01)	1,22 (2,12)	0,29 (0,76)	0,25 (0,41)	0,04 (0,68)	0,01 (0,06)
Saberio, 180	270	14,3 (17,3)	4,13 (4,33)	1,85 (2,46)	0,95 (1,10)	0,26 (0,42)	0,25 (0,37)	0,12 (0,63)	0,08 (0,16)
Radiev, 120	207	19,4	5,61	2,13	1,13	0,35	0,38	0,14	—

*The first value is for a 76 × 76 mm diameter NaI(Tl) scintillation counter; the second (in parentheses), for a 100 × 100 mm diameter NaI(Tl) detector with a 33 × 60 mm block.

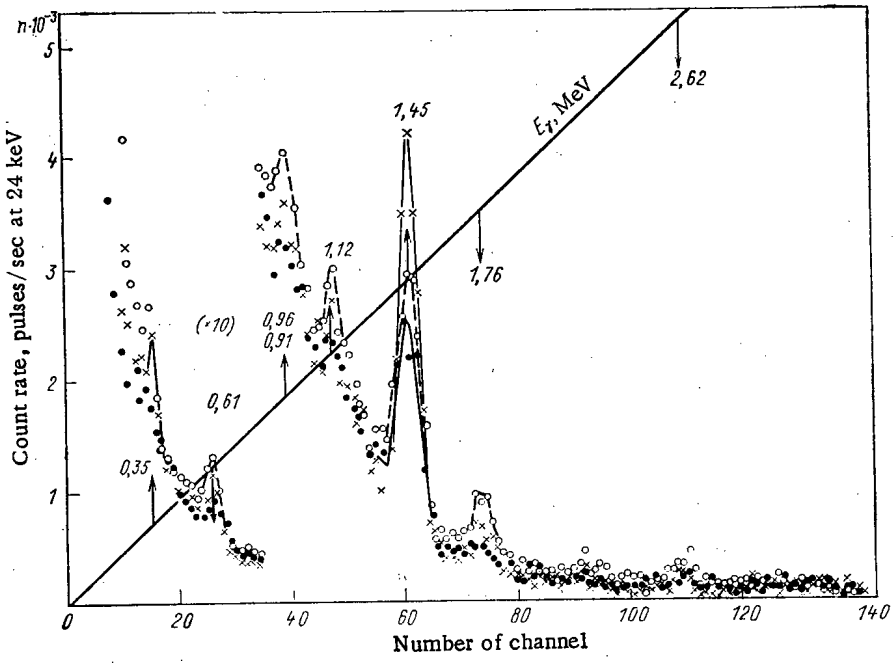

Fig. 3. Spectra of background for scintillation detector No. 274 with NaI(Tl) crystal, 76 × 76 mm diameter, in the underground laboratories at Baksan (×), Radiev (○), and Saberio (●).

Irradiation from the medium surrounding the chamber is attenuated by layers of steel 100 mm thick, lead 100-150 mm thick, copper 25-40 mm thick, and tungsten 30-40 mm thick (Fig. 2). The position of the last two layers and their thickness can be varied in relation to the configuration of the detector and can accommodate a maximum diameter and height of the sensitive part of the detector of 200 × 200 mm. The upper wall of the chamber comprises a cover weighing 700 kg, which can be freely moved in guides to permit access to the chamber when replacing samples or changing detectors.

The temperature in the tunnel at the site of the equipment room tends to vary throughout the day by not more than 0.3°C (for variations of charge temperature of up to 20°C). The temperature is 16-17°C during hot weather. For this reason, the instruments located in the chamber (high-voltage power packs, preamplifiers, and analyzers) are guaranteed stable long-term operation. The content of radioactive nuclides in the rock surrounding the tunnel and the natural ventilation due to its connection with a tunnel carrying river water to a reservoir ensure a low concentration of radon in the air and a reduction in the contribution of radon decay products in the background spectrum of the gamma spectrometer.

The same scintillation counters (ScC) were used to compare the screening conditions of the chamber as were used in [5]. The results of the present investigations were comparable with those achieved in the best Soviet underground laboratories, such as the Baksan Neutrino Observatory of the Institute of Nuclear Research of the Academy Sciences of the USSR and the laboratory of the V. G. Khlopin Radiev Institute (Table 1). The measurements were carried out with the aid of multichannel amplitude analyzers types NTA-512B and AI-1024-95, mounted in the low-background chamber and in the surface laboratory at a distance of 650 m. The error in determining count rate comprised 1-5% for $E < 3.4$ MeV and 10 and 30% for > 3.4 MeV ($P = 0.95$) using multiple exposure of $5 \cdot 10^4$ sec (13h, 53min). The background spectra obtained in the range 0.3-7.0 MeV were processed in a similar manner to [5]. Figure 3 gives the results of background measurements made on the same scintillation counter in three different laboratories.

Comparison of the data given in Table 1 and Fig. 3 shows that the integral count rate of the background in the energy range 0.3-3.4 MeV (including a summated stage of ^{208}Tl radiation) is lower in the Saberio chamber than in the Baksan and Radiev laboratories. Contributions to the background radiation at energies > 3.4 MeV of α radiation, due to the decay products of U and Th, are found in the detector [5], together with the muon component from the cosmic rays. The contribution of cosmic rays proved to be less effective in this range at the Baksan Observatory, due to the vast amount of overlying rock (660 mwe). Consequently, the analytical problem in the energy range that includes the γ lines of all the radionuclides of the gamma radiators is easier to solve at Saberio, despite its shallower overlay of rock and the less sophisticated equipment included in the first stage of construction.

A comparison of the measurements of the content of natural radioactive elements in samples of rock taken from the tailings of the excavation work at Baksan and the bedrock penetrated by the Saberio tunnel (Table 2) shows that the bedrock in the latter case is considerably less radioactive. The higher count rate at Baksan in the 1.35-1.55-MeV range (incorporating the ^{40}K photopeak) has also been noted by workers at the Radiev Institute [3]. It seems that the chamber itself and the dunite used for shielding the bedrock were not able entirely to eliminate the radiation from the potassium contained in the protection material. Lower background count rates in the range 1.7-2.0 MeV (in the region of the total absorption peak for ^{214}Bi, 1.76 MeV) were registered than at Baksan or Radiev. From this, we are able

TABLE 2. Content of Natural Radionuclides in Rocks Surrounding Laboratory, %

Radionuclide	Baksan	Saberio
K	3,20—6,22	0,04±0,01 *
U (Ra), 10^{-4}	2,0—3,7	0,6±0,2
Th, 10^{-4}	13,3—27,6	0,4±0,2

*Corresponds to average content of potassium in dunites.

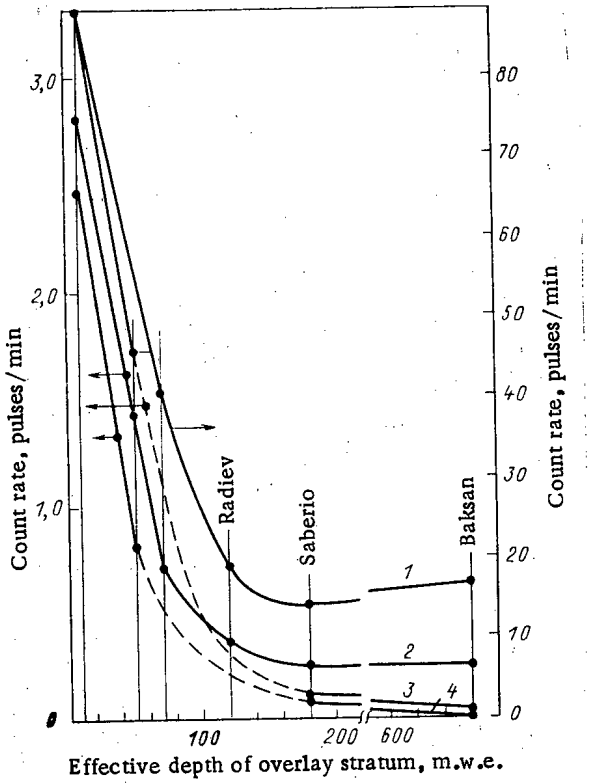

Fig. 4. Relationship of background count rate to depth of detector in passive protection in the energy ranges ΔE_γ = 0.3-3.4 MeV (1), 2.5-3.4 (2), 3.4-5.0 (3) and 5.0-7.0 (4), based on the data given in [5].

to conclude that the contribution of the γ radiation due to decay products was lower in the spectrum of Saberio. The investigation also showed that the contribution depended to some extent on the weather conditions (the humidity in the tunnel). Further improvements in the laboratory could bring the background count rate down by hermetically sealing the chamber. The lower count rate of the background radiation registered at Saberio in the range 0.3-3.4 MeV by the two monitor detectors is due to the lower contribution of gamma radiation from ^{40}K and a number of radionuclides representing decay products of radon.

A comparison of the count rates in various energy ranges in relation to the depth of the laboratory in which they were taken (Fig. 4) shows that a depth of 100-120 mwe is adequate for virtually full absorption of cosmic rays under real conditions of measurement in the laboratories we have been comparing, taking the differences in the protection of the chambers into account. The contribution of the muon component becomes negligible at a depth of 180 mwe, in comparison with the natural radiation of the materials.

The Saberio laboratory is used for determining low contents of radionuclides (K < 0.01%, U(Ra) and Th $n \cdot 1 \cdot 10^{-5}$%) in small one-off samples (from 5 g) and for estimating the intrinsic radioactivity of various types of detector.

The authors would like to express their gratitude to workers at the Institute of Geophysics of the Academy of Sciences of the Georgian SSR and the Institute of Geochemistry of the Academy of Sciences of the USSR A. M. Nikoladze, A. M. Kritarasov, V. G. Gelashvili, E. M. Sizov, E. B. Konovalova, M. L. Rivkin, I. L. Artemenkov, G. V. Petrov, and G. A. Fedoseev for their assistance in carrying out the preliminary investigations, in creating the underground laboratory, and in discussing the results.

LITERATURE CITED

1. A. A. Pomanskii, At. Energ., 44, No. 4, 376 (1978).
2. É. I. Al'terman and A. V. Stepanov, Preprint RI-78, Leningrad (1978).

3. O. S. Tsvetkov, in: Spectrometric Methods of Analyzing Radioactive Ground Pollution and Aerosols [in Russian], Gidrometeoizdat, Moscow (1974), p. 26.
4. W. Helbig et al., Nukleare Analysenverfahren, Dresden, 11-15, April, 1983.
5. O. P. Sobornov, At. Energ., 50, No. 1, 43 (1981).

MEASUREMENT OF THE RANGES OF RECOIL NUCLEI OF HEAVY ACTINIDES FORMED IN MULTINUCLEON TRANSFER REACTIONS INITIATED BY ^{22}Ne IONS

A. G. Demin, V. A. Druin, Yu. V. Lobanov, R. N. Sagaidak, and V. K. Utenkov

UDC 539.172.6:539.16.17.015

In experiments on the synthesis and study of the properties of the transfermium elements in reactions with heavy ions, a serious problem is the separation of the synthesized nuclide usually produced in the total-fusion reaction of the impinging ion and the target nucleus, on a background of the numerous reaction products of multinucleon transfers, the yields of which, as a rule, considerably exceed the yields of the total-fusion reaction products [1-3]. This problem is particularly complex in experiments on the synthesis of spontaneously fissile nuclides, as their identification causes additional difficulties.

In experiments on the synthesis of spontaneously fissile nuclides with $Z \geq 104$, using transuranic targets, the differences in the radioactive properties and in the angular distribution of the recoil nuclei formed via the composite nucleus and in the multinucleon transfer reactions were used for the separation of the total-fusion reaction products [4, 5]. Additionally, it is possible to improve the background conditions during separation of the total-fusion reaction products by means of the differences in the kinetic energy of the recoil nuclei. Thus, when investigating quasielastic transfer in nuclei of the fissile region over a wide range of mass and energy values of the incident ions, it was found that the ranges of the recoil nuclei in the direction of the beam are markedly different from the ranges of the reaction products of total fusion, and depend in a quite complex way on the energy of the incident ion [6].

The purpose of this project has been the measurement of the ranges and angular distribution of the recoil nuclei ^{256}Md, formed in the reaction ^{249}Bk + ^{22}Ne, and also the measurement of the ranges in the direction of the beam for the recoil nuclei ^{252}Fm and ^{256}Md, formed in the same reaction, and the recoil nuclei ^{246}Cf, ^{242}Cm, and ^{240}Cm, formed in the reaction ^{239}Pu + ^{22}Ne, in order to assess the feasibility of isolating the total-fusion reaction products from the reaction products of multinucleon transfers in the experiments on the synthesis of transfermium nuclides. An abstract of this paper was published earlier [7].

Experimental Procedure. The experiments were conducted on the U-300 cyclotron in the Nuclear Reaction Laboratory of the Joint Institute of Nuclear Research. The facility, shown schematically in Fig. 1, was used for the measurement of the angular distribution and ranges of the ^{256}Md atoms with different angles of flight from the target. The target of ^{249}Bk, with a thickness of 0.3 mg/cm^2 and an area of 0.1 cm^2, was irradiated with a stream of ^{22}Ne ions with an energy of 118 MeV. The energy of the ion beam at the target was established by means of aluminum absorbers and was monitored by the elastic scattering of the ions by a thin gold target located in front of the inlet to the reaction chamber (not shown in Fig. 1). The absorbers were chosen on the basis of tables of ranges [8], taking account of the thickness of the inlet window of the target and its backing.

The recoil nuclei ejected from the target were collected in aluminum collectors, forming the lateral surface and the base of the Faraday cylinder enclosing the target. The thickness of the collectors (0.1-0.3 mg/cm^2) was determined by the energy absorption of the α-particles of a spectrometric ^{238}Pu source by means of tables [9]. The error in determining the thickness amounted to ∿ 5%. For the purpose of preventing heating up of the target, the collec-

Translated from Atomnaya Énergiya, Vol. 57, No. 3, pp. 191-195, September, 1984. Original article submitted October 4, 1983.

0038-531X/84/5703-0637$08.50

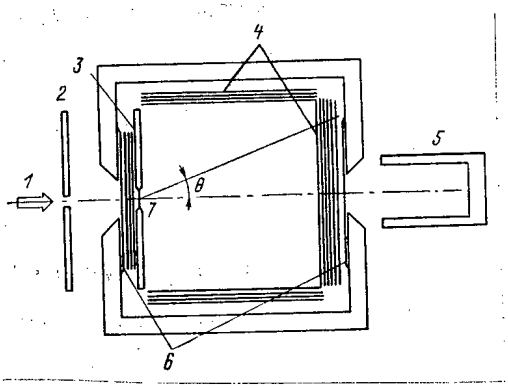

Fig. 1

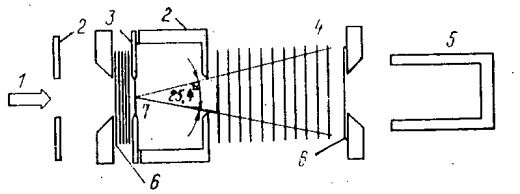

Fig. 2

Fig. 1. Diagram of the facility for measuring the angular distribution and ranges of the ^{256}Md recoil nuclei, formed in the reaction ^{249}Bk + ^{22}Ne: 1) ion beam; 2) ion beam collimator; 3) aluminum absorbers; 4) aluminum foil collectors of recoil nuclei; 5) Faraday cylinder; 6) inlet and outlet vacuum windows; 7) ^{249}Bk target.

Fig. 2. Diagram of the facility for measuring the ranges of recoil nuclei of multinucleon transfer reaction products, emitted in the direction of the beam (the maximum angle of flight of the recoil nuclei is shown): 1) ion beam; 2) ion beam and recoil nuclei collimators; 3-7) as in Fig. 1.

tors, and absorbers under the action of the intense ion beam, the reaction chamber was separated from the vacuum space of the cyclotron and the Faraday cylinder by aluminum windows and was filled with helium up to a pressure of $4 \cdot 10^3$ Pa.

The yield of ^{256}Md was determined from its spontaneously fissile daughter product ^{256}Fm, the direct formation of which in the reaction being considered is negligible at an energy of 118 MeV [2]. It was assumed, therefore, that all the spontaneous fission activity recorded at the collectors is due to the decay of ^{256}Md. The spontaneous fission fragments of the nuclei remaining in the collectors were recorded by means of solid-state track detectors (Lavsan, with a recording efficiency of the fragments of $\sim$ 90%).

The measurement of the range of the recoil nuclei in the direction of the beam was effected by means of a similar facility, shown in Fig. 2. In these experiments, targets of ^{249}Bk and ^{239}Pu were used, with thicknesses of 0.15 and 0.4 mg/cm^2 and areas of 2 and 0.5 cm^2, respectively. The stack of aluminum foils of the thickness shown above was located after the recoil nuclei collimator at some distance from the target. The maximum angle of flight of the reaction products achieved in this case was equal to 25.4°. The reaction chamber in working conditions was filled with helium to a pressure of 2000 Pa. The ranges of the recoil nuclei of the multinucleon transfer reaction products in ^{239}Pu were also measured in the stack of aluminum foils without collimator (angle of flight of the reaction products $\sim$ 120°). The energy of the ^{22}Ne ions at the target layer amounted to 118 MeV during the irradiation of ^{249}Bk and 121 MeV in the similar experiment with ^{239}Pu, which corresponds approximately to the calculated maxima of the excitation functions of the total-fusion reactions ^{249}Bk(^{22}Ne, 4n) and ^{239}Pu(^{22}Ne, 5n) [10].

The alpha-activity of the reaction products collected by the foil-collectors was measured with an eight-channel alpha-spectrometer with semiconductor surface barrier detectors. The resolution (lines width at one-half of its height) for the distribution over the thickness of the source located close to the detector amounted to 150-180 keV. The observed activity values of ^{252}Fm, ^{246}Cf, ^{242}Cm, and ^{240}Cm were identified by the characteristic α-decay energy and the half-life of the nuclide.

In view of the similar radioactive properties of ^{252}Fm and ^{255}Fm, for the purpose of additional identification of the 1-day activity attributed to ^{252}Fm, in a separate irradiation of ^{249}Bk with ^{22}Ne ions, it was shown that the ratio of the cross sections of formation $\sigma_{252+255}\text{Fm}/\sigma_{254}\text{Fm} > 10$. Allowing for the content in the target ^{249}Bk ($T_{1/2}$ = 314 days) of its daughter product ^{249}Cf (7%) and the data about the isotopic distributions of the actinides formed in reactions of ^{22}Ne ions with ^{249}Cf [2] and ^{248}Cm [3], it could be verified that the observed 1-day activity is associated mainly with the decay of ^{252}Fm, formed in the ^{249}Cf impurity in the berkelium target.

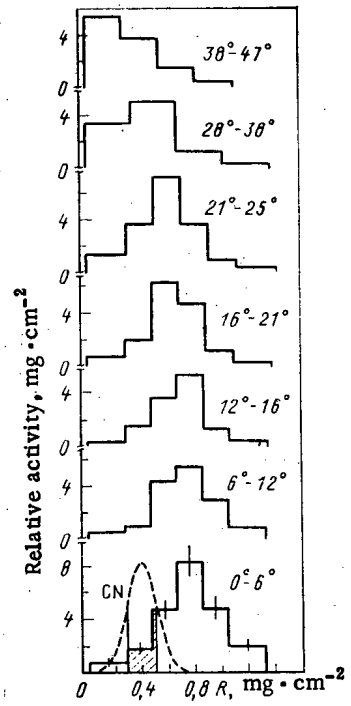

Fig. 3. Range distribution of the ^{256}Md recoil nuclei, formed in the reaction ^{249}Bk + ^{22}Ne with an energy of 118 MeV, for different angles of flight. For the angles 0-6°, the calculated distribution of the ranges of the total-fusion reaction products of ^{249}Bk(^{22}Ne, 4n)^{267}107 is shown.

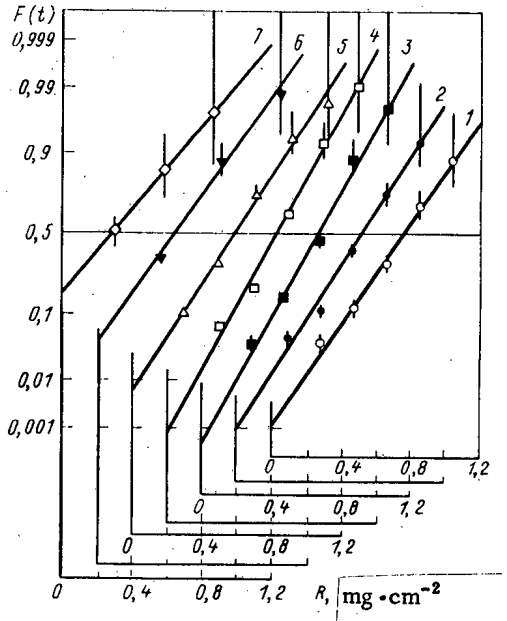

Fig. 4. Gaussian approximation of the range distributions of ^{256}Md recoil nucli in aluminum, shown in Fig. 3: 1) range of angle of flight of recoil nuclei 0-6°; 2) 6-12°; 3) 12-16°; 4) 16-21°; 5) 21-25°; 6) 28-38°; 7) 38-47°; F(t) is the buildup fraction of the total activity of the collectors (Gaussian scale).

Experimental Results. Figure 3 shows the distributions obtained of the ranges of ^{256}Md atoms formed in the reaction ^{249}Bk + ^{22}Ne, for different ranges of angles of flight of the products in the laboratory system of coordinates. The thickness of the foil, corrected for the average value of the given angle of flight of the recoil atom, is plotted along the abscissa, and the measured relative spontaneous fission activity of the foil-collectors in mg/cm^2 is plotted along the ordinate axis. The calculation of the average value of the

TABLE 1. Average Values and Dispersions of the ^{256}Md Recoil Nuclei Ranges in Aluminum, Measured in Different Intervals of Angles of Flight, in the Laboratory System of Coordinates

Interval of angles of flight of recoil nuclei, deg	Range, mg/cm^2	Dispersion, mg/cm^2	Energy of recoil nuclei, MeV
0—6	0,84±0,08	0,28	17,4±1,7
6—12	0,80±0,08	0,26	16,4±1,6
12—16	0,75±0,07	0,23	15,3±1,5
16—21	0,70±0,06	0,22	14,2±1,3
21—25	0,67±0,06	0,27	13,5±1,2
28—38	0,51±0,05	0,29	10,1±1,0
38—47	0,34±0,06	0,35	6,6±1,2

Note. The energy of the recoil nuclei, corresponding to the measured range, was obtained by means of tables [11].

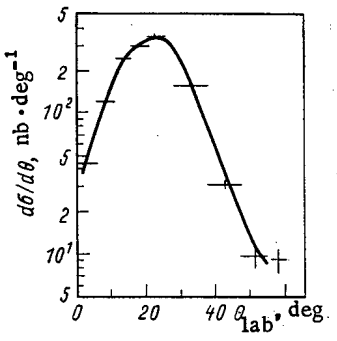

Fig. 5

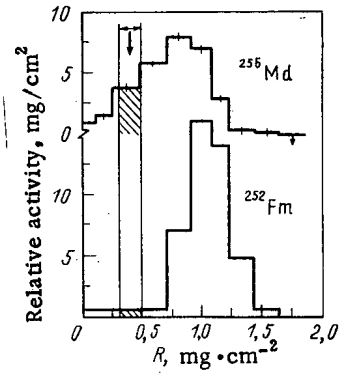

Fig. 6

Fig. 5. Angular distribution in aluminum of ^{256}Md recoil nuclei, formed in the reaction ^{249}Bk + ^{22}Ne with an energy of 118 MeV, in the laboratory system of coordinates. The statistical error is shown at each point of the distribution (by a vertical line), as is the interval of the defined angles θ (by a horizontal line).

Fig. 6. Distribution in aluminum of the ^{256}Md and ^{252}Fm recoil nuclei ranges, formed in the reaction ^{249}Bk + ^{22}Ne with an energy of 118 MeV, measured in the direction of the beam. The calculated distribution is shown of the ranges of the total-fusion reaction products; the arrow corresponds to the average value of the range, and the hatched section corresponds to the region in which 68% of the ^{267}107 (Fig. 6) and ^{256}Ku (Fig. 7) atoms are stopped.

range of the ^{267}107 atom was performed by extrapolation of the table data [11], which agreed quite well with the measured ranges of the heavy recoil atoms [6, 12]. For this, the energy of the recoil nucleus was calculated as

$$E_P = E_P M_P M_R / M_{CN}^2,$$

where the subscripts R, P, and CN relate to the recoil nucleus, the emitted particle, and the compound nucleus, respectively; E is the energy, and M is the mass. The effect of neutron emission on the range of the recoil nucleus was taken into account [13].

In the calculations of the straggling parameter (dispersion of the range distribution), representing the sum of several quantities, the contributions due to stopping processes of the

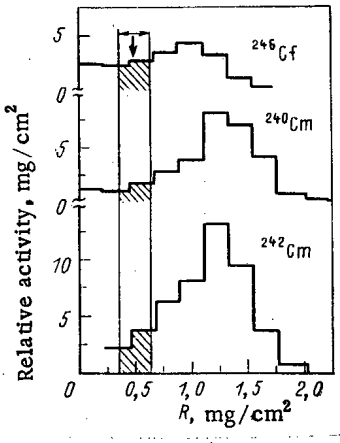

Fig. 7. Distribution in aluminum of the ranges of ^{246}Cf, ^{240}Cm, and ^{242}Cm recoil nuclei, formed in the reaction $^{239}Pu + ^{22}Ne$ with an energy of 121 MeV, measured in the direction of the beam.

TABLE 2. Degree of Separation of the Reaction Products of Total Fusion and Multinucleon Transfers η in the Interaction Reactions Investigated

Interaction reaction	Reaction product	η
$^{249}Bk + ^{22}Ne$	^{256}Md	7,7±0,8
	^{252}Fm	(2,5±0,3) 10^3
$^{239}Pu + ^{22}Ne$	^{246}Cf	7,8±1,0
	^{242}Cm	11,8±1,5
	^{240}Cm	16,3±2,1

heavy atom in the material, neutron boiloff from the compound nucleus, and the finite thickness of the target [13] were taken into account.

In order to determine the average values of the ranges of the atoms and their dispersion for ^{256}Md, a Gaussian approximation was used for the distributions obtained with fitting by the method of least squares, as shown in Fig. 4. The average values of the ranges of the atoms and their dispersion obtained in this way for different ranges of the angles of flight of the recoil nuclei are shown in Table 1. The average value of the range of ^{256}Md in aluminum was corrected for the thickness of the effective working layer of the target and the layer of helium filling the reaction chamber at the time of the experiment. The range correction was done by means of range–energy tables [11] and did not exceed 15% of the experimentally measured values. Table 1 also shows the average energy values of the recoil nuclei, obtained by means of table data [11].

Figure 5 shows the angular distribution of the ^{256}Md recoil nuclei in the laboratory system of coordinates for the reaction $^{249}Bk + ^{22}Ne$. In Figs. 6 and 7, the results are shown of the measurement of the recoil nuclei emitted in the direction of the beam: ^{256}Md and ^{252}Fm, formed in the reaction $^{249}Bk + ^{22}Ne$, and also ^{246}Cf, ^{242}Cm, and ^{240}Cm, formed in the reaction $^{239}Pu + ^{22}Ne$. Only the statistical errors of the measurement are shown in the distribution for ^{256}Md, and the errors are not shown for the distribution of α-active products. In the latter case, they were determined by the systemmatic error due to the geometry of counting and did not exceed 15%.

Discussion of Results and Conclusions. The results derived show that the ranges of the recoil atoms of the multinucleon transfer reaction products in the direction of the beam, with an energy of the impinging ions corresponding to the maxima of the excitation functions of the reactions (^{22}Ne, 4-5n), exceed the ranges of the total-fusion reaction products by a factor of more than two. This fact can be used in experiments for separating the reaction products of total fusion and multinucleon transfers. The data obtained allow quantitative estimates to be made of the degree of separation of these products η, for which was chosen the ratio of the total number of nuclei — multinucleon transfer reaction products — to the number of these nuclei remaining in the stopping region of the total-fusion reaction products. The regions in which 68% of these products are stopped are noted in Figs. 3, 6, and 7. The values of η are given in Table 2. Its data give an idea of the background suppression factor

from the reaction products of multinucleon transfers, which can be achieved by the use of recoil nuclei collectors of appropriate thickness and collimation of the recoil nuclei in experiments on the synthesis of the transfermium nuclides. It should be noted that the similar values for the reaction products of $^{239}Pu + ^{22}Ne$, obtained in the experiment without collimation of the recoil nuclei, did not exceed 2-3.

Thus, relatively shallow collimation and choice of the stopping conditions of the recoil nuclei (preliminary slowing down and appropriate thickness of the stopping layer) allow reaction products of total fusion and multinucleon transfers to be efficiently separated. The separation of the products should be revealed particularly distinctly when such light gases as hydrogen and helium are used as the stopping media. Then the contribution to straggling, due to the stopping process of the heavy atom in the material, which is fundamental in the case of the use of thin targets, will be significantly less [13].

The measurements of the ranges and angular distributions of the recoil nuclei may be found to be useful in the identification of the nuclides in the transfermium region, as they allow kinematic sampling of the most probable reaction channels to be carried out, leading to the formation of the nuclide being observed [14].

In conclusion, the authors consider it their duty to express their acknowledgement to G. N. Flerov and Yu. Ts. Oganesyan for the formulation of the problem and for interest in the project. We also thank S. P. Tret'yakova for ensuring processing of the track detectors, and G. V. Buklanov for the preparation of the targets.

LITERATURE CITED

1. G. V. Buklanov et al., JINR Preprint R7-83-91 [in Russian], Dubna (1983).
2. R. N. Sagaidak et al., JINR Preprint R7-82-890 [in Russian], Dubna (1982).
3. D. Lee et al., Phys. Rev., C25, 286 (1982).
4. Yu. Ts. Oganesyan et al., At. Energ., 28, No. 5, 393 (1970).
5. G. N. Flerov et al., JINR Preprint R7-4932 [in Russian], Dubna (1970).
6. D. Gardes et al., Phys. Rev., C21, 2447 (1980).
7. A. G. Demin et al., JINR Preprint D7-80-556 [in Russian], Dubna (1980), p. 74.
8. F. Hubert et al., Ann. Phys., 5S, 1223 (1980).
9. F. Williamson et al., CEA N 3042, Sasley (1966).
10. A. S. Il'inov and E. A. Cherepanov, Preprint Institute of Nuclear Research P-0090 [in Russian], Moscow (1978).
11. L. Northcliffe and R. Schilling, Nucl. Data Tabl., A7, 223 (1970).
12. R. Hahn et al., Phys. Rev., C10, 1889 (1974).
13. L. Winsberg and J. Alexander, Phys. Rev., 121, 518 (1961).
14. A. G. Demin et al., JINR Preprint D7-82-891 [in Russian], Dubna (1982), p. 52.

ENERGY AND ANGULAR DISTRIBUTIONS OF ELECTRON BREMSSTRAHLUNG FROM THICK TARGETS

V. I. Isaev and V. P. Kovalev

UDC 539.163:539.124

In view of the fact that electron accelerators for an energy of several tens of megaelectron volts are used extensively in industry and the applied sciences it is important to know the energy spectra and angular distributions of bremsstrahlung from targets of different materials and configurations.

At the present time the theory enables us to calculate these characteristics over a limited range of angles, corresponding to roughly half the radiation intensity [1-3]; calculation using the Monte Carlo method is laborious [4, 5] and practically no experimental data are available for the range of large angles. It is of great practical interest to derive an analytic expression for the angular and energy distributions of bremsstrahlung that would permit rapid calculation of these characteristics for different targets.

In this work, using the method of summation with the aid of an approximation series we have obtained analytic expressions for the energy and angular distributions of bremsstrahlung from electrons of energy 10-100 MeV for targets of different configurations in the range of angles from 0 to 90°.

In deriving the formulas we assumed that as it penetrates into the target, an electron continuously loses energy and at a depth t its state is characterized by an average energy E(t); the bremsstrahlung emitted is directed forward, along the ray (line) of electron scattering, and is attenuated according to an exponential law with a minimum absorption coefficient for the given material [6].

The general expression for the calculation of the number of γ-ray quanta of energy k that are emitted from the target at an angle θ into a unit solid angle has the form

$$N(T, \theta, k)\, d\Omega = \frac{N_0}{A} \int_0^y n(t)\, A(t)\, \sigma(E,\ t)\, e^{-\mu(x-t)}\, dt, \tag{1}$$

where N_0 is the Avogadro number, A is the atomic weight, n(t) is the number of electrons at the depth t, A(t) is the angular distribution of the electrons, σ(E, k) is the cross section for the formation of γ-ray quanta of energy k, E is the average electron energy at the depth t, (x − t) is the distance that a γ-ray quantum traverses in the target after formation in the direction of the line of scattering of the electron, μ is the γ-quantum absorption coefficient, T is the target thickness ($g \cdot cm^{-2}$), and y is determined in formula (18).

The principal difficulty in calculating expression (1) is that at this time the integrands n(t) and A(t) are not sufficiently well known for high-energy electrons. We shall calculate expression (1) approximately.

We take n(t) in the form [7]

$$n(t) = \exp\left[-a\,(t/R_e)^b\right], \tag{2}$$

where $b = [387\, E_0/Z\,(1 + 7.5 \cdot 10^{-5}\, ZE_0^2)]^{0.25}$; $a = (1 - 1/b)^{1-b}$, E_0 is the initial electron energy (MeV), and R_e is the extrapolated range,

$$R_e = 0.565 \left(\frac{125}{Z+112}\right) E_0^{0.935}. \tag{3}$$

The angular distribution A(t, θ) of electrons will be written as

Translated from Atomnaya Énergiya, Vol. 57, No. 3, pp. 195-198, September, 1984. Original article submitted January 23, 1984.

0038-531X/84/5703-0643$08.50

$$A(t) = \Gamma(t) \exp[-\alpha(t)\theta^2]. \quad (4)$$

The normalization condition

$$1 = \int_0^{2\pi}\int_0^{\pi} A(t) \sin\theta \, d\theta \, d\varphi = \int_0^{2\pi}\int_0^{\pi} \Gamma(t) e^{-\alpha(t)\theta^2} d\theta \, d\varphi. \quad (5)$$

should be satisfied for A(t, θ).

When integrating over θ we can set the upper limit of integration equal to infinity since the value of the exponent for θ = π is small. The calculation yields

$$1 = 2\pi\Gamma(t) \int_0^{\infty} e^{-\alpha(t)\theta^2} \sin\theta \, d\theta \approx \frac{2\pi\Gamma(t)}{2\alpha}\left[1 - \frac{1}{6\alpha}\right] \approx \frac{\pi}{\alpha}\Gamma(t).$$

The last approximation was obtained for α > 1.

Thus, Γ(t) and α(t) are related by

$$\Gamma(t) = \alpha(t)/\pi. \quad (6)$$

It is known that when the diffusion thickness is reached the angular electron distribution does not change and is described approximately by

$$A(t_d) = \cos^2\theta.$$

We assume that the distribution (4) and the diffusion distribution are equal for θ = 45°:

$$\exp\left[-\alpha(t_d)\left(\frac{\pi}{4}\right)^2\right] = \cos^2 45°.$$

Hence, $\alpha(t_d) = 1.12$. This means that α(t) should have a form such that as the diffusion thickness is approached it tends to the value 1.12 and then does not change (or changes only very little) upon a further increase in the thickness.

For thin targets electron scattering is described by the Moliere distribution [8]

$$A(t) \exp\left(-\frac{\theta^2}{\theta_0^2}\right), \quad (7)$$

where $\theta_0^2 = (44.8)^2 \Big/ \left(\frac{E_0 + mc^2}{mc^2} - \frac{mc^2}{E_0^2 + mc^2}\right)^2 \frac{t}{A} B$ (deg).

It thus follows that α(t) ∿ 1/t.

We choose α(t) in the form

$$\alpha(t) = \frac{U_0}{t + t^2} + 1. \quad (8)$$

For small values of t expression (8) leads to α(t) ∿ 1/t, since the first term is considerably greater than unity; for a larger thickness, equal to the diffusion thickness, α(t) → 1.

For targets in which electrons lose only an insignificant part of their initial energy but are scattered many times, the angular distribution of the bremsstrahlung is determined almost completely by the angular distribution of the electrons [9]. It was shown in [10] that in this case the part I(0) of the electron energy that is emitted into a unit solid angle in the forward direction is given by

$$I(0) = \frac{E_0^2 \tau}{440\pi} \ln(950 t_r). \quad (9)$$

Here, t_r is the target thickness and the radiation length and τ is the radiation energy loss per radiation length.

The range of thicknesses corresponding to this case lies between the limits $5 \cdot 10^{-4} \ll t \ll 1$ (in radiation lengths X_0).

From this we can determine the constant U_0 in expression (8). Multiplying by k and integrating both parts of equality (1) over the photon energy from zero to the maximum value E_0, we get the intensity (or energy) of the bremsstrahlung radiated in the direction of the given angle. Using the approximate equality

$$(dE/dx)_{\text{rad}} \approx cE \approx \frac{N_0}{A} \int_0^E \sigma(E, k)\, k\, dk, \tag{10}$$

we get

$$I(\theta) = \int_0^y cE(t)\, n(t) \frac{\alpha(t)}{\pi} e^{-\alpha(t)\theta^2} e^{-\mu(x-t)}\, dt. \tag{11}$$

For high-energy electrons [1] we have

$$E(t) = E_0 \exp(-\xi t), \tag{12}$$

where $(dE/dx)_{\text{rad}}$ is the radiation energy loss by an electron per unit length, $\xi = (dE/dx)_{\text{tot}}/E_0$, and $(dE/dx)_{\text{tot}}$ is the total electron energy loss per unit length.

For thin targets $n(t) \approx 1$, $e^{-\xi t} \approx 1$, $e^{-\mu(x-t)} \approx 1$, and for zero degrees $e^{-\alpha(t)\theta^2} = 1$, we find that equality (9) is equal to expression (11):

$$I(0) = \frac{E_0^2 \tau}{444\pi} \ln(950 t_p) = \int_0^y cE_0 \frac{\alpha(t)}{\pi}\, dt. \tag{13}$$

For a small thickness, $\alpha(t)$ can be written as $\alpha(t) = (U_0/t) + 1$. Then, integrating the right-hand side of expression (13) and setting the lower limit of integration equal to $0.00105X_0$, we get an equality in which we neglect the insignificant terms and from this we determine U_0:

$$U_0 = \frac{E_0 \tau}{440c}. \tag{14}$$

Thus,

$$\alpha(t) = \frac{E_0 \tau}{440c\,(t + t^2)} + 1. \tag{15}$$

The bremsstrahlung cross section is written as

$$\sigma(E, k) \approx \left(\frac{1}{k} - \frac{1}{E}\right) \tag{16}$$

and the proportionality factor is found from the condition

$$(dE/dx)_{\text{rad}} \approx cE = \int_0^E \sigma(E, k)\, k\, dk = d \int_0^E \left(\frac{1}{k} - \frac{1}{E}\right) k\, dk;\ d = 2c. \tag{17}$$

We substitute all the necessary functions into expression (1) and make the change

$$\exp[-\alpha(t)\,\theta^2] \approx \frac{1}{1 + c_2^2 \theta^2};$$

we determine c_2^2 from the condition

$$0.5 = \exp[-\alpha(t)\,\theta_{1/2}^2] = \frac{1}{1 + c_2^2 \theta_{1/2}^2}, \qquad \theta_{1/2}^2 = \frac{\ln 2}{\alpha(t)}, \quad c_2^2 = \frac{\alpha(t)}{\ln 2}, \qquad \frac{1}{1 + c_2^2 \theta^2} = \frac{\ln 2}{\ln 2 + \theta^2} \frac{t}{\frac{U_0 \theta^2}{\ln 2 + \theta^2} + t}, \quad u = \frac{U_0 \theta^2}{\ln 2 + \theta^2},$$

$$\exp[-a\,(t/R_e)^b + \mu t] \approx \frac{1}{1 + c_3^2 t^2},$$

where $c_3^2 = [2 \exp(\mu t_0) - 1]/t_0^2$, $t_0 = R_e (\ln 2/a)^{1/b}$, $z = 1/c_3^2$.

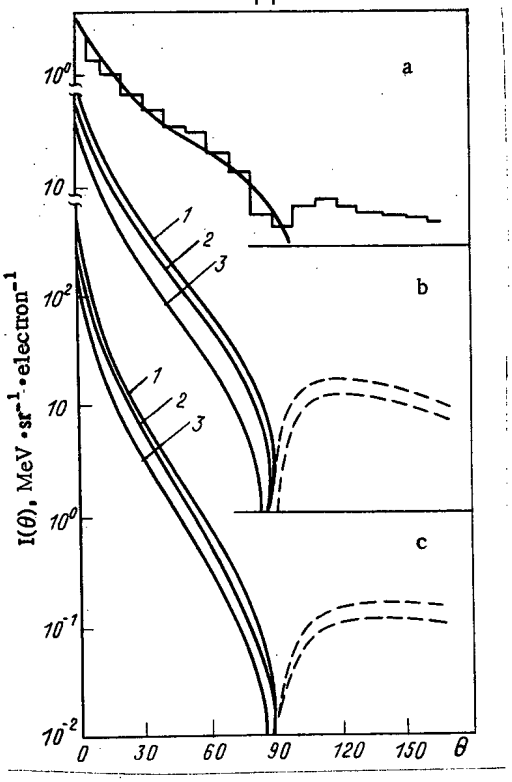

Fig. 1. Angular distribution of the bremsstrahlung of electrons from a tungsten target: a) E_0 = 10 MeV, T = 3.1 g·cm^{-2}; b) 30 MeV [1) 6 g·cm^{-2}, 2) 12 g·cm^{-2}, 3) 24 g·cm^{-2}]; c) 60 MeV [1) 8.25 g·cm^{-2}, 2) 16.5 g·cm^{-2}, 3) 33 g·cm^{-2}]; the histogram and the dashed lines represent Monte Carlo calculations [4, 5]; for b and c the results of the calculation from formula (19) and by the Monte Carlo method practically coincide in the range of angles 0-90°.

Then solving Eq. (1) reduces to the calculation of the expression

$$N(\theta)\,d\Omega = \frac{\ln 2}{\ln 2+\theta^2}\,\frac{2cz}{\pi}\,e^{-\mu x}\left(\frac{1}{k}-\frac{1}{E_0}\right)\int_0^y \frac{1}{z+t^2}\,\frac{U_0+t+t^2}{t+t^2}\,\frac{t}{u+t}\,dt.$$

This calculation gives for the bremsstrahlung spectrum the expression

$$N(\theta)\,d\Omega = \frac{\ln 2}{\ln 2+\theta^2}\,\frac{2cz}{\pi}\,e^{-\mu x}\left(\frac{1}{k}-\frac{1}{E_0}\right)\left\{A\ln(1+y)+B\ln\frac{u+y}{u+0{,}001X_0}+\frac{C}{2}\ln\frac{z+y^2}{z}+\frac{D}{\sqrt{z}}\operatorname{arctg}\frac{y}{\sqrt{z}}\right\}, \quad (18)$$

where X_0 is the radiation length,

$$A = U_0/[(z+1)(u-1)],\ B = [-u(1-\mu u) + (z+1)A]/(z+u^2),\ C = \mu - A - B,\ D = 1 - \mu u + A + uB,\ y = \frac{1}{\xi}\ln(E_0/k_x) \text{ if } 0 \leqslant k \leqslant k_x,\ y = \frac{1}{\xi}\ln(E_0/k) \text{ if } k_x < k \leqslant E_0.$$

Here $k_x = E_0 \exp(-\xi x)$.

When calculating the energy (intensity) (11) of the bremsstrahlung emitted in the direction of a given angle per unit solid angle, we make the substitution

$$\exp[-a(t/R_e)^b - (\xi-\mu)] \approx \frac{1}{1+c_1^2t^2},$$

where $c_1^2 = \{2\exp[(\xi-\mu)t_0] - 1\}/t_0^2$,

and we denote $v = 1/c_1^2$.

Calculation of Eq. (11) gives the following expression for the bremsstrahlung intensity:

$$I(T,\ \theta)\,d\Omega = \frac{\ln 2}{\ln 2+\theta^2}\,\frac{cvE_0}{\pi}\exp(-\mu x)\left\{A\ln(1+x)+B\ln\frac{u+x}{u+0{,}001X_0}+\frac{C}{2}\ln\frac{v+x^2}{v}+\frac{D}{\sqrt{v}}\operatorname{arctg}\frac{x}{\sqrt{v}}\right\}, \quad (19)$$

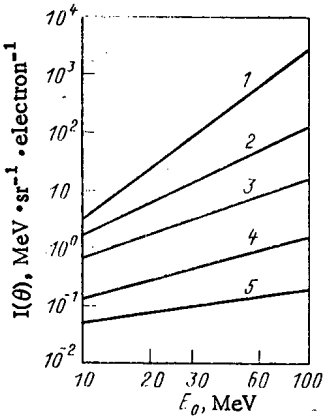

Fig. 2. Bremsstrahlung yields from a target (tungsten) of optimum thickness in the direction θ as a function of the electron energy E_0: 1) 0°, 2) 10°, 3) 30°, 4) 90°, 5) 180°.

where $A = U_0/[(1+v)(u-1)]$, $B = -[u+(1+v)A]/(v+u^2)$, $C = -A-B$, $D = 1+A+B$.

For the intensity in the forward direction at θ = 0° formula (19) gives us the expression

$$I(T,\ \theta)\,d\Omega = \frac{cvE_0}{\pi}\exp(-\mu T)\left\{A\ln(1+T) + B\ln\frac{950T}{X_0} + \frac{C}{2}\ln\frac{v+T^2}{v} + \frac{D}{\sqrt{v}}\operatorname{arctg}\frac{T}{\sqrt{v}}\right\}, \qquad (20)$$

where x is defined as the distance calculated along the ray in the direction of the angle θ from the point of incidence of the electron to the point of intersection of the ray with the line forming the external profile of the target.

Formulas (18)-(20) enable us to calculate the bremsstrahlung spectrum and intensity for a target of any material and any configuration for angles ranging from 0 to 90°. The results are expressed for the spectra [photon·MeV^{-1}·sr^{-1}] and for the intensity [MeV·sr^{-1}] and are normalized to one incident electron.

For a plane-parallel plate of thickness T that is infinite in the transverse direction

$$x = T/\cos\theta,$$

while for a disk of height T and radius r

$$x = T/\cos\theta, \quad \text{if} \quad \theta \leqslant \operatorname{arctg}\frac{r}{T};$$

$$x = r/\sin\theta, \quad \text{if} \quad \operatorname{arctg}\frac{r}{T} \leqslant \theta \leqslant 90°.$$

Figure 1 presents the values of the intensity of bremsstrahlung at angles of 0-90°, calculated from formula (19) and by the Monte Carlo method for angles 0-180° [4, 5].

In some cases, e.g., when assessing radiation hazard, it is necessary to know the maximum values of the intensity of bremsstrahlung emitted from a target in a given direction. Analysis of expression (19) shows that for the forward direction the optimum thickness of a target of heavy elements (tungsten—uranium) is 1.5-2.5 g·cm^{-2} for an electron energy range of 10 to 100 MeV. When the angle increases, the value of the optimum thickness increases and at 90° reaches a value of 0.5 of the electron mean free path. From the data of [4, 5] we can conclude that for angles of 180° the optimum thickness is close to the electron mean free path.

Figure 2 shows the yields of bremsstrahlung from a target of optimum thickness for the chosen direction, plotted as a function of the electron energy. The intensity in the forward direction from the target of optimum thickness is proportional to the third power E_0^3 of the electron energy. The proportionality factor is $3.16\cdot10^{-3}$. With increasing angle the degree of dependence of the intensity on the electron energy decreases and is 1.1 at 90° and 0.6 at 180°.

LITERATURE CITED

1. C. Emigh, "Thick target bremsstrahlung theory," LA4097-MS (1971).
2. Ferdinande et al., Nucl. Instrum. Methods, 91, 135 (1971).

3. V. E. Zhuchko and Yu. M. Tsipenyuk, At. Energ., 39, No. 1, 66 (1975).
4. M. Berger and S. Seltzer, Phys. Rev., 2, 621 (1970).
5. V. I. Tsovbun, Preprint R16-11132, Joint Institute for Nuclear Research, Dubna (1977).
6. D. L. Broder et al., Concrete in Shielding for Nuclear Installations [in Russian], 2nd ed., Atomizdat, Moscow (1973).
7. P. Ebert et al., Phys. Rev., 183, 422 (1969).
8. G. Moliere, Z. Naturforsch., 3, 78 (1948).
9. W. J. Price et al., Nuclear Radiation Detection, McGraw-Hill (1964).
10. J. Lawson, Nucleonics, 10(11), 61 (1952).

LETTERS TO THE EDITOR

CALCULATION OF EQUIVALENT AND ABSORBED PHOTONEUTRON DOSES

V. I. Isaev and V. P. Kovalev

UDC 539.136:539.124

Since electron accelerators are widely used as neutron sources, it is necessary to estimate dose rates at operating areas due to photoneutrons from accelerator targets.

The dose rate produced by neutrons with an energy distribution N(E) [neutrons/(cm^2·sec·MeV)] is calculated from the expression

$$P=\int_0^\infty N(E)\,\beta(E)\,dE, \tag{1}$$

where $\beta(E)$ is the dose factor [1].

Since the functions N(E) and $\beta(E)$ cannot generally be expressed analytically, the integration is replaced by a summation, the neutron energy distribution is represented by a set of monoenergetic groups, and the continuous function $\beta(E)$ is replaced by a group distribution, i.e., by a set of factors β averaged over the neutron energy-group limits.

The spectrum of the photoneutrons produced by electron accelerator targets is continuous, and in most cases is satisfactorily described by the simple expression

$$N(E)=T^{-2}E\exp(-E/T), \tag{2}$$

where T is the effective nuclear temperature.

If $\beta(E)$ is expressible in analytic form, an analytic expression can be obtained for the photoneutron dose rate.

For the equivalent dose the dose factor $\beta(E)$ is represented by the Snyder–Neufeld dose relation. This relation is difficult to express by a single curve over the photneutron spectrum, which extends from zero to several MeV. In order to represent it in piecewise component form, we divide the whole range into three regions:

$$\begin{aligned}&\text{for } 100\text{ eV}\leq E<9\text{ keV},\ \beta(E)=1.6\times10^{-9}\text{ rem/(neutron/cm}^2);\\&\text{for } 9\text{ keV}\leq E<1.1\text{ MeV},\ \beta(E)=10^{-7.35}\,E^{0.682}\text{ rem/(neutron/cm}^2);\\&\text{for } 1.1\text{ MeV}\leq E<\infty,\ \beta(E)=5\times10^{-8}\text{ rem/(neutron/cm}^2).\end{aligned} \tag{3}$$

Since the photoneutron spectrum has few low-energy neutrons, the first region in the integration can be neglected, and for convenience of calculation the relation for the second region can be extended to zero. Then the integral in Eq. (1) can be written as the sum of two integrals:

$$\int_0^\infty N(E)\,\beta(E)\,dE=10^{-7.35}\int_0^{1.1}T^{-2}Ee^{-E/T}E^{0.682}\,dE+\int_0^\infty 5\cdot10^{-8}T^{-2}Ee^{-E/T}\,dE. \tag{4}$$

Calculation yields the equivalent dose (in rem) from a unit flux of photoneutrons incident on an area of 1 cm^2 (1 rem = 10 mSv):

$$P=[4.47T^{0.682}\gamma(2.682;\ 1.1/T)+5(1.1-T)e^{-1.1T}]\,10^{-8}, \tag{5}$$

where $\gamma(\alpha, x)$ is the incomplete gamma function [2], $\alpha = 2.682$, and $x = 1.1/T$.

In the energy range 0.02–7 MeV the dose factor $\beta(E)$ (rad) for the absorbed dose is expressed in the form [3] (1 rad = 0.01 Gy)

Translated from Atomnaya Énergiya, Vol. 57, No. 3, pp. 199–200, September, 1984. Original article submitted October 27, 1983.

0038-531X/84/5703-0649$08.50

$$\beta(E) = 2{,}9 \cdot 10^{-9} E^{0{,}43}. \quad (6)$$

Substituting it into Eq. (1), performing the integration, and taking the upper limit as infinity, we obtain the absorbed dose (in rad/neutron) for one photoneutron incident on an area of 1 cm^2:

$$P = 3.67 \cdot 10^{-9} T^{0.43}. \quad (7)$$

With an accuracy sufficient for practical purposes, we assume that the photoneutron spectrum does not depend on the angle of emission of a photoneutron, the angular distribution of the photoneutrons is isotropic, and the target region in which most of the photoneutrons are produced is a point in comparison with the distance R to the operating area. Under these conditions the dose rate at the operating area due to photoneutrons produced in a target of atomic number Z and thickness t by electrons of energy E_0 and a current I is

$$D = \frac{6.25 \cdot 10^{18} I B(E_0, Z, t)}{4\pi R^2} P, \quad (8)$$

where 6.25×10^{18} is the number of electrons corresponding to a current of 1 A, $B(E_0, Z, t)$ is the photoneutron yield from a target on which one electron is incident [4], and P is the equivalent or absorbed dose produced by one photoneutron [cf. Eqs. (5) or (7)].

To transform the results obtained into SI units, Eqs. (5) and (7) must be multiplied by 10^{-2}. The errors of the final results are determined mainly by the error of the effective temperature, the photoneutron yield, and the approximation of the dose factor. The estimated error of the calculation of the equivalent and absorbed doses is 20-40%.

Let us compare the calculated values with published experimental data. Kovalev [5] measured the absorbed doses of photoneutrons produced by a 6-cm-diam. spherical lead target bombarded with 25-MeV electrons. Dosimeters were located at an angle of 90° with the direction of the electron beam at a distance of 20 cm from the target, and lead shields 10-20 cm thick were located between the target and the dosimeters. The following values were obtained for the absorbed doses: for a 10-cm-thick shield 1.3 rad/μA·min; for a 20-cm-thick shield 1.0 rad/μA·min.

Let us calculate the absorbed dose with Eqs. (7) and (8). For a 4-cm-thick lead target and T = 1 MeV, $B(25, 82, 4) = 70 \times 10^{-4}$ neutrons/electron. The photoneutrons are attenuated by a factor of 2.7 in passing through a 20-cm-thick lead shield, and by 1.73 in passing through a 10-cm-thick lead shield [5].

Substituting these values into Eqs. (7) and (8), we obtain

$$D = \frac{6.25 \cdot 10^{12} \cdot 60 \cdot 75 \cdot 10^{-4}}{4 \cdot 3{,}14 \cdot 400 \cdot 2.7} 3.67 \cdot 10^{-9} = 0.76 \text{ rad/μA·min for a 20-cm-thick shield,}$$

$$D = \frac{6.25 \cdot 10^{12} \cdot 1 \cdot 60 \cdot 75 \cdot 10^{-4}}{4 \cdot 3{,}14 \cdot 400 \cdot 1.73} 3.67 \cdot 10^{-9} = 1.19 \text{ rad/μA·min for a 10-cm-thick shield.}$$

The differences between the calculated and experimental values are 32 and 5%, respectively, which is consistent with the errors of the data used in the computations.

LITERATURE CITED

1. Yu. A. Egorov, Principles of Radiation Safety of Nuclear Power Plants [in Russian], Énergoatomizdat, Moscow (1982).
2. I. S. Gradshtein and I. M. Ryzhik, Tables of Integrals, Series, and Products, Academic Press, New York (1965).
3. V. I. Ivanov, A Course in Dosimetry [in Russian], Atomizdat, Moscow (1970).
4. V. P. Kovalev and V. I. Isaev, "Calculation of the yield of photoneutrons in the bombardment of thick targets by 10-150-MeV electrons," in: Neutron Physics. Materials from the Fifth All-Union Conf. on Neutron Physics [in Russian], TsNIIatominform (1980), pp. 124-129.
5. V. P. Kovalev, Secondary Radiations of Electron Accelerators [in Russian], Atomizdat, Moscow (1979).

INVESTIGATION OF THE INFLUENCE OF THE SURROUNDING MATERIAL ON THE ACTIVATION OF SAMPLES IN A NEUTRON-ACTIVATION APPARATUS WITH CENTRALLY LOCATED SOURCE

B. S. Vakhtin, V. S. Ivanov, and G. A. Kuznetsov

UDC 543.53

In a previous paper [1] we showed that when a californium source is placed inside a cassette along with a sample (so-called central geometry) the fast-neutron flux is used more efficiently than in a geometry providing for plutonium–beryllium source outside the sample. Even though the average energy of neutrons from californium sources is lower than the average energy of neutrons from plutonium–beryllium sources (2.34 and 4.0–4.5 MeV, respectively), the effect of activation of silicon and aluminum is sufficient for the more accessible californium sources, which are small in comparison, e.g., with plutonium–beryllium sources, to be used in neutron-activation analysis.

As already mentioned, this apparatus is provided with a cassette of a special shape: its lower part has a vertical cylindrical channel to half the cassette height. In the irradiation position the cassette is inserted by means of this channel onto a neutron source and as a result the source is in the center of the cassette with the sample. The radiation from the source is used in almost a 4π geometry.

In this work we carried out a series of measurements to assess how the materials surrounding the sample affect the activation of aluminum and silicon specifically for the given neutron-activation apparatus. Two artificial samples were used in our studies. The first consisted of a mixture of chemically pure aluminum oxide and calcium carbonate (content 10% Al_2O_3) and the other consisted of quartz glass powder (100% SiO_2). The mass of each sample was 290 g.

In the experiments these samples were irradiated with neutrons from a californium source inside the cassette containing the sample, with and without neutron-scattering or absorbing materials near the sample; the induced γ-ray activity of these samples was then measured. As a result, the (n, γ) and (n, p) nuclear reactions occurring in aluminum and silicon nuclei, respectively, produce ^{28}Al which has a half-period $T_{1/2} = 2.3$ min and a γ-ray energy $E = 1.78$ MeV.

In the first experiment no scattering or absorbing materials were present next to the sample in the channel. The holder with the source was set up on a vertical support (a rod of diameter about 10 mm and height 1.6 m) at a distance of no less than 1.5 m from the walls or other protruding objects (see Fig. 1a). For the duration of the irradiation (6 min) the cassette with the sample was inserted onto the holder with the neutron source. After the irradiation the sample was removed from the holder and put into the detection unit where in 5.4 min (according to the timer of the instrument) its induced γ-ray activity was measured. The interval between the completion of irradiation and the onset of the measurement was 20 sec. The samples were re-irradiated no sooner than 1 h after completion of the measurement. The times of the irradiation, interval, and measurement were the same in all the experiments.

The detection unit was made up of a scintillation detector, consisting of a thallium-activated sodium iodide single cyrstal (diameter 160 mm and height 200 mm) with a well of diameter 70 mm, and an FÉI-49 photomultiplier. In order to reduce the background the detector was placed in a lead housing (wall thickness 10 cm). An AI-256-6 pulse-height analyzer served as the recording instrument. The ^{28}Al photopeak was identified on the basis of 26 selected channels. The stability of the channels was checked with the aid of ^{40}K γ-rays ($E = 1.46$ MeV) from a potassium preparation. We also checked the position of the photopeak (channel number) and its magnitude. The neutron yield of the californium source (diameter 7 mm and length 14 mm) was 1.8×10^7 sec^{-1}.

Translated from Atomnaya Énergiya, Vol. 57, No. 3, pp. 200–201, September, 1984.

0038-531X/84/5703-0651$08.50

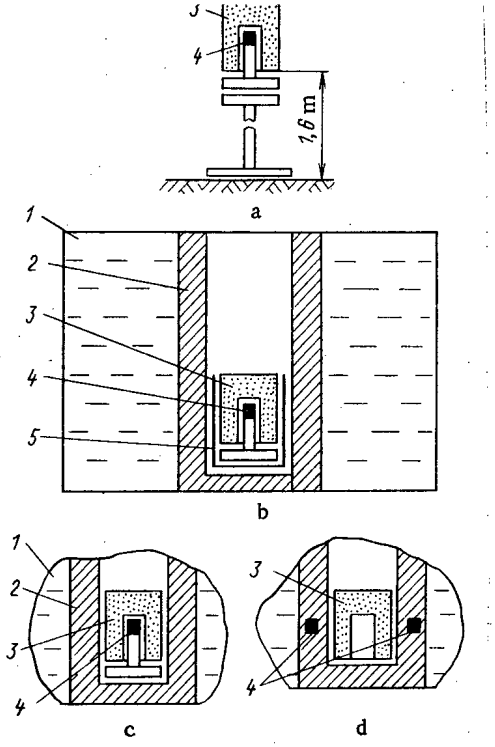

Fig. 1. Diagram of irradiation of samples (in experiment): a) in absence of absorbing or scattering materials; b) in cadmium shield; c) in moderator; d) from two sources outside the sample; 1) water; 2) organic glass; 3) sample; 4) neutron source; 5) cadmium shield.

TABLE 1. Influence of the Surrounding Material on the Activation of Aluminum and Silicon from a Californium Neutron Source

Position	Position of source, cassette, surrounding material	Sample	Total count in photopeak	Normalized count
1	Source inside cassette. Cassette at distance ≥ 1.5 m from floor and wall	10 % Al_2O_3	1393	0,22
		100 % SiO_2	72490	2,48
2	Source inside cassette. Cassette inside cadmium shield. Shield surrounded by organic glass and water	10 % Al_2O_3	3150	0,83
		100 % SiO_2	72596	2,46
3	Source inside cassette. Cassette in organic glass block surrounded by water	10 % Al_2O_3	63682	21,7
		100 % SiO_2	73122	2,49
4	Two sources outside sample in organic glass block surrounded by water	10 % Al_2O_3	39879	28,2
		100 % SiO_2	9334	0,60

Notes: 1. The background count was 730 pulses for the standard aluminum sample and 700 pulses for the standard silicon sample.
2. The table gives the arithmetical mean of two measurements for each sample.

Table 1 gives the results of this experiment: the count, in pulses (without background), in the region of the ^{28}Al photopeak, normalized to a mass of 1 g and an oxide concentration of 1%. This count is 2.48 pulses for silicon and 0.22 pulse for aluminum (position 1). The next experiments were carried out in the irradiation unit of the neutron-activation apparatus. Upon irradiating the samples with fast neutrons (in a cadmium shield, i.e., a thermal-neutron absorber), we established that the silicon activation remained at the same level (position 2), i.e., fast neutrons do not return into the bulk of the sample from the surrounding scattering material (Fig. 1b), i.e., organic glass and water. The increase in the aluminum activation can be attributed to the influence of the neutron scatterer (organic glass) in the upper part of the working channel.

In position 3 (see Fig. 1c) the cassette with the sample is surrounded by scattering materials (organic glass, water); an intensive zone of thermal neutrons forms in the scatterers and part of these neutrons diffuse into the sample, causing an aluminum activation of 21.7 pulses. The silicon activation increased insignificantly, by roughly 1 rel. %. The final experiment was carried out with two californium sources which were located outside the sample (Fig. 1d) and has a total neutron yield of $8.0 \cdot 10^6$ sec^{-1}. The aluminum activation, converted to the yield of the source used in the "central" geometry, is 28.2 pulses (position 4).

Upon analyzing the results of the experiments, we can note that the silicon is activated only by the fast neutrons of the source itself; there are no reflected or scattered fast neutrons here and, therefore, it does not matter what medium lies behind the cadmium shield. The aluminum activation by thermal neutrons in the "central" geometry per unit neutron yield is lower than for the case when two californium sources are outside the sample but higher than for plutonium–beryllium sources (see [1]). Moreover, when samples are irradiated in the "central" geometry the total induced activity from the silicon includes a contribution due to the activation of the silicon by fast neutrons from the source. When the californium sources are located laterally this contribution decreases by a factor of almost 7. Thus, the arrangement in which the source is centrally located is optimum for the silicon determination while the lateral arrangement is optimum for the aluminum determination.

In designing the irradiation unit of the neutron-activation apparatus, in order to simplify the operations of irradiating samples and to reduce the radiation hazard we adopted the "central" geometry optimum for silicon analysis. Although the possibilities of improving the conditions of sample irradiation with thermal neutrons are not realized completely in this geometry, as already mentioned these conditions are more favorable than when two plutonium–beryllium sources located outside the sample are used.

The irradiation unit of the neutron-activation apparatus with a centrally located source is described in [1]. The neutron source is placed in a yoke of the holder and is set on the bottom of the working channel. For the irradiation of a sample with fast neutrons a cup-shaped cadmium shield 1 mm thick, which has in its bottom a hole equal in diameter to the yoke of the source holder, is put into the working channel. For the irradiation of a sample with thermal neutrons the cadmium shield is removed and a "neutral" shield (of organic glass, polyethylene, etc.) is put in its place so as to maintain the diameter of the working channel.

This arrangement is used for neutron-activation analysis of potassium-bearing ores to determine the presence of aluminum and silicon. Upon comparison of the measured values we see that there is no loss of statistics in relation to the arrangement in which plutonium–beryllium sources were used. The relative change in the counting rate for plutonium–beryllium and californium sources as a function of the silicon concentration upon irradiation with fast neutrons is roughly the same: for a sample containing 61.2% SiO_2 the activation increased by 25-28% in comparison with a sample containing 49.6% SiO_2. When thermal neutrons were used, the activation of samples containing 11.82 and 24.02% Al_2O_3 increased 2.16 times for a californium source and 1.8 times for plutonium–beryllium sources. This apparatus is also used for the neutron-activation determination of sodium on the basis of ^{24}Na ($T_{1/2} = 15$ h, $E = 1.37$ and 2.75 MeV) as well as for γ-ray spectrometric analysis for potassium (on the basis of the natural γ-ray activity of ^{40}K).

LITERATURE CITED

1. B. S. Vakhtin and G. A. Kuznetsov, At. Energ., 54, No. 1, 60 (1983).

EFFECT OF TEMPERATURE ON THE INDICATIONS OF MAGNETIC FLOWMETERS IN THE SODIUM LOOPS OF THE POWER BLOCK OF BN-600

A. I. Karpenko, A. A. Lyzhin, V. P. Minin, and A. G. Sheinkman

UDC 621.039.564.5

The validity of information obtained from magnetic flowmeters (MF) in the sodium loops of the power block of BN-600 is of great significance for ensuring plant reliability and safety. The indications of these flowmeters are used in the accident containment system, for operational control of the flow rate through the active zone of the reactor, for determining the maximal temperature of the jackets of the fuel elements, in the remote control system, and in determining the hydraulic characteristics of the secondary loops in the second main loop and the distribution of flow rates of the heat carrier along sections of the steam generators. In this connection, it is necessary to know how different factors, including the temperature of the heat carrier, which can vary over a wide range, can affect the indications of MF during reactor operation. However, up to now, the effect of the temperature of the heat carrier on the indications of the MF, especially for pipes with large diameter, has not been studied systematically [1, 2].

After the power block with the fast BN-600 reactor was started up at the Beloyarskoi Nuclear Power Plant, constant observations were made of the indications of the MF, placed in the bypass secondary loop of the first main loop with a pipe diameter of 50 mm and in the pipelines with a diameter of 300 mm at the outlet from each section of all steam generators. The MF of the first main loop were calibrated during the power start-up of the power block of BN-600 with a sodium temperature of $\sim$240°C.

As the power of the reactor increases, the temperature of the heat carrier increases up to 360°C. An experiment was therefore performed to determine the effect of a change in the sodium temperature on the indications of the MF in the bypass secondary loop of the reactor with a constant rate of rotation of the principal circulation pumps in the first main loop (PCP-1). The experimental results are presented in the form of the dependence $K_t = u_{305}/u_t$, where u_{305} and u_t are the signals (in mV) at 305°C and the temperature t, respectively (Fig. 1). In the range of variation of the sodium temperature studied, the variations in the indications of the MF do not exceed ±1.5% of the average value.

The sectioned MF in the second main loop were calibrated by a correlation method with a sodium temperature of $\sim$260°C [3, 4]. The results of the calibration were used to determine the dependence of the flow rate of sodium in the secondary loop on the rate of rotation on the principal circulation pump in the second main loop (PCP-2) for each secondary loop. In order to determine the effect of the sodium temperature at the outlet from the sections of the steam generators on the indications of the MF, placed in the pipes with an inner diameter of 300 mm, we measured the signals from the MF accompanying a change in the sodium temperature from 225 to 315°C with a constant rate of rotation of PCP-2.

In the analysis of the results obtained, it was established that the signal from each sectioned MF decreases as the sodium temperature is increased practically linearly, while the absolute increment in the signal does not depend on the initial level. Thus the results of experiments with MF in pipelines with diameters of 50 and 300 mm showed that as the diameter of the pipeline is increased, the effect of the temperature of the liquid metal on the indications of the MF increases. This phenomenon is explained by the change in the physical characteristics of the flow and a change in the size and properties of the gap between the pipeline and the magnetic mass.

The computed increase in the signal from the MF due to the change in dimensions and the electrical resistance of the wall of the pipe made of Kh18N10T steel with an increase of 100°C

Translated from Atomnaya Énergiya, Vol. 57, No. 3, p. 202, September, 1984. Original article submitted November 9, 1983.

0038-531X/84/5703- 0654$08.50

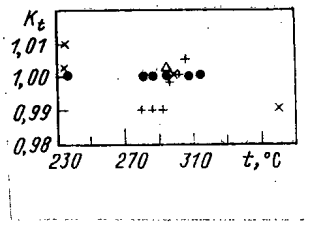

Fig. 1

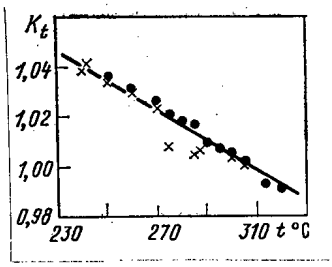

Fig. 2

Fig. 1. Effect of the temperature on the indications of the MF in the bypass secondary loop in the pipeline with a diameter of 50 mm with a rate of rotation of PCP-1 of 280 (•), 315 (Δ), 340 (+), and 680 (×) rpm.

Fig. 2. Effect of the temperature in a pipeline with a diameter of 300 mm on the indications of the MF in the section A4 of the steam generators 5 (×) and 6 (●).

in the sodium temperature is equal to ∿0.7% [2]. This value is much smaller than the observed changes in the signal. Figure 2 shows how the coefficient of change of the MF signal ($K_t = u_{305}/u_i$) in the second main loop depends on the temperature. It was established that k_t depends practically linearly on the sodium temperature and does not depend on the rate of rotation of PCP-2.

It is shown in [4] that the flow rate of the heat carrier through the section of the steam generator is an indirectly measured quantity, related to the signal of the MF by an approximate relation of the form

$$u = AG - BG^2, \tag{1}$$

where u is the signal in mV; G is the volume flow rate in m^3/h; and A and B are the approximation coefficients.

In order to account for the dependence of the signal u on the temperature of the heat carrier, the values of the coefficient K_t obtained must be introduced into the relation (1). In this case, the volume flow rate of the heat carrier will be related to the MF signal by the formula

$$u_{red} = K_t u_t = (A_1 G - B_1 G^2), \tag{2}$$

where u_{red} is the reduced value of the signal with respect to the selected reference temperature.

Thus, in the range of the heat-carrier temperatures in the first main loop from 220 to 360°C studied, the signal of the MF placed in the pipeline with an inner diameter of 50 mm is virtually independent of the temperature. The indications of the MF placed in a pipeline with an inner diameter of 300 mm depends strongly and almost linearly on the temperature. The true flow rate of the heat carrier can be determined from the measured signal by introducing into it an empirical correction factor that takes into account the effect of the temperature.

LITERATURE CITED

1. L. A. Adamovskii, K. A. Aleksandrov, and V. V. Golovanov, "Methods and means for measuring the flow rate of the sodium heat carrier in the power blocks of sodium reactors," Review, NIIAR, Dimitrovgrad (1982).
2. N. I. Loginov, Electromagnetic Transducers of the Flow Rate of Liquid Metals [in Russian], Énergoizdat, Moscow (1981).
3. B. V. Kebadze, N. V. Krasnoyarov, L. A. Adamovskii, et al., "Correlation measurements of the sodium flow rate with the help of magnetic sensors," At. Energ., 45, No. 1, 30-35 (1978).

4. L. A. Adamovskii, V. G. Vysotskii, and V. V. Golovanov, et al., "Correlation measurements of the sodium flow rate in the BN-600 plant," ibid., 54, No. 2, 100-103 (1983).

INFLUENCE OF A RESONANCE BUFFER GAS ON THE CHARACTERISTICS OF THE PROCESS OF INFRARED MULTIPHOTON DISSOCIATION OF 2-CHLOROETHENYL DICHLOROBORANE

G. I. Abdushelishvili, T. G. Abzianidze, A. S. Egiazarov, G. I. Tkeshelashvili, and T. B. Tsinadze

UDC 621.033.343:546.262.7

Jensen in [1] and we in [2] investigated the isotopic effect and the process of multiphoton dissociation (MPD) of molecules of 2-chloroethenyl dichloroborane in the radiation field of a pulsed CO_2 laser. In the present article we study the influence of buffer gases on the process of infrared multiphoton dissociation (hereinafter called IR dissociation) of $HClC{=}CHBCl_2$ molecules, as well as the frequency characteristics of their isotopically selective dissociation.

Figure 1a shows the spectral variation of the yield of the dissociation of the molecules $HClC{=}CH^{10}BCl_2$ and $HClC{=}CH^{11}BCl_2$ in the laser radiation frequency range from 990 to 930 cm^{-1}. The data were obtained in the direct case of a CO_2 laser at p = 13.3 Pa and a laser-radiation energy density $\Phi = 2.5$ J/cm^2. From the spectral dependence of the dissociation yield β it can be seen that the MPD spectrum is characterized by several maxima. The first maximum for β^{10} (radiation frequency 982 cm^{-1}, curve 1) is displaced from the contour of the linear absorption by 10 ± 2 cm^{-1}, and the second (radiation frequency 966 cm^{-1}, curve 1) by 26 ± 2 cm^{-1}. At a frequency of 978 cm^{-1} the dissociation yield with respect to ^{10}B is minimal, which is apparently due to the properties of IR excitation at low oscillatory levels and to the transitions of the excitation to other resonance levels in the process of variation of the laser radiation frequency.

Starting at a radiation frequency of 972 cm^{-1}, the molecule $CHCl{=}CH^{11}BCl_2$ also dissociates. The dissociation reaches its maximum value at a frequency of 947 cm^{-1}. The displacement of the peak for β^{11} with respect to the maximum of the linear absorption is equal in this case to 12 ± 2 cm^{-1}. The shift of the MPD peaks with respect to the contour of linear absorption (curve 3) is due to the anharmonic oscillations of the molecules [3].

Figure 1b shows the variation of the selectivity of dissociation ($\alpha = \beta^{10}/\beta^{11}$) as a function of the laser radiation frequency (ν) at a pressure of 13.3 Pa. The relation $\alpha = f(\nu)$, as in the case of boron trichloride [4], is asymmetric. In the short-wave region we observe a sharp increase in α, with preferential dissociation of the $HClC{=}CH^{10}BCl_2$ molecules. When the laser radiation was shifted further toward the short-wave region (in the 975-986 cm^{-1} frequency range) at the given pressure of the substance being investigated (p = 13.3 Pa), the selectivity of the process was not determined, since the change in the peak of the absorption for $HClC{=}CH^{11}BCl_2$ during IR dissociation of the molecules is commensurable with the error of measurement of the IR spectrometer itself.

As the pressure of the material increases, i.e., as the collision processes increase, there is clearly observable in the short-wave portion of the spectrum a dissociation of both isotopic modifications. Figure 2 shows the variation of the yield of the dissociation of 2-chloroethenyl dichloroborane as a function of the laser radiation density Φ when p = 133 Pa and $\nu = 987.6$ cm^{-1}. Even though the oscillatory transition of the isotopic modification $HClC{=}CH^{11}BCl_2$ is out of resonance with the frequency of the laser radiation, for values of $\Phi > 2.5$ J/cm^2 we observe considerable dissociation of the molecules to BCl_3 and acetylene.

The dissociation of $HClC{=}CH^{11}BCl_2$ becomes possible as a result of the collision processes between the isotopic modifications of 2-chloroethenyl dichloroborane, which leads to a decrease in the isotopic selectivity of the process. The selectivity of dissociation also

Translated from Atomnaya Énergiya, Vol. 57, No. 3, pp. 203-204, September, 1984. Original article submitted November 11, 1983.

 0038-531X/84/5703-0656$08.50

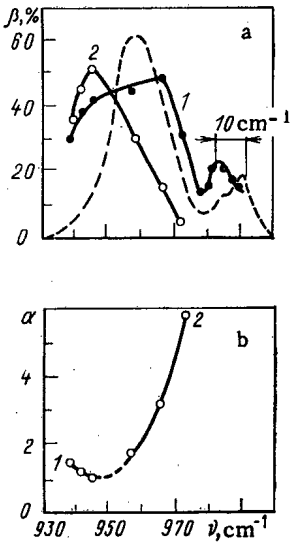

Fig. 1. Spectral dependence of the yield of the dissociation of 2-chloroethenyl dichloroborane (a) and variation of the selectivity of dissociation as a function of the laser radiation frequency (b): a) 1, 2 show the yield of the dissociation of $HClC{=}CH^{10}BCl_2$ and $HClC{=}CH^{11}BCl_2$, respectively; the dashed curve shows the IR spectrum of the linear absorption on the transitions $v = 0 \rightarrow v = 1$; the arrows indicate the shift of the peak of the multiphoton absorption with respect to the peak of the linear absorption curve; b) 1: $\alpha = \beta^{11}/\beta^{10}$; 2: $\alpha = \beta^{10}/\beta^{11}$. Here and in Figs. 2-5 the symbols ○ and ● indicate experimental data.

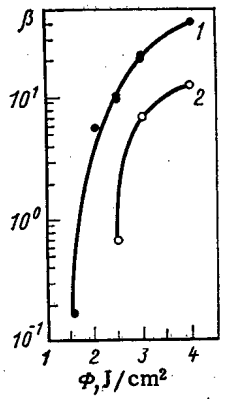

Fig. 2. Yield of the dissociation of $HClC{=}CH^{10}BCl_2$ (1) and $HClC{=}CH^{11}BCl_2$ (2) as a function of the laser energy density.

decreases when there is an increase in the intensity of the laser radiation owing to a field broadening of the absorption contour. When there is preferential dissociation of the $HClC{=}CH^{10}BCl_2$ molecules, in the decomposition product BCl_3 we observe an enrichment in ^{10}B, and in the remaining gas there is an enrichment in ^{11}B. In this case the enrichment is usually characterized by the degree of separation K.

In Fig. 3 we show the variation of the degree of separation K as a function of the time of irradiation of the molecules in units of βN (N is the number of pulses) when $p = 133$ Pa, $\nu = 987.6$ cm^{-1}, and $\Phi = 2.8$ J/cm^2. It follows from the figure that as the material is further irradiated, the degree of separation with respect to ^{10}B in the dissociation product and with respect to ^{11}B in the remaining gas will increase. These results contradict the published data according to which the degree of separation in the dissociation products decreases as

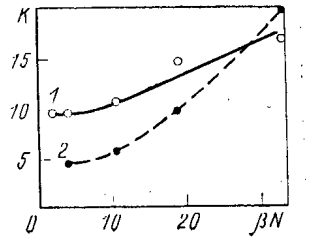

Fig. 3. Degree of separation as a function of the time of irradiation in the case of excitation of $HClC{=}CH^{10}BCl_2$ molecules: 1) enrichment in ^{10}B in the dissociation product BCl_3; 2) enrichment in ^{11}B in the remaining gas $HClC{=}CHBCl_2$.

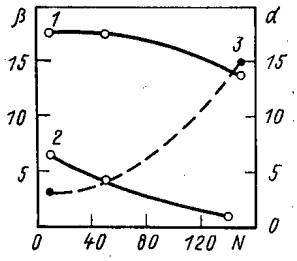

Fig. 4. Dissociation yield as a function of the number of pulses: 1, 2) yield of the dissociation of $HClC{=}CH^{10}BCl_2$ and $HClC{=}CH^{11}BCl_2$, respectively; 3) selectivity of the dissociation process.

the number of pulses increases [5]. The yield of the dissociation with respect to ^{10}B in the present case $\beta^{10} = \beta^{10}_{sp} - \Delta\beta^{10}_{col}$, where β^{10}_{sp} is the spectral value of the dissociation yield and $\Delta\beta^{10}_{col}$ is the decrease in the dissociation yield caused by the deexcitation of the molecules in the collision processes.

For a low gas flow rate at the beginning of the irradiation the deactivation of the $HClC{=}CH^{10}BCl_2$ molecules takes place mainly as a result of V–V exchange with the $HClC{=}CH^{11}BCl_2$ molecules which are out of resonance with the laser field. In this case the $HClC{=}CH^{11}BCl_2$ molecules, participating in the collision processes, can gather enough energy for dissociation, and eventually they can increase the total yield in ^{11}B. Then the yield of the dissociation is $\beta^{11} = \beta^{11}_{sp} + \Delta\beta^{11}_{col}$; where β^{11}_{sp} means the spectral values of the dissociation yield which are caused by the overlapping of the absorption field of the two isotopic modifications for the chosen laser wavelength, and $\Delta\beta^{11}_{col}$ is the additional yield of the dissociation resulting from the V–V exchange between the molecules. As the material is further irradiated and there is an accumulation of BCl_3 molecules, there appears an additional collision channel, which leads to deexcitation of the molecules of both the light and the heavy isotope. However, the influence of the V–V exchange on the β^{10} and on the β^{11} will be different. For the dissociation of the $HCl{=}CH^{10}BCl_2$ the BCl_3 molecules can compensate for the increase in β^{10} caused by the reduction in the partial pressure of the original material. Thus, the result of this phenomenon will be that the dissociation with respect to ^{10}B remains the same (Fig. 4, curve 1). The dissociation yield with respect to ^{11}B will decrease, since the $HClC{=}CH^{11}BCl_2$ molecule obtains energy mainly through the V–V exchange. The appearance of an additional deactivation channel can therefore lead to a decrease in its observed yield. Figure 4 shows that as the material is further irradiated, the β^{11} dissociation yield decreases (curve 2) and the selectivity α of the process increases correspondingly (curve 3).

To confirm the influence of the resonance buffer gas on the increase in the selectivity of the process of dissociation of $HClC{=}CHBCl_2$, we conducted special experiments in which we added to the main material a resonance buffer gas BCl_3 at different partial pressures. The variation of the dissociation yield as a function of the BCl_3 partial pressure was determined for a constant laser radiation frequency of $\nu = 987.6$ cm^{-1} and different values of the laser energy density.

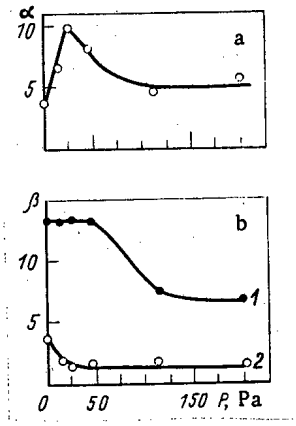

Fig. 5. Selectivity of the process (a) and dissociation yield (b) as functions of the pressure of the resonance buffer gas: 1, 2) yield of the dissociation of $HClC{=}CH^{10}BCl_2$ and $HClC{=}CH^{11}BCl_2$.

In all the experiments the qualitative variation in the dissociation yield and in the selectivity of the separation process over the range of increasing partial pressures of the resonance buffer gas from zero to 27 Pa was the same and was analogous to what was observed in the process of formation of BCl_3 directly during the decomposition of $HClC{=}CHBCl_2$ in the IR field of the laser radiation (Fig. 5).

Thus, the presence of a resonance buffer gas during IR multiphoton dissociation of $HClC{=}CH^{10}BCl_2$ enables us to obtain at the same time the enrichment in ^{10}B in the decomposition product BCl_3 and in ^{11}B in the remaining gas ($HClC{=}CH^{11}BCl_2$).

We also investigated the influence of a nonresonance buffer gas (argon) on the process of dissociation of 2-chloroethenyl dichloroborane. The addition of argon led to a decrease in the yields of both of the isotopic modifications and to a decrease in the selectivity of the process.

As we noted earlier [2], a molecule of 2-chloroethenyl dichloroborane can be regarded as promising for use as a working substance in developing a laser method for separating boron isotopes. Our investigation confirms these hypotheses and at the same time indicates that the appearance of a resonance buffer gas in the dissociation of molecules of 2-chloroethenyl dichloroborane or the addition of this gas to the zone of interaction of laser radiation with the material leads to an increase in the selectivity of the dissociation process.

LITERATURE CITED

1. R. Jensen et al., IEEE J. Quantum Electronics, QE-16, 1352 (1980).
2. T. G. Abzianidze et al., Pis'ma Zh. Tekh. Fiz., 8, No. 20, 1234 (1982).
3. V. N. Bagratashvili et al., Multiphoton Processes in Molecules in an Infrared Laser Field [in Russian], VINITI, Moscow (1980).
4. Yu. R. Kolomiiskii and E. A. Ryabov, Kvantovaya Elektron., 5, 651 (1978).
5. E. P. Velikhov et al., ibid., 6, 317 (1979).

EFFECTIVE FISSION-PRODUCT YIELDS IN VVÉR-365 AND VVÉR-440 FUEL

V. Ya. Gabeskiriya
and V. I. Borisenkov

UDC 621.039.516.22:
621.039.524.4-98

The most accurate (error ∿1.5%) method of determining the depth of burnup of nuclear fuel is based on the measurement of the quantity of heavy atoms N_h and any fission product (FP), which is a monitor of the nuclear fuel burnup N_M. Knowing the effective yield Y_{eff} for fission [1], the burnup F (rel. units) is calculated by the formula

$$F=\frac{N_M/Y_{eff}}{N_h+N_M/Y_{eff}}, \quad (1)$$

where

$$Y_{eff}=\sum_j g_j Y_{jh}; \quad (2)$$

g_j is the fraction of fissions of nuclei j in the total number of fissions; Y_{jk} is the yield of the k-th nuclide from fission of the j-th nucleus.

Using the results of analysis of fuel and also data about the nuclear constants and design of the reactor, the value of g_j can be calculated by the method of heavy atoms [1]. The measurement of the content of the nuclides uranium, plutonium, americium, curium, and fission products in samples of spent VVÉR fuel with a different burnup [2, 3], carried out by mass-spectrometric methods, has allowed the numerical relationships between the values of g_j and the fuel characteristics, verified by experiment, to be established (see Table 1).

TABLE 1. Fraction of Fissions of Uranium and Plutonium Nuclides and Effective Fission-Product Yield*

Fuel burnup depth (with respect to U), kg/ton	Fraction of fissions, %				Effective yield, %		
	^{235}U	^{238}U	^{239}Pu	^{241}Pu	^{137}Cs	^{144}Ce	^{148}Nd
			VVÉR-365				
5	89,15; 86,13	5,029; 5,948	5,791; 7,864	0,030; 0,055	6,286; 6,290	5,306; 5,259	1,703; 1,706
10	84,07; 79,70	5,147; 6,048	10,58; 13,91	0,205; 0,355	6,296; 6,304	5,210; 5,160	1,705; 1,708
15	79,45; 74,05	5,291; 6,185	14,66; 18,79	0,599; 0,979	6,306; 6,315	5,149; 5,073	1,707; 1,710
20	75,09; 68,91	5,456; 6,346	18,22; 22,83	1,235; 1,918	6,315; 6,326	5,084; 5,000	1,709; 1,713
25	70,89; 64,12	5,636; 6,521	21,37; 26,25	2,100; 3,104	6,320; 6,336	5,020; 4,926	1,711; 1,716
30	66,84; 59,65	6,828; 6,705	24,17; 29,19	3,146; 4,452	6,331; 6,346	5,962; 4,860	1,714; 1,710
35	62,93; 55,46	6,024; 6,893	26,71; 31,77	4,321; 5,872	6,339; 6,355	4,904; 4,800	1,717; 1,723
			VVÉR-440				
5	88,78; 85,71	5,302; 6,264	5,891; 7,981	0,028; 0,050	6,285; 6,289	5,294; 5,323	1,704; 1,706
10	83,59; 79,16	5,409; 6,353	10,53; 14,15	0,175; 0,325	6,296; 6,304	5,219; 5,154	1,705; 1,709
15	78,92; 73,40	5,555; 6,479	14,97; 19,17	0,552; 0,901	6,307; 6,316	5,139; 5,067	1,707; 1,710
20	74,51; 68,28	5,713; 6,627	18,63; 23,32	1,142; 1,770	6,315; 6,327	5,077; 4,990	1,710; 1,714
25	70,30; 63,31	5,884; 6,788	21,87; 26,82	1,947; 2,878	6,324; 6,337	5,014; 4,918	1,712; 1,717
30	66,25; 59,06	6,067; 6,955	24,75; 29,83	2,932; 4,144	6,333; 6,346	4,955; 4,851	1,715; 1,720
35	62,35; 54,93	6,254; 7,127	27,34; 32,45	4,047; 5,500	6,341; 6,356	4,898; 4,793	1,718; 1,723

*The first value is for a ^{235}U enrichment of 3.6%, and the second for 3%.

Translated from Atomnaya Énergiya, Vol. 57, No. 3, pp. 204-205, September, 1984. Original article submitted November 18, 1983.

 0038-531X/84/5703- 0660$08.50

When calculating the effective yields of ^{137}Cs, ^{144}Ce, and ^{148}Nd, given in Table 1, data were used about the yields of these nuclides from the fission of ^{235}U, ^{239}Pu, ^{241}Pu [4], and ^{238}U [5]. Similarly, the effective yields of any fission product can be calculated by formula (2), using the values of g_j given in the table and published data on fission-product yields.

The error in the determination of Y_{eff} depends slightly on the accuracy of the values of g_j. This is explained by the fact that $\Sigma g_j = 1$, as a result of which a reduction of the contribution to Y_{eff} of fissions of a single nucleus $g_j Y_{jk}$ is almost completely compensated by the increase of the contribution of fissions of the other nuclides. Therefore, the error in the determination of the effective yield

$$\Delta Y_{eff} = \sum_j g_j \Delta Y_{jk} \qquad (3)$$

is determined completely by the error of the fission-product yield values ΔY_{jk} used, and is almost independent of the error in the calculation of the values of g_j, which amounts to 5-10%.

An excellent monitor of the fuel burnup is ^{144}Ce, as it has an acceptable half-life and does not migrate in the fuel. It can be seen from the analysis given that the effective yield of this nuclide is significantly different from the yield by the fission of ^{235}U. Therefore, if ^{144}Ce is the fuel burnup monitor, it is necessary to use only the values of the effective yields of this nuclide.

It can be seen from an analysis of the table that the effective yield depends on the depth of burnup of the spent fuel. For VVÉR-365 and VVÉR-440, it is almost identical. Although the effective yield depends slightly on the initial enrichment of the fuel, in a number of cases this dependence cannot be neglected, for example, in the mass-spectrometric method of determining the depth of burnup. It follows from the table that the effective yield of ^{144}Ce, from fuel with an initial enrichment of 3 and 3.6%, is different by 1%, which is comparable with the error in the determination of the depth of burnup.

LITERATURE CITED

1. Yu. B. Novikov et al., At. Energ., 43, No. 4, 240 (1977).
2. V. Ya. Gabeskiriya et al., At. Energ., 44, No. 5, 446 (1978).
3. V. Ya. Gabeskiriya et al., At. Energ., 55, No. 3, 175 (1983).
4. E. Crouch, in: Proceedings of the IAEA Symposium "Nuclear Data in Science and Technology," Paris, March 12-16 (1973), Vol. 1, p. 393.
5. Yu. A. Zysin, A. A. Lbov and L. I. Sel'chenkov, Yields of Fission Products and Their Distribution by Mass [in Russian], Atomizdat, Moscow (1963).

EFFECT OF GEOMETRICAL PARAMETERS ON THE CIRCULATION CHARACTERISTICS OF AN EVAPORATIVE ELEMENT

V. A. Farafonov
and V. I. Churyumov

UDC 621.039.534.25

The creation of a heat-exchange surface using Field tubes is of definite interest in the calculation and design of high-temperature steam generators. In order to provide for the reliable operation of steam generators and good technicoeconomic indices of them, workers have devoted special attention to the choice of the optimal geometry of the evaporator channel, especially its circulation channel.

Theoretical and experimental investigations of an evaporator channel of the Field-tube type have been carried out in [1, 2] for the determination of its geometry for the maximum circulation characteristics. On the basis of analysis of the data, a geometry has been suggested for the channel which corresponds to maximum circulation possibilities. Under these conditions the ratio of the cross section of the rising annular channel to the cross section in the descending tube is $S_{a.c}/S_{desc} = 2\text{-}4$, which permits obtaining the greatest multiplicity of circulation for a given average specific heat flux.

However, one should note that all the computational formulas in [1, 2] are obtained in the solution of a system of differential equations. The assumption is adopted that heat exchange between the rising and descending sections is absent, since the temperature of the water in the descending channel is close to the saturation temperature at the average pressure. This assumption first of all makes the calculation insufficiently rigorous for an evaporator channel fabricated in the form of a Field tube and secondly is unsuitable for use in cases in which the supply water enters the descending tube with strong underheating.

The ideas presented have forced making a more detailed study of the effect of the geometry of a Field tube on its circulation parameters. A mathematical model was developed for the investigation of heat exchange processes in a Field steam-generating tube with natural circulation and study of the effect of its geometry on the circulation parameters. We did a calculation for "direct-flow" and "counterflow" schemes of the motion of a warming coolant.

For the counterflow scheme the differential equations in a Field tube have the following form. The evaporator section:

temperature of the supply water in the inner tube

$$c_p G \frac{dt}{dx} = k_1 (t_s - t); \tag{1}$$

enthalpy of the steam–water mixture in the annular channel

$$-G_2 \frac{di}{dx} = k_1 (t - t_s) + k_2 (T - t_s); \tag{2}$$

and temperature of the warming coolant

$$c_{pT} G_1 \frac{dT}{dx} = k_2 (t_s - T). \tag{3}$$

The economizer section:

temperature of the supply water in the inner tube

$$c_p G_2 \frac{dt}{dx} = k_1' (\Theta - t); \tag{4}$$

Translated from Atomnaya Énergiya, Vol. 57, No. 3, pp. 206-207, September, 1984. Original article submitted December 22, 1983.

 0038-531X/84/5703-0662$08.50

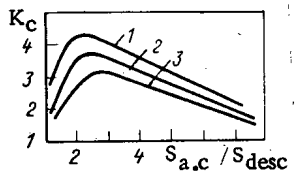

Fig. 1

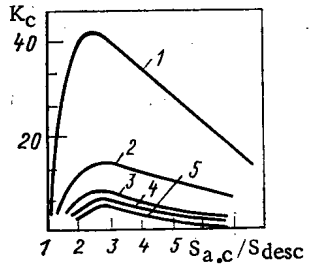

Fig. 2

Fig. 1. Dependence of the multiplicity of circulation on the ratio of the transitional cross sections of the annular channel and the descending section for a pressure in the loop of 5.2 MPa: (1) $q_{av} = 135$, (2) 145, and (3) 175 kW/m^2; $\Delta t = 22°C$.

Fig. 2. Dependence of the multiplicity of circulation on the ratio of the transitional cross sections of the annular channel and the descending section for p = 5.2 MPa: $q_{av} = 145$ kW/m^2 and (1) $\Delta t = 100$, (2) 86, (3) 62, (4) 42, and (5) 22°C.

temperature of the supply water in the annular channel

$$-c_p G_2 \frac{d\Theta}{dx} = k_1'(t-\Theta) + k_2'(T-\Theta); \tag{5}$$

and temperature of the warming coolant

$$c_{pT} G_1 \frac{dT}{dx} = k_2'(\Theta - T). \tag{6}$$

Here t, Θ, and T are the temperatures of the water in the inner tube, the annular channel, and of the warming coolant; i is the enthalpy of the steam-water mixture in the annular channel; G_1 and G_2 are the flow rates of the warming coolant and the supply water; k_1, k_1', k_2, and k_2' are the linear heat-exchange coefficients of the inner and outer tubes in the evaporator and economizer sections; and c_p and c_{pT} are the specific heats of the water and warming coolant.

The system of differential equations for the direct-flow scheme of coolant motion differs only in the signs of its terms on the left-hand side of Eqs. (1), (2), (4), and (5).

A mathematical description of the problem was carried out under the following assumptions: the inner and outer tubes have the identical length, and the specific heats of the coolants are constant within the limits of the section under discussion. We solved the system of differential equations on a computer by a numerical method which permits finding the distribution of the temperature of the warming medium and of the supply water, the weighted steam content along the length of the field tube, as well as the variation of the heat exchange coefficients along the length of the section under discussion as a function of the temperature of the warming coolant and the supply water in a specific cross section.

In order to determine the effect of the channel geometry on its circulation characteristics, we used the ratio $S_{a.c}/S_{desc}$ as the main geometrical parameter. We varied only the transitional cross section of the descending tube in the computational analysis. The diameter of the heat-transfer tube bounding the annular channel was left unchanged. The multiplicity of the circulation K_c was calculated as the inverse of the exit steam content x_{out}. We did the calculation with different flow rates of the warming coolant, i.e., with different values of the average specific heat fluxes. We also analyzed the effect on K_c of the input temperature of the warming coolant and the supply water. The pressure in the steam-water loop was varied from 2.6 to 5.2 MPa. The computational results for three values of the

specific heat fluxes are shown in Fig. 1. It follows from Fig. 1 that as the average specific heat flux increases, the multiplicity of circulation decreases and its maximum is shifted in the direction of large values of $S_{a.c}/S_{desc}$.

Investigations of the effect of underheating of the supply water on the multiplicity of circulation have shown the following (Fig. 2):

with appreciable underheating to t_s the multiplicity of circulation increases sharply; thus with $\Delta t = 100°C$, $K_c^{max} = 40$;

as the underheating increases, the maximum multiplicity of the circulation is shifted, depending on $S_{a.c}/S_{desc}$, in the direction of smaller values of this ratio;

with appreciable underheating to boiling the maximum multiplicity of circulation is observed for $S_{a.c}/S_{desc} = 2-3$. The calculations performed have also shown that the optimal ratio of the transitional cross sections of the steam-water loop for motion of the coolant by the direct-flow scheme is $S_{a.c}/S_{desc} = 2.0-4.0$. The value $S_{a.c}/S_{desc} = 1.5-3.0$ is recommended for motion of the coolant by the counter-flow scheme. When the coolant moves according to the direct-flow scheme, the multiplicity of the circulation is somewhat higher for the given values of the average specific heat flux than in the case of the counter-flow scheme. A change in the length of the steam-generating Field tube with the input parameters of the coolants unchanged exerts no significant effect on the multiplicity of circulation.

Thus the investigations performed have shown that in the range of recommended values of $S_{a.c}/S_{desc}$ with the counter-flow and direct-flow schemes of motion of the warming coolant, conditions which provide for the reliable operation of the heat-exchange surface of a Field tube under conditions of developed bubble boiling will be satisfied for values of the output steam content less than the critical value.

LITERATURE CITED

1. L. F. Fedorov and V. G. Popov, Teploenergetika, No. 2, 78 (1976).
2. L. F. Fedorov, V. G. Popov, and E. N. Voropaeva, Teploenergetika, No. 8, 37 (1978).

TEMPERATURE INTERVALS OF Si(Li)p-i-n DETECTOR USE

R. A. Muminov, B. N. Zaveryukhin,
V. D. Krevchik, Kh. Kh. Ismailov,
and A. Sh. Shamagdiev

UDC 621.315.592

Si(Li)p–i–n detectors are nowadays widely employed in the spectrometry of electrons and low-energy x rays. Investigations of the spectrometric characteristics of such semiconductor detectors have revealed substantial limitations for their applicability in certain temperature intervals (4.2-180°K) [1]. Substantial changes in the amplitude $\bar{A}$ of the charge-induced signal were explained at $T < 50$°K by fine impurity levels causing the capture of nonequilibrium charge carriers or by the "polarization" of the semiconductor detector (total loss of the spectrometric properties) and at $T \approx 50$–150°K by the temperature dependence of the average energy $\varepsilon(T)$ of electron–hole pair generation. When we studied the temperature dependences of the signal amplitude in the range 77-250°K, we detected particular details in the function $\bar{A}(T)$ which are associated not only with the dependence $\varepsilon(T)$ but also with other physical processes taking place in the sensitive detector region. An analysis of the resulting experimental dependences $\bar{A}(T)$ has shown that at 77–150°K the contribution of $\varepsilon(T)$ to the change in the signal amplitude may be considered constant and insignificant.*

We therefore made experiments to study the processes which determine the amplitude changes of the charge-induced signal in the particular temperature interval. Si(Li)p–i–n detectors having a thickness $w = 0.1$ cm of the sensitive region were examined. p-Type silicon with the initial specific resistivity $\rho \approx 2$–4 kΩ•cm, the charge carrier lifetime $\tau \approx 500$–800 μsec, the dislocation density $N_d \approx 10^4$ cm^{-2}, and the oxygen concentration $N_{O_2} \approx 10^{16}$ cm^{-3} was used in the manufacture of the detectors. A diffusion-drift technique was employed to manufacture the semiconductor detectors.

Detectors with T-shaped geometry, which were mounted in a metal housing, had an inverse current I_{inv} and an energy equivalent E_n of the noise not exceeding 1.5 μA and 15 keV at the operating voltage and at $T = 300$°K, respectively. In order to separately determine the behavior of the electron and the hole components of the charge losses, the spectrometric characteristics of the detectors were studied while the detectors were irradiated with collimated ^{137}Cs β- and ^{239}Pu α-particle sources. A cryostat made it possible to adjust smoothly and at a given rate the temperature in the interval 77-300°K. The temperature was monitored with a copper–Constantan thermocouple and a digital VK2-20 voltmeter. The spectrometric setup included a charge-sensitive amplifier, a BUS-2-97 pulse-shaping amplifier, a BUS-2-06 expander, and an AI-256-6 pulse analyzer. In order to increase the curvature of the characteristics of the transistors used and in order to expand the range of the dynamic capacitance of the charge-sensitive amplifier, two KP-307Zh field-effect transistors were inserted in parallel in the head stage of the preamplifier. The stability of the spectrometric channel was monitored with a pulse generator of stable amplitude; the pulse amplitude was measured with an error of ∿0.01%.

The experimental dependences $\bar{A}(T)$ and $\bar{A}(E)$ which were obtained in counting α and β particles are illustrated in Figs. 1 and 2. The step of the $\bar{A}_\alpha(T)$ dependence and the "hump" attest to an impurity level and large-scale traps [3, 4], respectively. The analysis of the authors of [3] has shown that steps in the $\bar{A}_\alpha(T)$ and $\bar{A}_{\beta_2}(T)$ dependences are caused by admixed oxygen ($E_c = 0.16$ eV, $N_t \approx 10^{11}$ cm^{-3}, and $\sigma_t \approx 10^{-13}$ cm^2), with the impurity being "frozen" at $T = 77$°K. When the temperature is increased ($T \geqslant 87$°K) the oxygen impurity begins to be ionized; at $T \approx 107$–154°K, a transition of the ionized oxygen from its atomic form into the associated form takes place whereupon vacancy–oxygen complexes are being formed (the so-called A centers of [5]). In the field strength dependence $\bar{A}_\alpha(E)$, two sections (I – a linear section,

*Owing to the temperature dependence of the width of the forbidden energy gap E_g, the change of the average energy $\varepsilon(T)$ required for generating an electron–hole pair in Si is very small in the range 77-250°K and amounts to ∿0.02 eV [2].

Translated from Atomnaya Énergiya, Vol. 57, No. 3, pp. 207-208, September, 1984. Original article sumitted January 30, 1984.

0038-531X/84/5703- 0665$08.50

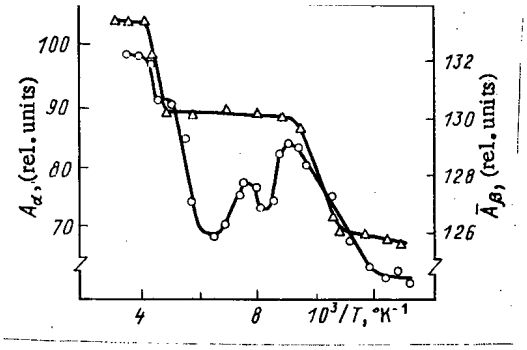

Fig. 1. Experimental temperature dependences of the signal amplitude A(T); the dependences were obtained with Si(Li)p—i—n detectors in the spectrometry of (o) α particles and (Δ) β particles at V = 70 V.

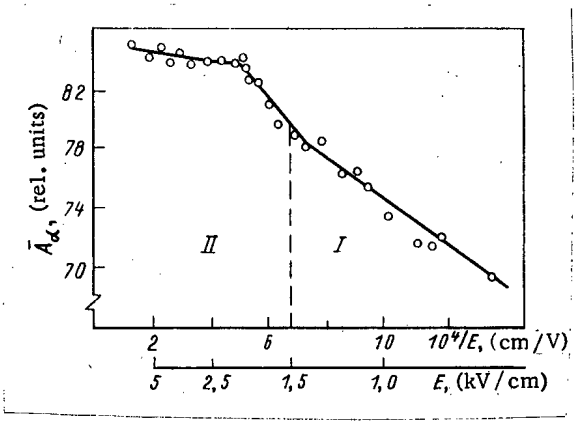

Fig. 2. Dependence of the signal amplitude $\bar{A}_\alpha(E)$ generated by I) the ionization of single oxygen impurity atoms and II) the activation of large complexes upon the electric field strength at T = 77°K.

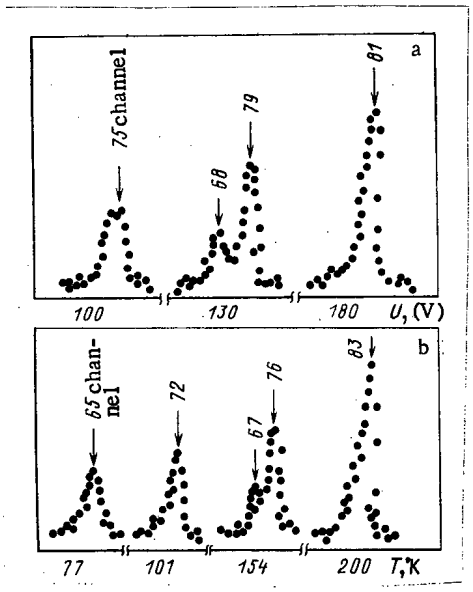

Fig. 3. Transformation of the shape of the α-particle induced amplitude spectra of Si(Li)p—i—n detectors; a) in changes of the electric field strength (T = 77°K); b) in temperature changes (V = 100 V).

and II — a superlinear section) correspond to the transition of atomic oxygen to the A centers; the sections characterize the losses of charge at isolated oxygen atoms and vacancy—oxygen complexes, respectively (see Fig. 2). Finally, the investigations of the shape of the α- and β- amplitude spectra have revealed doublets (in the same temperature interval of 107-154°K) which attest to the large scale of the inhomogeneities formed [6]. The transformation of the amplitude spectrum from the doublet form to the single-line form was observed at electric field strength $E \approx 1.5$-2 kV/cm and T = 154-200°K (Figures 3a and 3b). This means that in the range 77-150°K there exist intervals in which the spectrometric characteristics of the semiconductor detector deteriorate as a consequence of the accumulation of A centers which are formed by thermal ionization of impurity-oxygen levels. The capacitive dependencies C(V) and C(T) of the semiconductor detectors also attest to large-scale formations in the sensitive region of the detector.

Thus, when excellent spectrometric characteristics of silicon semiconductor detectors are to be obtained, the optimal intervals of the operating temperature and bias voltage must be selected in dependence upon the degree of inhomogeneity in the concentration of uncontrollable impurities, particularly oxygen, in the initial material.

LITERATURE CITED

1. N. P. Afanas'eva et al., Prib. Tekh. Eksp., No. 1, 73 (1982).
2. G. MacFarlane et al., Phys. Rev., 11, No. 5, 1245 (1958).
3. V. K. Eremin et al., in: Applied Nuclear Spectroscopy [in Russian], No. 8, Atomizdat, Moscow (1978), p. 207.
4. V. K. Eremin et al., Fiz. Tekh. Poluprovodn., 12, No. 4, 718 (1978).
5. V. V. Emtsev and T. V. Mashovets, Impurity-Induced Defects and Point Defects in Semiconductors [in Russian], Radio i Svyaz', Moscow (1981).
6. V. K. Eremin et al, Fiz. Tekh. Poluprovodn., 13, No. 12, 2407 (1979).

DENSITY DISTRIBUTION OF THE PHOTONEUTRON FLUX IN A THICK LEAD TARGET

V. I. Kasilov, N. I. Lapin,
and S. F. Shcherbak

UDC 539.172.284

We present in the present work results of measurements of the radial and longitudinal distributions of fast neutrons in electron-irradiated lead; we describe the change which occurs in these distributions when oriented Si single crystals are placed before the target on the path of the electrons.

Our work was done on the beam of the linear 2-GeV electron accelerator of the Khar'kov Physicotechnical Institute of the Academy of Sciences of the Ukrainian SSR. A beam of 1200-MeV electrons with a divergence of $2 \cdot 10^{-4}$ rad passed through a 1.5-mm-thick Si single crystal positioned in a goniometer; then the beam was incident on a 300-mm-long lead block with a diameter of 150 mm; the block consisted of 5-mm-thick disks. The crystal was oriented with an error of $5 \cdot 10^{-5}$ rad with respect to the electron beam axis with the aid of readings of an ionization chamber [1]. The activation method of [2] was used to measure the neutron yield: the $^{27}Al(n, p)^{27}Mg$ reaction with a threshold of 4.5 MeV and a half-life of 9.5 min was employed. The detectors, which were 2.5-mm-thick aluminum disks with a diameter of 15 mm, were placed as indicated in Fig. 1. The activity of the detectors was measured with a semiconductor gamma spectrometer equipped with a Ge—Li crystal. The statistical error of the measurements did not exceed 1%.

Figure 2 depicts the longitudinal distribution of fast ($E_n > 4.5$ MeV) neutrons generated in the lead block by the electrons which had passed through the Si single crystal. The <111> axis of the single crystal was parallel to the electron beam direction. Figure 2 also shows the longitudinal distribution of the fast neutrons generated by electrons which were directly

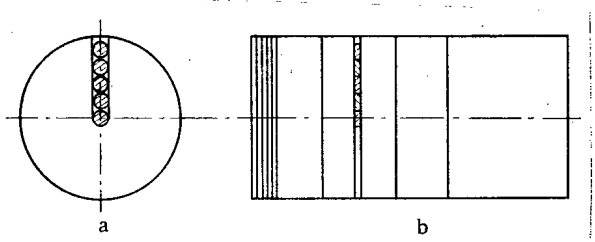

Fig. 1. Scheme of the detector arrangement.

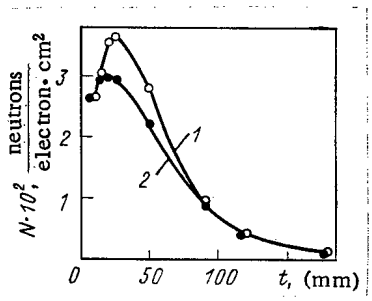

Fig. 2. Longitudinal distribution of the fast neutrons: 1) with the oriented Si single crystal; 2) without the Si single crystal.

Translated from Atomnaya Énergiya, Vol. 57, No. 3, pp. 208-209, September, 1984. Original article submitted February 23, 1984.

 0038-531X/84/5703-0668$08.50

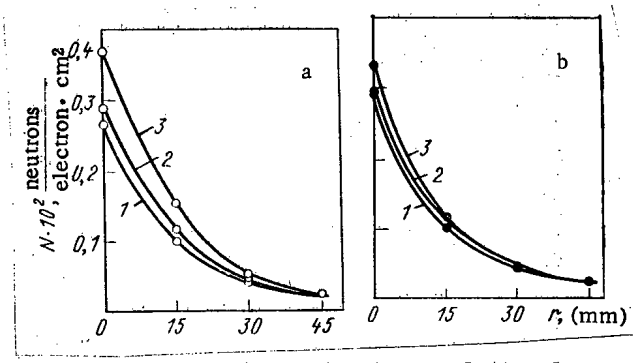

Fig. 3. Radial distributions of the fast neutrons with a 1) 10-mm, 2) 15-mm, and 3) 20-mm-thick lead block.

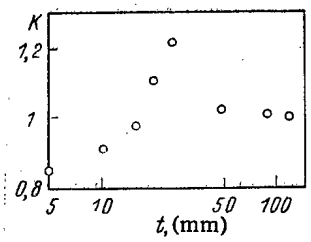

Fig. 4. Dependence of the neutron yield ratio upon the thickness of the lead block with an oriented single crystal and without it.

incident on the lead block. A maximum at t = 20-25 mm is observed on both curves (this is equal to approximately four radiation lengths). At the maximum the yield of the secondary gamma quanta with an energy in excess of 10 MeV has its highest value [3] (the threshold of the photoproduction of neutrons in the lead is ∿8 MeV). Curve 1 is situated above curve 2. This can be explained by the increase in the gamma radiation intensity when oriented single crystals are employed. The increase occurs at the low-energy part of the spectrum, which part coincides with the "giant" resonance in the cross sections of photonuclear reactions [4, 5].

Figure 3 depicts the radial distributions of the fast neutrons for lead block thicknesses of 10, 15, and 20 mm. The distributions were obtained a) with the oriented Si single crystal and b) without it. The substantial difference between the curves corresponding to a particular thickness (Fig. 3a and Fig. 3b) is observed only in the case of small radii (in the region of the electron–photon avalanche propagation). At large radii the difference is small because the absorption [6] and the neutron scattering are of dominating importance. Therefore, only detectors situated on the axis of the lead block were taken into account in Fig. 4 which depicts the yield ratio of the neutrons for the cases of Figs. 3a and 3b in dependence upon the thickness of the lead block. The value is $K < 1$ for thicknesses of 5-15 mm because of the scattering of the electron beam passing through the Si single crystal, i.e., because of the decreased density of the electrons incident on the target.

The authors also measured the number of neutrons leaving the lead block when an oriented Si single crystal was used or omitted. The results do not differ within the error limits of the measurements and the corresponding value is 0.05 neutron per electron ($E_n > 4.5$ MeV).

The above experimental results may be useful in the design of sources of fast neutrons on the basis of linear accelerators of electrons.

The authors thank A. P. Antipenko for his help in the experiment.

LITERATURE CITED

1. V. L. Morokhovskii et al., Problems of Atomic Science and Technology, Series Physics of High Energies and the Atomic Nucleus [in Russian], No. 5 (7), 58 (1973).
2. E. A. Kramer-Ageev et al., Activation Techniques in Neutron Spectrometry [in Russian], Atomizdat, Moscow (1976).
3. H. Nagel, Z. Phys., No. 186, 319 (1965).
4. V. B. Ganenko et al., Pis'ma Zh. Eksp. Teor. Fiz., 32, No. 6, 397 (1980).
5. V. I. Vit'ko et al., Pis'ma Zh. Tekh. Fiz., 7, No. 22, 1343 (1981).
6. L. R. Kimel' and V. P. Mashkovich, Protection from Ionizing Radiation [in Russian], Atomizdat, Moscow (1972).

CROSS SECTION OF THE ^{111}Cd(n, n')^{111m}Cd REACTION IN THE INTERVAL EXTENDING FROM THE THRESHOLD ENERGY TO 2.2 MeV

Yu. N. Trofimov

UDC 539.171.017

The sparse data which are currently available on the cross sections of inelastic neutron scattering at ^{111}Cd have been listed in two papers [1, 2]. We have attempted to measure the cross sections of these reactions with the activation method in order to obtain data of greater accuracy and in a greater amount.

The measurements were made between the threshold energy of 0.4 MeV and 2.2 MeV relative to the known cross sections of the (n, n') and (n, γ) reactions of ^{115}In [3]. In order to increase the precision of the measurements, an enriched ^{111}Cd isotope of the following percentage composition was irradiated: 0.35 ^{110}Cd, 95.1 ± 0.3 ^{111}Cd, 2.98 ^{112}Cd, 0.48 ^{113}Cd, 0.93 ^{114}Cd, and 0.16 ^{116}Cd. Targets with a diameter of 6 mm and a low weight (20 mg) were irradiated in order to minimize the corrections for self-absorption. Neutrons were obtained from the ^{3}H(p, n)^{3}He reaction when tritium–titanium targets were bombarded with protons accelerated in the electrostatic accelerator of the V. G. Khlopin Radium Institute. The integral neutron flux was measured with ^{115}In activation detectors. Two detectors with a diameter of 6 mm and a thickness of 0.2 mm were mounted on the two sides of the sample and close to it. The difference in the activation of a detector close to the sample and one far from it did not exceed 8%. The sample and the ^{115}In detectors were mounted 12 mm from the neutron source and irradiated for 20 min. Slight changes in the neutron flux during the relatively short irradiation time influenced the activation of ^{111}Cd and ^{115}In in the same way; the activation products have very similar half-lives (49.1 min in the case of ^{111m}Cd and 54.15 min in the case of ^{116m}In). The activity of the reaction products was determined from the 245.35-keV gamma line of ^{111m}Cd and the 336.25-keV and 416.98-keV gamma lines of ^{115m}In and ^{116m}In, respectively. The energy and the intensity of the γ peaks were determined

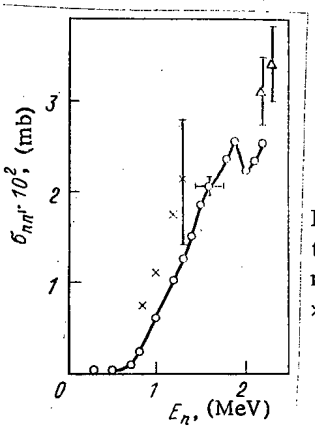

Fig. 1. Dependence of the cross section of the ^{111}Cd(n, n')^{111m}Cd reaction upon the neutron energy: ○) data of the present work; ×) data of [1]; Δ) data of [2].

Translated from Atomnaya Énergiya, Vol. 57, No. 3, p. 210, September, 1984. Original article submitted April 5, 1984.

 0038-531X/84/5703-0670$08.50

TABLE 1. Cross Sections of the $^{111}Cd(n, n')^{111m}Cd$ Reaction and Cross Sections Used in the Case of the $^{115}In(n, \gamma)^{116m}In$ and $^{115}In(n, n')^{115m}In$ Reactions [3]

E_n, MeV	$\pm\Delta E_n$, MeV	^{111}Cd		^{115}In	
		$\sigma^*_{nn'}$, mb	$\pm\Delta\sigma_{nn'}$, mb	$\sigma_{n\gamma}$, mb	$\sigma_{nn'}$, mb
0,3	0,14	0	0	180	0
0,5	0,13	0,3	0,1	183	3,75
0,7	0,13	8	1	190	14
0,8	0,13	25	2	200	23
1,0	0,12	62	5	188	59
1,2	0,11	103	8	178	101
1,4	0,10	150	12	166	136
1,5	0,10	174	14	160	167
1,6	0,09	205	16	153	189
1,8	0,09	236	17	137	232
1,9	0,09	248	18	129	246
2,0	0,08	220	17	121	260
2,1	0,08	232	18	115	270
2,2	0,08	253	20	108	280

* $1 b = 10^{-28} m^2$.

with a Ge(Li) spectrometer having a detector with a volume of 38 cm^3 and a resolution of 3 keV at the 1332 keV line. The spectrometer was calibrated with a set of standard gamma nuclides (OSGI) and reference gamma sources of the D. I. Mendeleev All-Union Scientific-Research Institute of Metrology.

The product of the $^{111}Cd(n, n')$ reaction, the ^{111m}Cd isomer, can also be produced by radiative capture of neutrons by ^{110}Cd, a small amount (0.35%) of which is present in the enriched ^{111}Cd. However, the lack of the ^{111m}Cd isomer in the reaction products at neutron energies below 0.4 MeV indicates that the radiative capture of neutrons by ^{110}Cd is negligible.

The results of the measurements of the cross section of the $^{111}Cd(n, n')^{111m}Cd$ reaction are listed in Table 1 which includes the cross section figures employed for the $^{115}In(n, \gamma)$-^{116m}In and $^{115}In(n, n')^{115m}In$ reactions [3]. Figure 1 depicts the results of the present work and of [1, 2]. The results of our work are smaller than the data of [1, 2] by 50-70%, but the errors of the cross sections of the cited papers overlap our cross section figures. The experimentally observed reaction threshold of 0.4 MeV corresponds to the energy of the isomeric level (396 keV).

In calculating the cross sections, we introduced corrections of $3 \pm 1\%$ for the neutron scattering and of $1.5 \pm 0.3\%$ for the summation of the pulses from ^{111m}Cd. The counting efficiency of the Ge(Li) detector was determined with an accuracy of 4%. Corrections for the nonstationary flux of the neutrons, differences in the geometry, neutrons generated in the (p, n) reaction at target components, self-absorption of the radiation in the sample, and counting losses of the analyzer by superposition of the pulse edges were negligibly small. The statistical error in the measurement of the ^{111m}Cd activity was 0.5% and amounted to 1% in the case of the ^{116m}In activity. The following published data were used by the authors: ^{111m}Cd half-life 49.1 ± 0.1 min; ^{116m}In half-life 54.15 ± 0.05 min; quantum yield of the gamma radiation with $E_\gamma = 245.35$ keV amounting to $94.2 \pm 0.1\%$ for ^{111m}Cd and to $33 \pm 1\%$ for ^{116m}In with $E_\gamma = 416.98$ keV [4].

The total relative mean-square error of the measured cross section (indicated in Fig. 1 for $E_n = 1.6$ MeV) amounted to 8%. Figure 1 also depicts the characteristic spread of the neutron energies. The spread results from the energy losses of the protons in the titanium-tritium targets and the solid angle formed by the sample vis-a-vis the neutron source.

MEASUREMENT TECHNIQUES
Izmeritel'naya Tekhnika
Vol. 27, 1984 (12 issues) $520

MECHANICS OF COMPOSITE MATERIALS
Mekhanika Kompozitnykh Materialov
Vol. 20, 1984 (6 issues) $430

METAL SCIENCE AND HEAT TREATMENT
Metallovedenie i Termicheskaya Obrabotka Metallov
Vol. 26, 1984 (12 issues) $540

METALLURGIST
Metallurg
Vol. 28, 1984 (12 issues) $555

PROBLEMS OF INFORMATION TRANSMISSION
Problemy Peredachi Informatsii
Vol. 20, 1984 (4 issues) $420

PROGRAMMING AND COMPUTER SOFTWARE
Programmirovanie
Vol. 10, 1984 (6 issues) $175

PROTECTION OF METALS
Zashchita Metallov
Vol. 20, 1984 (6 issues) $480

RADIOPHYSICS AND QUANTUM ELECTRONICS
Izvestiya Vysshikh Uchebnykh Zavedenii, Radiofizika
Vol. 27, 1984 (12 issues) $520

REFRACTORIES
Ogneupory
Vol. 25, 1984 (12 issues) $480

SIBERIAN MATHEMATICAL JOURNAL
Sibirskii Matematicheskii Zhurnal
Vol. 25, 1984 (6 issues) $625

SOIL MECHANICS AND FOUNDATION ENGINEERING
Osnovaniya, Fundamenty i Mekhanika Gruntov
Vol. 21, 1984 (6 issues) $500

SOLAR SYSTEM RESEARCH
Astronomicheskii Vestnik
Vol. 18, 1984 (6 issues) $365

SOVIET APPLIED MECHANICS
Prikladnaya Mekhanika
Vol. 20, 1984 (12 issues) $520

SOVIET ATOMIC ENERGY
Atomnaya Énergiya
Vols. 56-57, 1984 (12 issues) $560

SOVIET JOURNAL OF GLASS PHYSICS AND CHEMISTRY
Fizika i Khimiya Stekla
Vol. 10, 1984 (6 issues) $235

SOVIET JOURNAL OF NONDESTRUCTIVE TESTING
Defektoskopiya
Vol. 20, 1984 (12 issues) $615

SOVIET MATERIALS SCIENCE
Fiziko-khimicheskaya Mekhanika Materialov
Vol. 20, 1984 (6 issues) $445

SOVIET MICROELECTRONICS
Mikroélektronika
Vol. 13, 1984 (6 issues) $255

SOVIET MINING SCIENCE
Fiziko-tekhnicheskie Problemy Razrabotki Poleznykh Iskopaemykh
Vol. 20, 1984 (6 issues) $540

SOVIET PHYSICS JOURNAL
Izvestiya Vysshikh Uchebnykh Zavedenii, Fizika
Vol. 27, 1984 (12 issues) $520

SOVIET POWDER METALLURGY AND METAL CERAMICS
Poroshkovaya Metallurgiya
Vol. 23, 1984 (12 issues) $555

STRENGTH OF MATERIALS
Problemy Prochnosti
Vol. 16, 1984 (12 issues) $625

THEORETICAL AND MATHEMATICAL PHYSICS
Teoreticheskaya i Matematicheskaya Fizika
Vol. 58-61, 1984 (12 issues) $500

UKRAINIAN MATHEMATICAL JOURNAL
Ukrainskii Matematicheskii Zhurnal
Vol. 36, 1984 (6 issues) $500

Send for Your Free Examination Copy

Plenum Publishing Corporation, 233 Spring St., New York, N.Y. 10013
In United Kingdom: 88/90 Middlesex St., London E1 7EZ, England
Prices slightly higher outside the U.S. Prices subject to change without notice.

RUSSIAN JOURNALS IN THE PHYSICAL AND MATHEMATICAL SCIENCES

AVAILABLE IN ENGLISH TRANSLATION

ALGEBRA AND LOGIC
Algebra i Logika
Vol. 23, 1984 (6 issues) $360

ASTROPHYSICS
Astrofizika
Vol. 20, 1984 (4 issues) $420

AUTOMATION AND REMOTE CONTROL
Avtomatika i Telemekhanika
Vol. 45, 1984 (24 issues) $625

COMBUSTION, EXPLOSION, AND SHOCK WAVES
Fizika Goreniya i Vzryva
Vol. 20, 1984 (6 issues) $445

COSMIC RESEARCH
Kosmicheskie Issledovaniya
Vol. 22, 1984 (6 issues) $545

CYBERNETICS
Kibernetika
Vol. 20, 1984 (6 issues) $445

DIFFERENTIAL EQUATIONS
Differentsial'nye Uravneniya
Vol. 20, 1984 (12 issues) $505

DOKLADY BIOPHYSICS
Doklady Akademii Nauk SSSR
Vols. 274-279, 1984 (2 issues) $145

FLUID DYNAMICS
Izvestiya Akademii Nauk SSSR, Mekhanika Zhidkosti i Gaza
Vol. 19, 1984 (6 issues) $500

FUNCTIONAL ANALYSIS AND ITS APPLICATIONS
Funktsional'nyi Analiz i Ego Prilozheniya
Vol. 18, 1984 (4 issues) $410

GLASS AND CERAMICS
Steklo i Keramika
Vol. 41, 1984 (6 issues) $590

HIGH TEMPERATURE
Teplofizika Vysokikh Temperatur
Vol. 22, 1984 (6 issues) $520

HYDROTECHNICAL CONSTRUCTION
Gidrotekhnicheskoe Stroitel'stvo
Vol. 18, 1984 (12 issues) $385

INDUSTRIAL LABORATORY
Zavodskaya Laboratoriya
Vol. 50, 1984 (12 issues) $520

INSTRUMENTS AND EXPERIMENTAL TECHNIQUES
Pribory i Tekhnika Éksperimenta
Vol. 27, 1984 (12 issues) $590

JOURNAL OF APPLIED MECHANICS AND TECHNICAL PHYSICS
Zhurnal Prikladnoi Mekhaniki i Tekhnicheskoi Fiziki
Vol. 25, 1984 (6 issues) $540

JOURNAL OF APPLIED SPECTROSCOPY
Zhurnal Prikladnoi Spektroskopii
Vols. 40-41, 1984 (12 issues) $540

JOURNAL OF ENGINEERING PHYSICS
Inzhenerno-fizicheskii Zhurnal
Vols. 46-47, 1984 (12 issues) $540

JOURNAL OF SOVIET LASER RESEARCH
A translation of articles based on the best Soviet research in the field of lasers
Vol. 5, 1984 (6 issues) $180

JOURNAL OF SOVIET MATHEMATICS
A translation of Itogi Nauki i Tekhniki and *Zapiski Nauchnykh Seminarov Leningradskogo Otdeleniya Matematicheskogo Instituta im. V. A. Steklova AN SSSR*
Vols. 24-27, 1984 (24 issues) $1035

LITHOLOGY AND MINERAL RESOURCES
Litologiya i Poleznye Iskopaemye
Vol. 19, 1984 (6 issues) $540

LITHUANIAN MATHEMATICAL JOURNAL
Litovskii Matematicheskii Sbornik
Vol. 24, 1984 (4 issues) $255

MAGNETOHYDRODYNAMICS
Magnitnaya Gidrodinamika
Vol. 20, 1984 (4 issues) $415

MATHEMATICAL NOTES
Matematicheskie Zametki
Vols. 35-36, 1984 (12 issues) $520

continued on inside back cover